DESIGN, ECONOMIC, AND ENVIRONMENTAL ASSESSMENT OF RENEWABLE ENERGY SYSTEMS

By

Siddharth Shukla

A DISSERTATION

Submitted to
Michigan State University
in partial fulfillment of the requirements
for the degree of

Environmental Engineering – Doctor of Philosophy

2022

ABSTRACT

The renewable energy systems for residential, commercial, and transportation sectors need to be designed to minimize cost and environmental impacts. Key considerations in energy systems' design are energy demand estimation and inclusion of location-specific electricity pricing structures. Due to different energy demand patterns, electricity pricing, and location, designing renewable systems for each sector is complex.

In the residential sector, microgrid systems capacity design is based on deterministic loads assuming that all individual houses have an identical appliance usage throughout the year. Also, residential photovoltaic (PV) systems with second-life batteries are designed based on the in-vehicle degradation behavior of the second-life batteries. Therefore, an alternate stochastic load modeling strategy and optimization algorithm to design PV and battery systems with reduced cost and carbon footprint for the residential sector is proposed in this work.

In commercial and utility sectors, renewable energy systems need to provide energy, cost, and environmental benefits considering different constraints. For commercial buildings, producing electricity and reducing peak demand are key objectives of renewable energy systems without compromising the aesthetics. The agricultural sector is another commercial sector where land use of energy systems needs to be minimized to avoid food security issues. In utility-level applications, large battery capacities can be required to improve grid stability by minimizing the impact of PV variability. Depending on the specific energy challenge, the PV and battery-based renewable energy solutions will differ in terms of materials and systems design. In this work, we analyze the cost and energy benefits of novel PV and battery-based solutions such as transparent organic photovoltaics and second-life batteries for commercial and utility sectors.

In the transportation sector, using battery electric vehicles and generating conventional hydrocarbon fuels from atmosphere-captured carbon dioxide (e-fuels) are two ways to reduce vehicle carbon emissions. However, both these technologies have high electricity demand that should be supplied from renewable energy resources like solar PV and wind turbines. No study has yet analyzed the feasibility of solar PV and wind energy in terms of land and material requirements to support battery electric vehicles and refueling infrastructure for e-fuel. Therefore in this work, the land use and material requirements for solar PV and wind turbines required to decarbonize the light-duty vehicle fleet are analyzed.

Overall, the results of this dissertation highlight the importance of energy demand estimation for designing renewable energy systems at both micro and macro levels. At the micro or individual level, the systems' design can target specific characteristics of the hourly demand, like peak intensity and duration, for reduced cost and environmental impacts. At the macro or national level, forecasting the energy demand can lead to selecting renewable energy solutions which avoid material and supply chain constraints.

To my family and friends!

I dedicate this dissertation to every soul out there that is struggling and trying to accomplish something great. Please believe in yourself; you are capable of much more than you think.

ACKNOWLEDGEMENTS

I want to express my gratitude to my advisor Dr. Annick Anctil, who believed in me, especially when I did not believe in myself. I would also like to thank my committee members (Dr. Anthony Kendall. Dr. Kristen Cetin, and Dr. Yadu Pokhrel), who gave their valuable feedback in shaping this dissertation.

A big thanks goes out to my family, who always supported when the times were hard. A special shout out to my lab mates, who proved to be my support system, family, and friends in a foreign land. Thanks to Angela, Mohammad, and Eunsang for making this Ph.D. journey worthwhile. A special thanks to you Dipti; one cannot ask for a better friend and colleague. You made everything easy when I transitioned to the U.S., whether it was doing research or knowing how to order vegetarian food and coffee.

I would like to thank all my friends in the U.S. and back home. I don't want to mention the names as I am sure I would miss someone important in the process. Please know that you all contributed immensely in making this dissertation possible. I would also like to thank all my teachers during my school, undergraduate, and graduate studies who inculcated the technical skills and hunger for knowledge in me.

TABLE OF CONTENTS

KEY TO ABBREVIATIONS

BAU: Business as usual

BEV: Battery electric vehicle

BIPV: Building integrated photovoltaics

BTM: Behind the meter

CED: Cumulative energy demand

ClAlPc: Chloroaluminum Phthalocyanine

CyTPFB: Cyanine heptamethine substituted with tetrakis(pentafluorophenyl)borate anion

DOD: Depth of Discharge

EIA: Energy Information Administration

EPA: Environmental protection agency

EPBT: Energy payback time

EV: Electric Vehicle

GHG: Greenhouse gas

GWP: Global warming potential

IEA: International Energy Agency

IECC: International energy conservation code

IPCC: Intergovernmental panel on climate change

ITC: Investment tax credit

LCA: Life cycle assessment

LCI: Life cycle inventory

LDV: Light duty vehicle

LIB: Lithium-ion battery

LCOE: Levelized cost of electricity

NEB: Net energy benefit

NIR: Near Infrared radiation

NPV: Net present value

NREL: National Renewable Energy Laboratory

OEM: Original equipment manufacturer

PV: Photovoltaic

RECS: Residential energy consumption survey

SOC: State of Charge

SOH: State of health

SLB: Second life battery

SSP: Shared socio-economic pathway

TMY: Typical meteorological year

TOPV: Transparent organic photovoltaics

Chapter 1 Introduction

The total energy demand from the U.S. in 2021 was 97 quadrillion BTU. 43% of this energy demand was generated from coal and natural gas [1], leading to 274 million metric tonnes of carbon dioxide emissions [2]. With high energy demand along with a coal and natural gas reliant grid, the carbon footprint of energy systems is expected to be significant. The IPCC sixth assessment report stated that global temperature is expected to rise by 1.5° C in the next two decades if stringent measures are not taken to reduce anthropogenic carbon emissions [3].

Renewable energy solutions like solar photovoltaics (PVs) and wind turbines have minimal anthropogenic carbon emissions. However, renewable energy projects can fail to achieve their desired economic and environmental goals because of inefficient systems design [4]. Recent studies have shown that system design is one of the key strategies to improve the cost and environmental benefits of renewable energy systems [5]. The energy systems design is a complex process that does not have a “one-fits-all” approach. The renewable systems design can be complex because of different hourly demands, varied electricity price structures, incentives, and utility policies for each sector.

1.1 Renewable energy systems for residential sector

In residential sector, residential microgrids have facilitated the penetration of renewable energy solutions at a distributed level by providing PV installation options with reduced upfront costs [6,7]. The rapid reduction in PV module prices in recent years [8] and improvements in microgrid control system technologies [9] are two key factors explaining the rapid growth in PV microgrid installations. Residential microgrids help utilities because consumers become prosumers or can at least offset their loads partly, thereby reducing the load on the grid [6,7]. However, the

PV + battery systems for residential microgrids are conventionally not designed based on the realistic hourly load pattern expected in the residential microgrids.

Most studies assume that all the consumers in the microgrids have identical loads [10]. Therefore, all the consumers are assumed to use their appliances at the exact same time, leading to a deterministic load profile. Such deterministic load estimates can lead to the inefficient design of renewable energy systems for residential microgrids. Thus, a novel microgrid load modeling algorithm was designed considering the stochasticity in the load due to consumer behavior. The LCOE and carbon footprint of the considered scenarios were calculated using the stochastic load and compared with the corresponding results for deterministic load in various U.S. locations.

The residential load demand is also evolving rapidly with the increased use of electric vehicles (EVs) [11]. EV energy demand is usually during the hours of no sunlight, requiring some form of energy storage for later use of PV-generated electricity [12]. Li-ion batteries are most suitable for energy storage because of their high energy density, roundtrip efficiency, and depth of discharge [13]. However, due to the high cost of new Li-ion batteries, second-life Li-ion batteries (SLBs) retired from electric vehicles are being sought as an alternate option.

Previous studies showed cost and carbon footprint savings in PV + battery systems when the SLBs are used instead of new Li-ion batteries [14–17]. However, most battery parameters like battery replacement time and depth of discharge are taken from previous literature, which assume that SLB capacity degradation is similar to the new Li-ion batteries' in-vehicle degradation [18,19]. Most of these studies assume SLBs' replacement times and depths of discharge values without considering different cyclic stresses faced by SLBs in stationary applications [20–22]. Thus, incorrect battery degradation modeling can lead to underestimation of the cost and carbon footprint benefits provided by SLBs in PV-based stationary storage systems.

Therefore, a novel PV+battery systems optimization algorithm was developed as a part of this work that accounted for the degradation of SLBs in stationary storage applications based on lab-based accelerated aging tests. The resultant systems optimization algorithm was used to identify the optimal retirement point of SLBs in home energy storage + EV charging applications to increase the cost and carbon footprint savings from PV + SLB systems.

1.2 Renewable energy systems for commercial and utility sector

In commercial buildings, PV and battery-based systems have demonstrated savings in cost and environmental impacts in numerous simulation-based studies and pilot plants [23,24]. However, in addition to the techno-economic and environmental benefits, aesthetic factors like visibility and degree of integration of PV with its surroundings are also becoming an important concern in commercial buildings [25]. One of the ways to produce renewable energy while preserving the aesthetic and architectural value of the buildings is by using Building integrated photovoltaics (BIPVs) [26]. Most BIPVs technologies, like semi-transparent and transparent PVs, suffer from low power conversion efficiencies [27]; however, larger surface areas like windows and façades are available for their installations.

We analyzed the energy benefits from one such BIPV technology, Transparent organic photovoltaics (TOPVs). TOPVs can also save building energy in addition to electricity generation due to the absorption of near-infrared (NIR) radiation [28], thereby acting as low emissivity coatings on the windows [29]. However, the energy benefits need to be analyzed for different types of TOPV donor materials and various commercial buildings due to their different load patterns. Therefore, the energy benefits from TOPVs made from two different donor materials in five types of commercial buildings and four U.S. climates were analyzed in this dissertation. The results helped analyze the relation between the energy benefits from TOPV in building windows and building energy demand and construction.

Currently, TOPV remains an immature technology with only lab-based tests and ongoing pilot-plant projects [30]. While TOPVs become commercially available, conventional silicon-based PV technology and battery storage need to serve the commercial loads. Unlike residential buildings, a considerable portion of electricity cost in commercial buildings gets reduced due to peak demand reduction using PV and battery systems [31]. However, there is little knowledge about the reduction in environmental impacts when the PV+battery systems are designed to reduce both the energy and demand charges in a commercial building. Thus, we analyzed the reduction in the environmental impacts like carbon footprint, photochemical oxidation potential, acidification potential, and abiotic depletion potential when PV+battery systems are used to simultaneously prevent the peak demand and reduce overall grid purchase in commercial buildings.

Another subset of the commercial sector is the agricultural sector. Energy benefits from agriculturally co-located PVs were analyzed in addition to how PVs can offset the agricultural energy demand while utilizing less land. Lastly, the second-life alternates to lithium-ion batteries were explored for utility level firming. The results highlighted the cost and carbon footprint savings with SLBs in utility-level firming applications.

1.3 Renewable energy systems for transportation sector

The transportation sector emits about 29 % of the total greenhouse gas emissions in the U.S., and most of this emission comes from passenger cars and medium and heavy-duty trucks [32]. With a continued expected increase in the vehicle miles traveled [33], the transportation sector's carbon emissions need to be controlled to prevent a more than 2°C rise in global temperature. Electrification of vehicle fleet using battery electric vehicles (BEVs) can be one of the ways to reduce the emissions from the transportation sector based on BEVs' growth and public acceptance [34,35]. Another way to reduce life-cycle carbon emissions from vehicles is using fuels made from carbon dioxide captured from atmosphere via physical or chemical methods [36]. The resultant carbon dioxide is combined with hydrogen to make conventional hydrocarbon fuels (also known as "e-fuels") such as diesel and gasoline for vehicles [37].

The electricity required for both BEV and e-fuels needs to come from renewable energy resources like solar PV or wind turbines to reduce the associated CO_2 emissions [38]. However, there is no knowledge about the materials and land-use implications of large-scale installations of solar PV and wind turbines to satisfy the energy demand of BEV or e-fuels. Therefore, we analyzed the land use and material requirements like aluminum, copper, silicon, neodymium, dysprosium, and praseodymium to set up the refueling infrastructure for BEV and e-fuel dominant future scenarios.

1.4 Dissertation outline

This dissertation identifies the key knowledge gaps and issues in design and benefit assessment of renewable energy systems for residential, commercial, utility, and transportation sectors. The impact of energy demand estimation in systems design and assessment was analyzed by:

a. Evaluating the levelized cost of electricity and carbon footprint in residential applications like microgrids and home energy storage + EV charging applications.
b. Analyzing PV-based solutions based on the energy demand and application that could reduce the commercial sector's environmental impacts while considering the constraints like aesthetics, land use, and cost.

c. Weighing the feasibility of the future BEV dominant vs. e-fuel dominant scenarios for light-duty vehicle fleet by comparing the associated land use and material requirements.

Various models and tools, like techno-economic analysis, life cycle assessment, building energy modeling, and systems optimization, were developed and used to achieve these objectives.

Chapter 2 focuses primarily on the micro-level analysis of the residential PV and battery systems for residential applications. The results and conclusions highlight the importance of considering stochastic load behavior in microgrids. Also, key insights were derived regarding the optimal size of the microgrids. Further, in chapter 2, we evaluate the optimal retirement point for SLBs in demand-intensive applications like home energy storage + EV charging applications.

In Chapter 3, we analyze different PV-based materials and systems design solutions to reduce the energy demand and environmental impacts from the commercial buildings while considering constraints like aesthetics and typical load behaviors. Chapter 3 also focuses on the demand from the agricultural and utility sectors and the ways to reduce their energy demand and carbon footprint.

Finally, a macro-scale feasibility analysis was done in chapter 4 to estimate the land use and material constraints to decarbonize the light-duty vehicle fleet. The land use and material constraints were compared for two future pathways for light-duty vehicles. The first pathway assumed a vehicle fleet dominated by battery electric vehicles, and the second pathway assumed a vehicle fleet operated primarily on e-fuels. Several socio-economic pathways were studied for these two future pathways in addition to the business-as-usual scenarios to estimate land use and materials constraints associated with each of them.

Each chapter and the corresponding analysis highlighted the important role of energy demand estimation in the design, economic, and environmental assessment of renewable energy systems. The result and conclusions highlighted that the demand estimates at the micro and macro level could guide the technological and policy implications such that maximum benefits can be derived from renewable energy solutions while considering constraints like aesthetics, land use, material availability, and cost.

Chapter 2 PV and battery systems design for residential sector

In the United States, the potential for rooftop photovoltaic (PV) electricity is estimated to be 1,000 TWh/year [39], of which only 0.28% have been installed as of 2019 [40]. The residential rooftop PV installations have increased by about 30%/year in the past decade [41]. Residential rooftop PVs are also cheaper in terms of initial investments and do not require any land use change [42]. Residential PV setups can be installed to offset grid purchase or sell back to the grid for a range of loads, including single houses, residential microgrids, and home energy storage + EV charging applications. However, the PV+battery systems design for each of these applications face unique challenges because of time-of-use pricing, stochasticity in the load, and challenges with cost and capacity fade of the battery-based energy storage.

2.1 Residential microgrids

The rapid reduction in PV module prices in recent years [8] and improvements in microgrid control system technologies [9] are two key factors explaining the rapid growth in PV microgrid installations. The U.S. Department of Energy defines microgrids as “a group of interconnected loads and distributed energy resources within clearly defined electrical boundaries that acts as a single controllable entity with respect to the grid to enable it to operate in both grid-connected or island mode” [43]. Microgrids have no size limitations and can range from residential to community or utility level [44,45].

Case studies and pilot-plant based literature across the world show benefits in the Levelized cost of electricity (LCOE) and global warming potential (GWP) when PV and battery-based microgrids were installed [46–52]. A residential microgrid is one subset of the microgrids which act as a local energy-sharing framework within a neighborhood [53]. Residential microgrids help consumers by providing a sustainable business model for PV installation with reduced upfront costs. Residential microgrids help utilities because consumers become prosumers or can offset their loads partly, thereby reducing the load on the grid [6,7]. However, the PV + battery systems for residential microgrids are not designed based on the realistic load patterns expected in the residential microgrids.

Most existing studies assume that all the consumers in the microgrids have identical loads meaning that the load for a 20 house microgrid is calculated by multiplying a single house's load by 20 [10]. Therefore, all the consumers in a microgrid are assumed to use all their appliances at the same time, which is inaccurate. A previous study showed that accounting for uncertainty in the loads, PV generation, and wind generation, can lead to a 2-23% change in cost benefits to consumers [54]. Some previous studies have given novel optimization algorithms and energy management frameworks to account for possible stochasticity in the load [55–58]. However, these studies focus their novel approaches to efficiently design microgrids considering the data privacy and power electronic issues. Also, these studies considered arbitrary stochasticity in the loads by varying the entire load by a certain percentage and do not consider the stochasticity due to consumer behavior. Thus, a novel microgrid load modeling algorithm was designed considering the stochasticity in the load due to consumer behavior. The LCOE and carbon footprint of the considered scenarios was calculated using the stochastic load and compared with the corresponding results for deterministic load in various U.S. locations. The results showed the importance of considering the stochasticity in the load modeling of microgrids for better cost and carbon footprint estimates.

Another question about the residential microgrid design was whether there is an optimal number of connected units in a microgrid and if this number changes with location. In a previous study, the optimal number of houses to lower the LCOE was found to be 10 houses for all considered locations. The analysis was limited to microgrids with 1, 10, and 50 houses in three U.S. locations (Arizona, Texas, and North Dakota) [10], and therefore the optimal value could only be one of these three values. The microgrid consumption was estimated by multiplying the single house consumption by the number of houses in the microgrid, an approach that overestimates the peak electricity demand. Therefore, the approach developed in this study was further used to study the optimal number of houses that can be connected in a residential microgrid while considering load stochasticity.

2.2 Second-life batteries for home energy storage + EV charging applications

The residential load demand is evolving rapidly with increasing electrification of space and water heating [59] and the use of electric vehicles (EVs) [11]. EV energy demand usually occurs during the hours of no sunlight, thereby requiring energy storage for later use of PV generated electricity [12]. Li-ion batteries are most suitable for energy storage because of their high energy density, roundtrip efficiency, and depth of discharge [13]. However, due to the high cost of new Li-ion batteries, second-life Li-ion batteries (SLBs) retired from electric vehicles are being sought as an alternate option.

SLBs can be remanufactured to pass quality checks and specifications for redeployment in stationary applications, as these applications require intermittent and less stressful use of the battery than EVs. Also, developing a secondary market for SLBs can lead to sharing of battery costs between primary and secondary users, ultimately leading to lower battery and EV costs. SLBs retain about 80% of the capacity of new batteries with a relatively smaller (4-8%) reduction in the roundtrip efficiency [60–62]. Previous studies showed cost and carbon footprint savings in PV + battery systems when the SLBs are used instead of new Li-ion batteries [14–17]. However, most battery parameters like battery replacement time and depth of discharge are taken from previous literature, which assumed that SLB capacity degradation is similar to the new Li-ion batteries' in-vehicle degradation [18,19]. Most of these studies assume SLBs' replacement times and depths of discharge values without considering different cyclic stresses faced by SLBs in stationary applications [20–22]. Thus, incorrect battery degradation modeling can lead to underestimation of the cost and carbon footprint benefits provided by SLBs in PV-based stationary storage systems.

A novel PV+battery systems optimization algorithm was developed as a part of this work that accounted for the degradation of SLBs in stationary storage applications based on lab-based accelerated aging tests. The resultant systems optimization algorithm was used to identify the optimal retirement point for SLBs in home energy storage + EV charging applications to increase the cost and carbon footprint savings from PV + SLB systems.

2.3 Methodology

The reduction in the Levelized cost of electricity (LCOE) and global warming potential (GWP) or carbon footprint was studied for PV systems with new and second-life batteries, considering the stochastic nature of the residential load. The results were compared with LCOE and GWP of PV and battery systems when the stochasticity in the load was not considered (Deterministic load). Also, a novel optimization algorithm was developed to design PV and battery system capacities considering the degradation of second-life batteries based on lab-based accelerated aging. This model was used to estimate the optimal replacement strategy for SLBs to reduce the GWP of the systems in residential home EV charging applications.

For analyzing residential microgrids a microgrid modeling framework (Figure 1) was developed in this work that had four stages. The proposed framework was divided into four stages: (1) electricity consumption modeling, (2) system design optimization, (3) cost assessment, and (4) environmental assessment. The first step was to model the hourly electricity load for a single-family house for one year and then extrapolate the load pattern for a microgrid with 20 houses. The cost and economic payback time for the microgrids were calculated based on the microgrid consumption using an economic optimization tool (in this case, HOMER Pro software (version-3.7) [63]). Finally, the life-cycle global warming potential (GWP) of the microgrids were calculated.

For this study, the reference year was 2020, and the project lifetime was assumed to be 25 years. The analysis was initially performed in five locations for a microgrid with 20 houses, which is the average reported residential microgrid size [50,64,65]. The inputs related to the cost, efficiency and lifetime of the system components are given in appendix A. A heatmap analysis for the entire PV and battery solution space was performed for two out of the five locations with the highest LCOE and GWP differences between stochastic and deterministic load. Also, a sensitivity analysis was performed to evaluate the variation of LCOE of PV + battery systems on the number of houses connected in a microgrid.

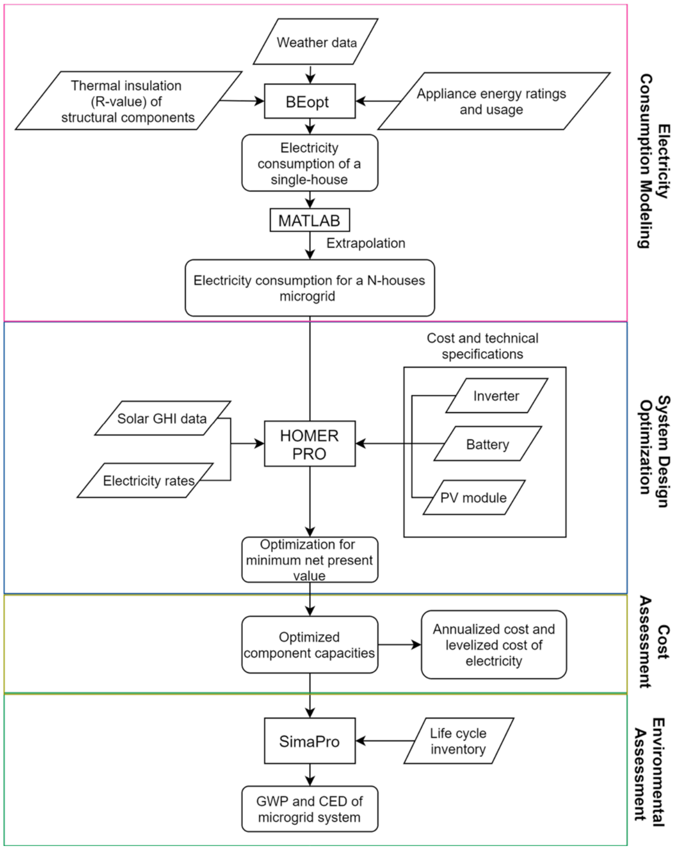

Figure 1. Microgrid modeling framework that combines electricity consumption modeling, system design optimization, cost analysis, and environmental impact analysis.

Five locations were selected for residential microgrid analysis: Detroit, Los Angeles, New York City, Phoenix, and Portland. The locations represent a range of factors that influence energy system design optimization, including average solar irradiance, temperature, as well as current and future electricity prices, which are summarized in Table 1. The time-of-use pricing variation in the residential electricity prices for the five locations are shown in Figure 2.

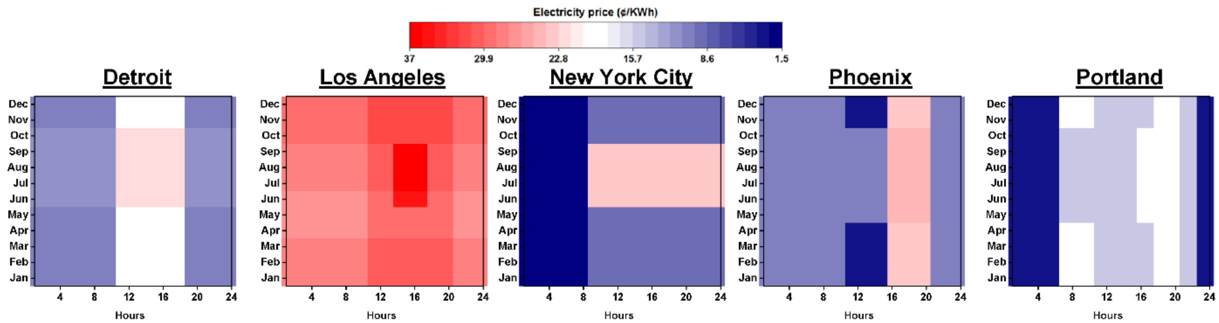

Figure 2. The time of use pricing variation in residential electricity pricing for the considered locations.

The residential microgrid were assumed to be located in the suburban area and not in the city since single-family houses are not common in large cities. The typical building construction and electricity consumption vary with location due to changes in climate and building codes, and single-family houses were modeled to represent those variations. The annual electricity consumption for an average household in 2017 is shown in Table 1, based on the Northwest Energy Efficiency Alliance report for Portland [66], and the Energy Information Administration's (EIA) Residential Energy Consumption Survey (RECS) [67–70] for the other locations. In addition, since rooftop PV are being considered, Table 1 summarizes the average solar irradiance for a system with optimal tilt, which corresponds to the location's latitude.

Table 1. The average solar irradiance incident on PV modules at the optimal tilt, the climate zones, annual electricity price increase, and state average single-house yearly electricity consumption for each location.

Suburban area	**Average solar irradiance incident on PV modules (kWh/m^2day)** [71]	**IECC climate Zone**	**State**	**State-level annual electricity price increase (2017-2027) (%)** [72]	**Single-house annual electricity consumption for 2017 in the state (MWh/year)**
Detroit	4.4	Zone-5 A [73]	Michigan	1.4	8.1 [67]
Los Angeles	6.1	Zone-3 B [74]	California	1.9	7.0 [68]
New York City	4.6	Zone-4 A [75]	New York	2.7	6.5 [69]
Phoenix	6.7	Zone-2 B [76]	Arizona	0.1	14.0 [70]
Portland	4.0	Zone-4 C [75]	Oregon	1.9	7.0 [66]

2.3.1 Load Modeling

The hourly electricity consumption from single houses in each location was modeled using the BEopt software (version-2.7) [77]. Required inputs for BEopt were the thermal insulation (R-value) of the building components, seasonal energy efficiency rating (SEER) of electrical appliances, and weather files. These inputs vary with location due to the changes in building codes, energy codes, and climate. The building and energy codes are selected for each location based on the average age of residential buildings in that state, as summarized in appendix A. If the older versions of the codes (corresponding to the building age) did not provide the R-values or SEER rating, then the first code where those values are provided was used. For example, in Los Angeles, most houses were built between 1970-1989, but the R-value for wooden wall stud specifications were from the 2005 building code since there was no specification for this component until this newer version of the building code.

The houses were assumed to have three bedrooms and two bathrooms with an occupancy of four individuals, based on the average U.S. single-family house survey [78]. Detailed inputs for all five of the modeled residential houses are available in appendix A. The energy source for water and space heating in each location was selected based on the EIA RECS data (Table 2). The heating source selected for modeling the energy consumption in each location is shaded in gray.

Table 2. Percentage distribution of energy sources for water heating, space heating, and space cooling per state based on EIA's 2017 RECS data [79–81].

State	**Water heating**		**Space heating**		**Space cooling**
	Natural gas (%)	**Electricity (%)**	**Natural gas (%)**	**Electricity (%)**	**Electricity (%)**
Michigan	**60.2**	34.1	**71.5**	18.4	**100**
California	**65.2**	31.5	**62.7**	32.7	**100**
New York	**51.9**	31.2	**62.2**	15.5	**100**
Arizona	42.3	**54.4**	46.3	**46.4**	**100**
Oregon	**65.2**	31.5	**62.7**	32.7	**100**

The individual houses in a residential microgrid were assumed to have similar types of occupancy and electrical appliances. However, since everybody is not using their appliances at the same time, each modeled consumption profile is represented using a stochastic pattern [82]. Thus, 20 houses may have 10 kW peak demand, but the probability is low that the combined demand will reach 200 kW at any instant. This reduction in combined demand is commonly represented by the After Diversity Maximum Demand (ADMD) index [83]. A microgrid consumption algorithm was developed to introduce ADMD in the microgrid consumption profile, as shown Figure 3. The hourly electricity consumption from a single-house (C_t) was divided into eight different categories: a) cooling, b) heating, c) cooling fan/pump, d) hot water, e) lights, f) large appliances (like air conditioner, refrigerator), g) vent fan, and h) miscellaneous, where t ranges between 1 and 8760. These categories were classified into "fixed" (F_t) and "variable" (V_t) consumption depending on the seasonal trends and intermittency of the usage patterns. For each category, when the daily consumption varied within a week in all the seasons, the consumption category was classified as "variable"; otherwise, it was classified as "fixed." Electricity consumption from cooling, heating, hot water, large appliances, and miscellaneous were "variable," while the remaining categories were "fixed" consumption.

New "variable" consumption profiles were generated to simulate the random use of appliances in different microgrid houses based on the level of activity (i.e., active or inactive). The variable consumption changes between 12:00 pm and 4:00 pm, based on a previous study [82]. The variable portion of the single-house consumption profile was displaced by 1 and 2 hours, both forward and backward, to create a total of five stochastic variable consumption profiles. To implement this algorithm in MATLAB, a random integer (k) between -2 and 2 was generated from a uniform random number generator. The indices of the "variable" profile (V_t) were shifted to get new variable profiles ($V_{t'}$) based on the value of (k) while ensuring the indices are always between 1 and 8760, as shown in Eq. (1).

$$V_{t'} = V_{t+k} \qquad (1)$$

Where, if $t + k > 8760$, ($t' = t + k - 8760$), and if $t + k < 1$, ($t' = 8760 + t + k$)

The total electricity consumption for each house was the sum of the fixed and a randomly selected variable consumption profile ($C_t = F_t + V_{t'}$). The procedure was repeated for each house in the microgrid, and the profiles were added to get the final consumption from the microgrid.

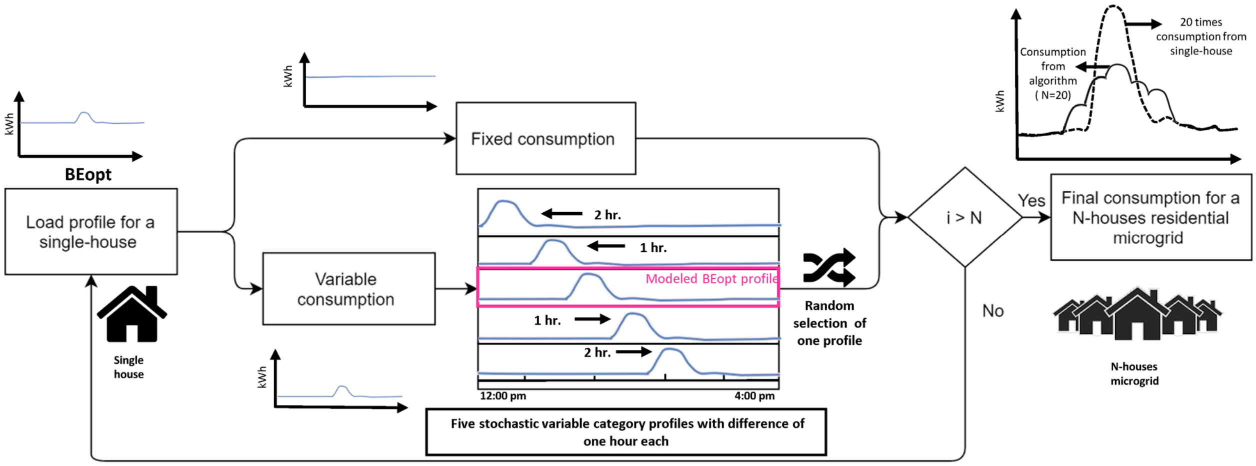

Figure 3. Microgrid consumption algorithm to calculate the total consumption for an n-house microgrid from a single-house consumption.

2.3.2 Systems design optimization for residential microgrids

The hourly consumption profile for a microgrid with 20 houses was the input load in HOMER Pro used for system optimization. The system design optimization minimizes the net present cost of the microgrids in HOMER Pro through the project lifetime (ten years). This study considers lithium-ion (Li-ion) batteries for energy storage due to their high-roundtrip efficiency, short discharge time, and longer lifetime than other batteries [13].

The LCOE and GWP of the PV and battery systems was considered using both new and the second-life Li-ion batteries. SLBs retain about 80% of their original capacity after retirement from electric vehicles, and can be used in stationary energy storage applications [84,85].

The minimum capacities for the PV and the battery in the microgrid was taken as 2 kW and 5 kWh, respectively. The minimum capacities were less than or equal to the average capacities for single-house residential systems installed in the U.S. in 2017 [86,87]. The maximum PV capacity for each location was assumed based on the maximum allowable PV capacity by the utility and the available roof space suitable for PV installation [88]. The maximum battery capacity to be installed in for 1 house was taken as 80 kWh based on limitations from the National fire protection agency [89]. The corresponding maximum PV capacities for each selected location are given in appendix A.

The solar irradiance data was from the National Renewable Energy Laboratory's (NREL's) TMY3 database [90]. The other inputs related to SLB, PV, and inverter are given in Table 3. New batteries are assumed to be replaced at 40% degradation from the initial capacity [91] while SLBs are assumed to be replaced at 20% fade from the initial capacity [92].

Table 3. Systems optimization model inputs from SLB, PV and inverter.

Variable	**Value**	**Reference**
New Battery cost ($/kWh)	253	[93]
SLB cost ($/kWh)	65	[16]
New battery roundtrip efficiency (%)	95	[94]
SLB roundtrip efficiency (%)	91	[16,95]
PV cost ($/kW)	940	[93]
PV O&M cost($/kW)	39	[93]
PV derating factor (%)	90.5	[93]
PV efficiency (%)	19.5	[93]
PV lifetime (years)	25	[93]
Inverter cost ($/kW)	103.6	[93]
Inverter efficiency (%)	98	[93]
Inverter lifetime (years)	10	[93]
Discount rate (%)	6.1	[93]
Inflation rate (%)	3.0	[93]

Six configurations were considered for the system design optimization: Grid only (*Grid*), New Li-ion battery systems connected to the grid (*Grid* + *NB*), second-life battery connected to the grid (*Grid* + *SLB*), PV microgrid connected to the grid with net metering (*Grid* + *PV (NM)*), PV microgrid with new battery connected to the grid (*Grid*+ *PV* +*NB*), and PV microgrid with SLB connected to the grid (*Grid*+ *PV* +*SLB*). The *Grid* configuration was the baseline for this study. The system capacities were first optimized assuming the deterministic load and the difference in LCOE and carbon footprint for each scenario was calculated using stochastic load.

2.3.3 Cost Assessment of residential microgrids

The annualized cost, levelized cost of electricity (LCOE), and the economic payback time for the optimized microgrid configurations specified in Section 2.2.2 are calculated for all locations. The annualized cost is the cash flow for the microgrid throughout its lifetime converted to an equal annual expenditure value [96]. The LCOE is the annualized cost of the microgrid divided by the lifetime electricity production and represents the cost of electricity for a microgrid over its lifetime (¢/kWh) [97,98]. The economic payback time (Eq. (2)) for a microgrid is the time required to pay back the initial investment (net present value of the system, NPV) based on the difference in annualized cost of electricity from the grid (AC_{grid}) and the microgrid ($AC_{microgrid}$) [64].

$$Economic\ Payback\ time = \frac{Net\ present\ value\ of\ (PV + SLB + Inverter + Balance\ of\ Systems)}{(AC_{grid} - AC_{microgrid})} \tag{2}$$

The LCOE and economic payback time was calculated with a 26% rebate or investment tax credit [99].

2.3.4 Novel genetic algorithm framework for PV and battery capacity optimization

An objective function was designed for system capacity optimization and attached to a genetic algorithm optimization framework [100] to assess the optimal use condition of SLBs in home EV charger applications. The flow diagram in Figure 4 shows the logic followed in the objective function. The objective function was used to calculate the LCOE and GWP for each scenario.

The optimization framework calculates the cost and GWP for random PV and battery capacities initially and then runs recursively to find better solutions over a user-specified solution space. Minimizing the objective function is treated as the fitness criteria of each individual solution. The solutions that rank the highest in the fitness criteria are mated and mutated to generate the next set of solutions, analogous to natural selection [100]. After a fixed number of generations, the optimum solutions are found and displayed to the user. The genetic algorithm used for this model was an open-source code developed by researchers at the Michigan State University [100].

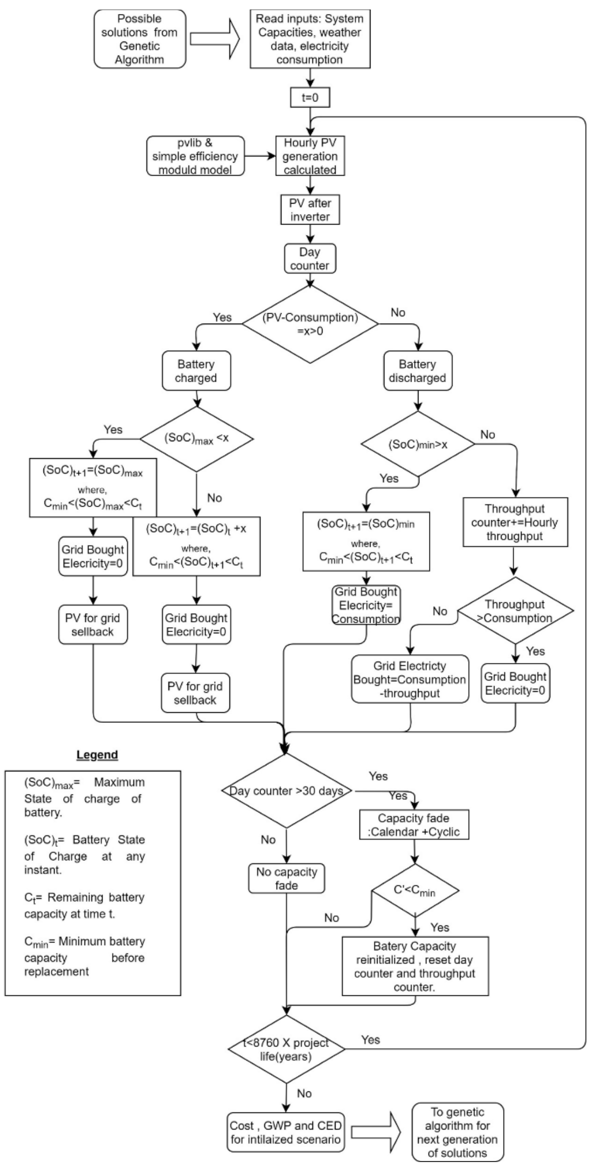

Figure 4. The objective function used inside the optimization algorithm.

Three locations were selected for this study: Detroit, Phoenix, and New York City. The cities were selected out of the five locations considered in section 2.3 because of their varied time-of-use pricing, grid electricity's carbon footprint and solar irradiance (Table 1).The electricity load profile for the three considered locations was modeled in BEopt as mentioned in the section 2.3.1. The project lifetime was considered as 10 years for home EV charger applications as the average life of an electric vehicle is 10 years [101,102]. The home EV charging was considered to have a load of 18.4 kWh and the consumers charge their EVs after midnight for two hours as given in [12]. The typical metrological year (TMY) weather data was taken from the National Solar Radiation Database [103]. Similar to the microgrids, the maximum allowable battery capacity was taken as 80 kWh per house based on [89], and the maximum PV capacity was based on the utility guidelines and the rooftop space suitable for PV installations (given in appendix A).

The total hourly irradiance incident on the PV module was calculated using the pvlib python module [104] developed by Sandia National Laboratory. This module calculated the total irradiance on a PV module based on irradiance from the weather file along with the latitude, longitude, azimuth, and tilt of the PV module. Based on the calculated irradiance, the hourly PV power generation was calculated using the "simple efficiency module" model [105] developed by the National Renewable Energy Laboratory. The annual PV module degradation was taken as 0.7% per year based on [8], and the inverter loading ratio (PV capacity/inverter capacity) was taken as 1.15 [93]. The SLBs in this study were assumed to be replaced at seven different levels battery state of health (SOH): 70%, 73%, 76%,79%,82%,85%, and 88%. That signifies different levels of the battery degradation. A detailed battery degradation model was used to account for calendar and cyclic capacity degradation of battery. A high SLB cost scenario and low SLB cost scenario was analyzed based on expected SLB costs given by [94,106].

2.3.4 1 Battery degradation

The battery capacity degradation was modeled in the optimization algorithm based on [107]. The selected model can be used for all applications to simulate the battery degradation and project the battery capacity fade after a given time [107]. The selected model was used to simulate the degradation of the battery capacity for SLB by calendar and cyclic aging based on Eq. 3

$$C_t = C_{initial}\left(1 - \alpha \cdot t^{0.75} - \beta \cdot \sqrt{Q}\,\right) \tag{3}$$

Where t is time in days, C_t is the battery capacity at instant t , $C_{initial}$ is the initial battery capacity, Q and is the cumulative battery throughput. The parameters α and β are calendar and cyclic aging parameters, respectively. The calendar aging parameter α is dependent on the temperature, T (Kelvin) and voltage, V, given by Eq. 4. The cyclic aging parameter is obtained by fitting the capacity vs. throughput curve and is dependent on the battery's state of charge range, current rate, and charge throughput.

$$\alpha(T, V) = (7.543 \cdot V - 23.75) \cdot 10^6 \cdot e^{-\frac{6976}{T}} \tag{4}$$

The battery degradation parameters for the second-life batteries for residential and fast charger applications were obtained from accelerated cycle testing data in the Arbin cycler, as shown in Figure 5. The curve fitting is done based on the two-step methodology provided by [107].

Firstly, the value of α is calculated from the average temperature (T_{meas}), and voltage (V_{meas}) values (Eq. 3). The capacity fade due to calendar ageing is calculated and added to the measured capacity fade data, which gives the degradation only due to the cyclic aging (C_{cyc}) as given by Eq 5.

$$C_{cyc} = C_{meas} + \ \alpha \cdot (V_{meas}, T_{meas}) \cdot t^{0.75} \tag{5}$$

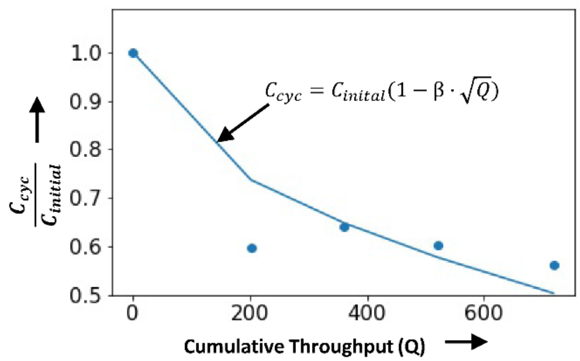

α= 0.000323 β= 0.018499

$R^2 = 0.818397$

Figure 5. Battery degradation model fitting for a residential sample data obtained from accelerated ageing test.

For residential samples, the typical number of charge-discharge cycles in a year is 750 based on [108]. Therefore, the samples with less than 750 cycles and a coefficient of determination (R^2) of less than 0.1 ("bad" fit) were excluded from the curve fitting. The corresponding parameters for the new lithium-ion battery were obtained from the curve fitting of capacity degradation data from the literature [109]. The calendar ageing parameters is kept same for new or second-life batteries for as it is only dependent on the temperature and voltage. The final parameter values are given in Table 4**.**

Table 4. Average calendar and cyclic ageing parameter values for new and second-life batteries.

Battery Type	Calendar ageing parameter (α)	Cyclic ageing parameter (β)
Second-life Battery	0.000337	0.006512
New Battery	0.000337	0.009525

2.3.5 Environmental assessment of microgrids and home energy storage + EV charging application

The GWP of all the microgrid and home EV charging configurations were calculated using the TRACI 2.1 [110] and the Cumulative Energy Demand [111] methods in SimaPro software (version-8.5) [112]. The functional unit was the delivery of electricity to meet the demand of the systems for 25 years in case of microgrids and 10 years in case of home energy storage + EV charging applications.

The life-cycle inventories for the PV system and other material inputs was taken from Ecoinvent 3 [113] and DATASMART LCI databases [114]. The electricity was updated with the fuel mix representative of the 2019 USEPA eGRID subregion generation for each location [115]. The SLB inventory was from an LCA of EV battery manufacturing [116] and the remanufacturing process was assumed to take place in the U.S. The material required for the enclosure was assumed to be 30% of the amount for a new lithium-ion battery, and the primary energy for pack assembly was assumed to be the same [95]. Inventory data is given in appendix A.

The GWP and the CED were calculated using the TRACI 2.1 method [110] and the Cumulative Energy Demand method [117] in Simapro v8.5 software [118]. The life cycle inventories for the PV-inverter system and other material inputs were from Ecoinvent 3 [119] and DATASMART LCI databases [114]. The EV SLB inventory was based on previous publications [94,120]. The assessment excludes transportation and the end of life treatment of the system. The electricity production sources in the US on average and the eGRID subregions were taken from the EIA's Annual Energy Report 2019 [121]. The relative fractions of the electricity generation sources for each year were calculated based on the total generation and were used to obtain the electricity inventory for each eGRID region based on the methodology from a previous study [28].

2.4 Results and discussion

2.4.1 Cost and carbon footprint in microgrids due to load stochasticity

Figure 6 shows the LCOE and the economic payback time for all the considered scenarios with deterministic loads and stochastic loads. All locations had lower (25-71%) LCOE than baseline with PV and PV + battery systems depending on the location's PV generation potential and the time-of-use pricing. With net metering, PV systems could lower the LCOE in the 78-109% range, depending on the location. However, utilities throughout the U.S. are revising their net metering programs to reduce the economic incentives to the consumers, so net metering results in this study are likely overestimated for a projected life of 25 years [122]. The economic payback time ranged from 1.9-10.7 years for all the scenarios (Figure 6(b)), which was smaller than the project life (25 years). Most systems with only a battery (and no PV) have a higher LCOE than the baseline scenario (*Grid only*) with no economic payback.

The LCOE difference for systems with stochastic and deterministic loads ranged from 0.1-38.6%, depending on the location and configuration, leading to a 0.3-16.1% difference in the payback times. For PV + battery systems, this LCOE difference translates into an annual cost difference of 29-981 \$/year to the consumers.

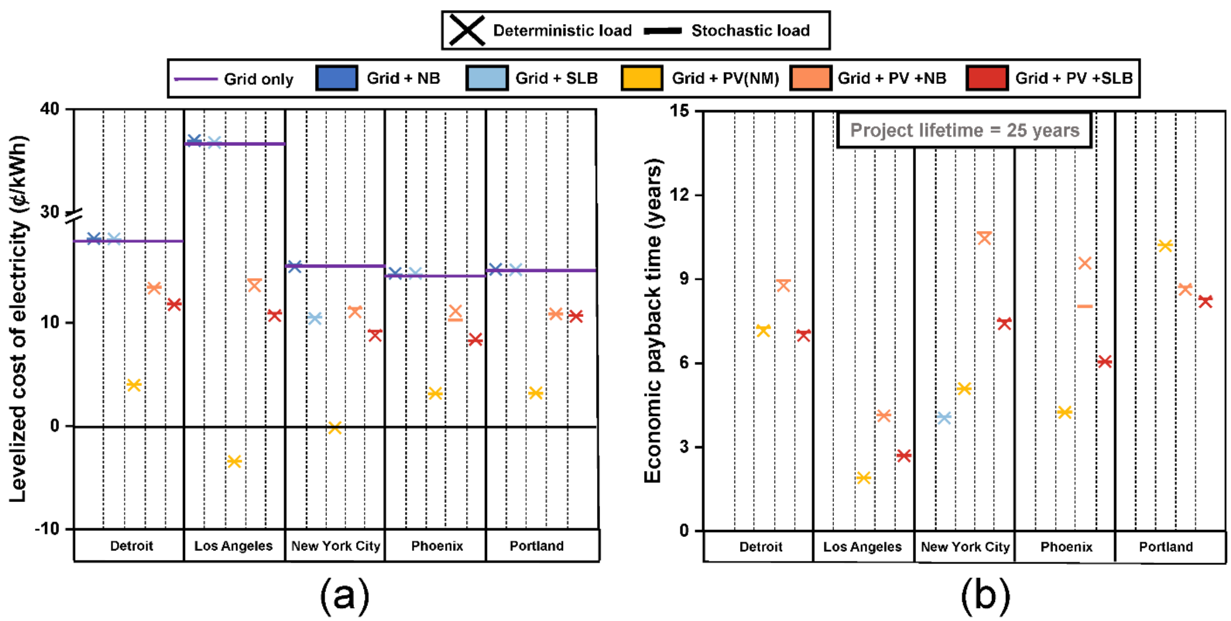

Figure 6. (a)Levelized cost of electricity (LCOE) and (b) Economic payback time for *Grid only*, Grid connected microgrid with new battery (*Grid+NB*), Grid connected microgrid with second-life batteries *(Grid+SLB),* Grid connected PV systems with net metering (*Grid+PV(NM)),* Grid connected PV+battery system with New Li-ion battery *(Grid+PV+NB), and* Grid connected PV+ battery system with SLB (*Grid+PV+SLB).*

The global warming potential (GWP) or carbon footprint of the microgrid scenarios in Figure 7 shows that all PV-based system configurations always reduce the carbon footprint of a 20 house microgrid regardless of the location. The reduced carbon footprint with PV + battery systems resulted from the 49-92% reduction in grid purchases. For net metering scenarios, the carbon footprint was reduced due to a combination of avoided grid purchase and sell back to the grid. The second-life "battery only" scenario in New York City was the only scenario with a higher carbon footprint than the baseline due to more purchase of grid electricity than the load for battery charging. Similar to LCOE and economic payback time, the GWP was also different (0.7-13.0%) when the deterministic load in the renewable energy systems was replaced with stochastic loads. For PV + battery systems, this GWP difference translated into a difference of 3.0-239.2 metric tonnes of CO_2-eq. over the project life, which is equivalent to operating an average gasoline-powered light-duty vehicle for 0.6-48.8 years.

The LCOE was 0.6-4.7% higher, and EPBT was 0.4-2% higher with stochastic load than deterministic load, meaning that microgrid systems generally have a higher cost to consumers than conventionally calculated costs. Similarly, the GWP was also higher (0.7-2.7%) for most locations when the renewable energy systems were assumed to operate with the stochastic load. However, in Phoenix, the LCOE was higher by up to 7.8%, EPBT was higher by up to 16.1%, and GWP was lower by up to 13.0% for the renewable energy systems with the stochasticity in load. A heatmap analysis was done for two out of five locations (New York City and Phoenix) over a range of PV and battery solution space to find the reason for the difference in LCOE with stochastic and deterministic load across the locations. New York City and Phoenix were selected for the LCOE heatmap analysis because they had the highest LCOE difference between stochastic and deterministic load among the five locations. Also, the LCOE was higher with the stochastic load than the deterministic load in New York City, while LCOE was lower with the stochastic load than the deterministic load in Phoenix.

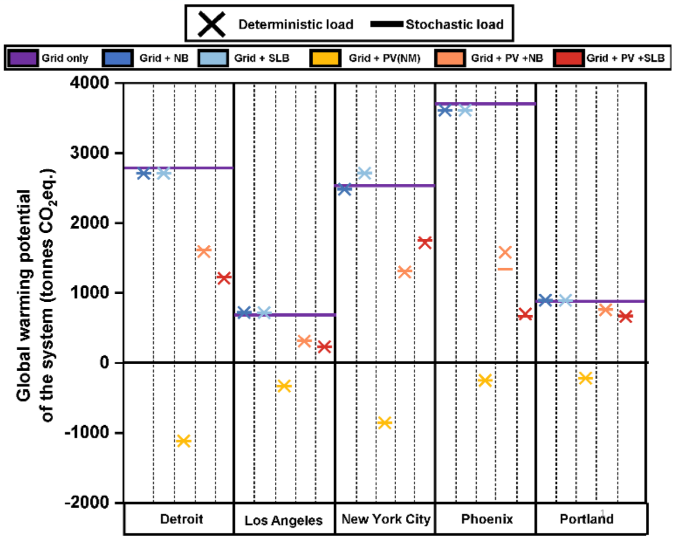

Figure 7. Global warming potential of the for *Grid only*, Grid connected microgrid with new battery (*Grid+NB*), Grid connected microgrid with second-life batteries *(Grid+SLB),* Grid connected PV systems with net metering (*Grid+PV(NM)),* Grid connected PV+battery system with New Li-ion battery *(Grid+PV+NB), and* Grid connected PV+battery system with SLB (*Grid+PV+SLB).*

The LCOE and carbon footprint results shown above are based on the cost, efficiencies and economic parameters given in table 2. The results may vary in the future depending on future costs and efficiencies of PV, battery and inverter systems along with electricity rates and rebates. However, the costs of PV+battery systems is likely to decrease in the future [123,124] with increased electricity prices with more time-of-use variation [125,126]. Both these future conditions would lead to higher PV + battery systems capacities thereby leading to higher cost savings from residential PV and battery systems.

Figure 8 shows the LCOE for different PV and battery systems combinations with deterministic and stochastic load for new and second-life batteries in New York City. The LCOE was lower for deterministic load than the stochastic load for most PV and battery capacities meaning that the cost savings from the PV + battery microgrids are conventionally overestimated.

The lower LCOE with deterministic load was because of an early evening (5 pm-6 pm) load peak in all the cities, which can be partially satisfied directly from the PV generation. There are no energy losses due to the battery storage when the PV generation satisfies the early evening peak load; therefore, the LCOE was lower with the deterministic load. The LCOE difference between stochastic and deterministic load was higher for SLB cases (up to 1.1 ¢/kWh) than for new battery scenarios (up to 0.6 ¢/kWh) due to the low cost of SLBs. When stochasticity is considered, the early evening peak load (around 5 pm-6 pm) shifted and merged with the late evening peak load (around 8:30 pm-9:30 pm), which could be satisfied by optimizing a higher SLB capacity due to its low cost. The higher battery capacity led to a lower grid purchase leading to a lower LCOE in the SLB scenario.

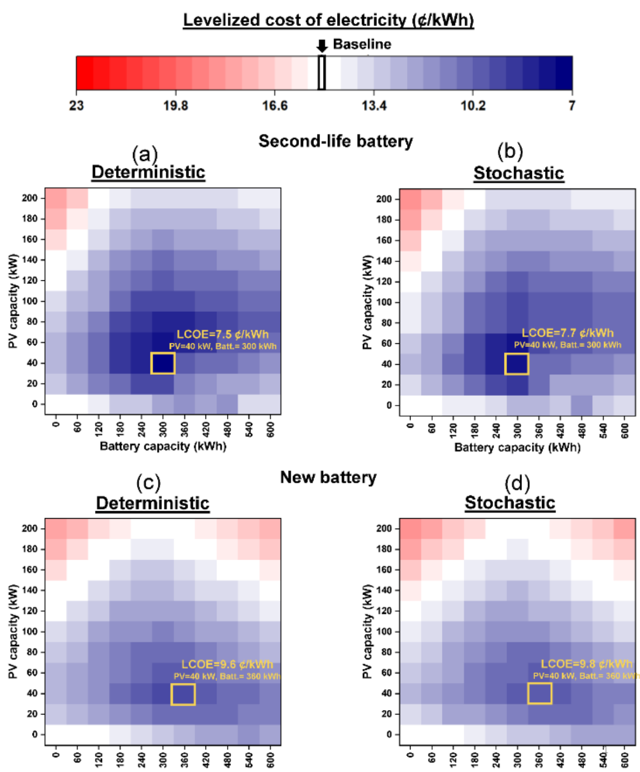

Figure 8. Heatmaps showing the Levelized cost of electricity (LCOE) for the New york city for second-life Li-ion batteries ((a) and (b)) and new Li-ion batteries ((b) and (c)) over a range of PV and battery solution space.

Figure 9(a) shows that LCOE was higher for stochastic load than the deterministic load because a higher percentage of the deterministic load was satisfied from PV generation over the project lifetime. Only for the 19th year, a higher percentage of the stochastic load was satisfied from PV generation as the battery was replaced in the 19th year for the stochastic load while the battery was replaced in the 20th year for the deterministic load. The higher percentage of the deterministic load was satisfied from PV because of an early evening peak, as shown in Figure 9(b). However, in stochastic load, the early and late evening peaks were combined and delayed (Figure 9(c)) so that PV generation could not directly satisfy the load, and higher battery capacity was required to satisfy this evening peak load.

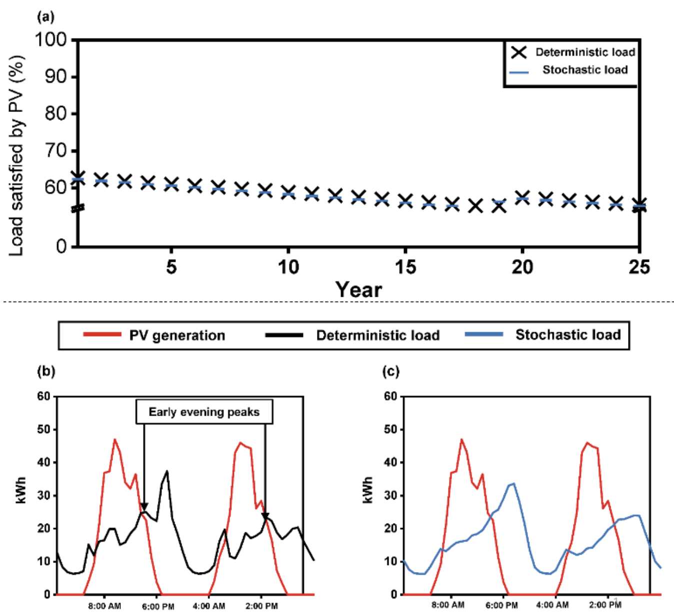

Figure 9. (a) Yearwise load satisified with PV generaated electricity with degrading PV efficiency and battery capacity. The corresponding reason is shown at the daily scale for (b) deterministic load, and (c) stochastic load.

Figure 10 shows the LCOE for different PV and battery systems combinations with deterministic and stochastic load for new and second-life batteries in Phoenix. The LCOE was higher for deterministic load than the stochastic load for most PV and battery capacities meaning that the cost savings from the PV + battery microgrids are conventionally underestimated, unlike all the other cities. The LCOE difference for the two loads was higher for the new battery than SLB due to the higher cost of the new battery and the low electricity cost that can be offset by increasing the battery capacity. The reason for a higher LCOE with deterministic loads in Phoenix was due to the higher overall load demand than any other location leading to higher evening peaks. This higher load in Phoenix was because electricity is used for space and water heating in Phoenix compared to other locations where natural gas is used for space and water heating (as given in Table 2).

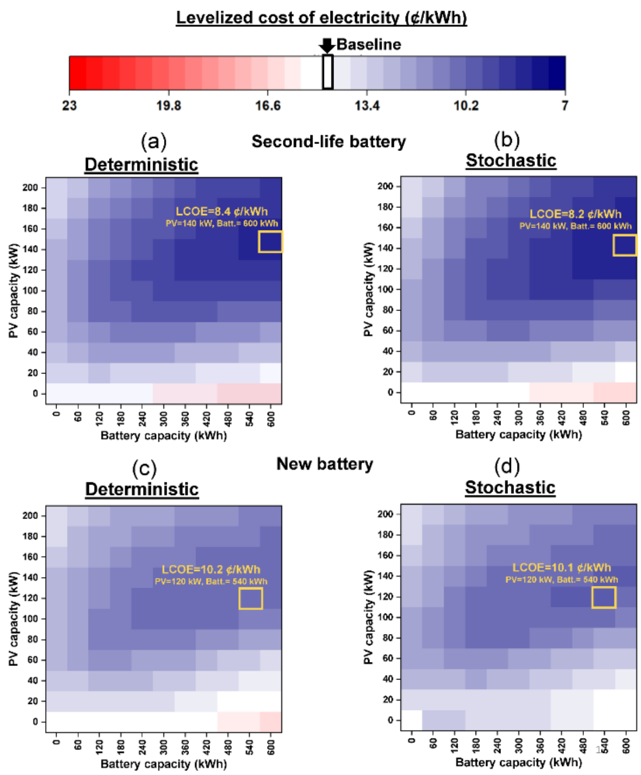

Figure 10. Heatmaps showing the Levelized cost of electricity (LCOE) for Phoenix for second-life Li-ion batteries ((a) and (b)) and new Li-ion batteries ((b) and (c)) over a range of PV and battery solution space.

Figure 11 shows the reason for the difference between the LCOE heatmaps for Phoenix by showing the load and grid-electricity bought in the PV and battery system in Phoenix for a week in August. The higher LCOE was because of the higher peaks in the deterministic load (Figure 11(a)), which were smoothed out and reduced in intensity when stochasticity was considered.

Thus, more electricity needed to be purchased from the grid (shown by the shaded black part) with the deterministic load than the stochastic load (shown by the shaded blue part). Also, the evening peak load needed to be satisfied by the grid purchase, and the deterministic load peaks occur at the same time as the evening peak pricing period (shown by the pink band). Therefore, the LCOE with deterministic load was higher than with stochastic load in Phoenix.

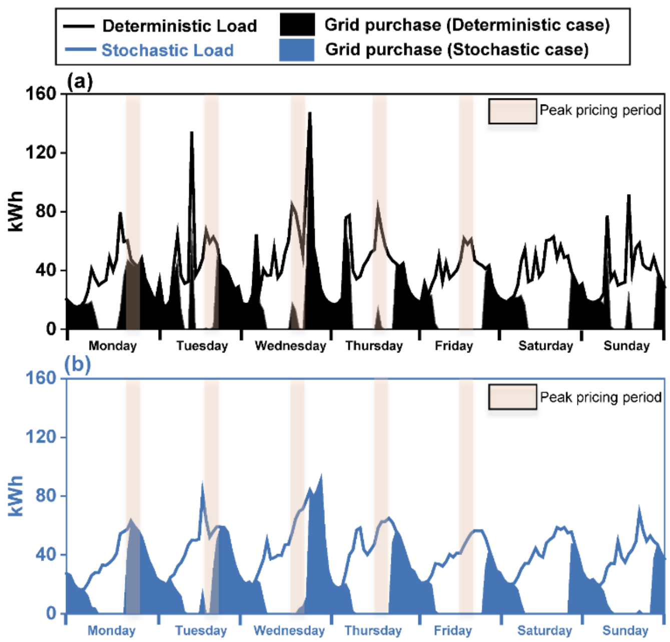

Figure 11. The load and the grid purchased electricity for week in summer in Grid connected PV+ battery system with SLB (*Grid+PV+SLB*) for (a) determinsitc load (b) stochastic load.

In addition to stochastic load modeling, the results also highlight the key role of battery systems in increasing the cost and environmental benefits of residential PV systems. This analysis was based on the federal tax rebate of 26% applied to the PV and battery systems and no rebate to the standalone battery projects. However, with the new inflation reduction act (IRA), the rebate on residential renewable energy-based systems has been increased to 30% (till 2032) with rebate provisions to the standalone battery projects as well [127]. Therefore, the cost and carbon footprint benefits of the upcoming residential microgrids will likely be more than the values calculated in this study.

2.4.2 Sensitivity analysis for the number of houses in a microgrid

A sensitivity analysis was also carried out to study the effect of the number of connected houses in a microgrid on LCOE, as shown in Figure 12, which showed that LCOE reduces with the number of houses in most locations. However, the number of houses was a more important consideration for LCOE in locations with high variation in base and peak prices (as shown in Figure 2), e.g., New York City and Portland. The difference between the LCOE for the stochastic and deterministic load was more when the number of houses in a microgrid was more than two as the LCOE change due to evening peak shifting becomes more prominent with the increasing number of houses. The sensitivity analysis showed that the maximum number of houses in a microgrid should be ten as there would be diminishing cost savings for more than ten connected houses, but there can be higher logistical and electrical connection costs to connect more than ten houses in a microgrid. In Portland, LCOE is considerably different for stochastic and deterministic load for 10 and 30 house microgrids as the PV capacity is minimal due to low PV generation potential and low electricity prices. Due to a smaller PV capacity, the battery charging mechanism was different for stochastic and deterministic loads for 10 and 30 house microgrids. For deterministic load, the battery is charged only during the daytime as the early evening peak can be satisfied directly from PV generation leading to low LCOE. However, the battery is charged both during the day and night due to more discharge of the battery to serve the delayed evening peak load that leads to a higher LCOE. Therefore, in bigger microgrids, considering the stochasticity of the load can also lead to battery charging from the grid that can eventually lead to a higher cost and carbon footprint than calculated conventionally.

Considering stochasticity in the microgrid loads can lead to a difference in cost and carbon footprint of the renewable energy systems in almost all locations depending on the microgrid sizes. Therefore, even locations with low PV generation potential and low time-of-use pricing variation like Portland may have a considerable difference in cost to the consumers and the system's carbon footprint.

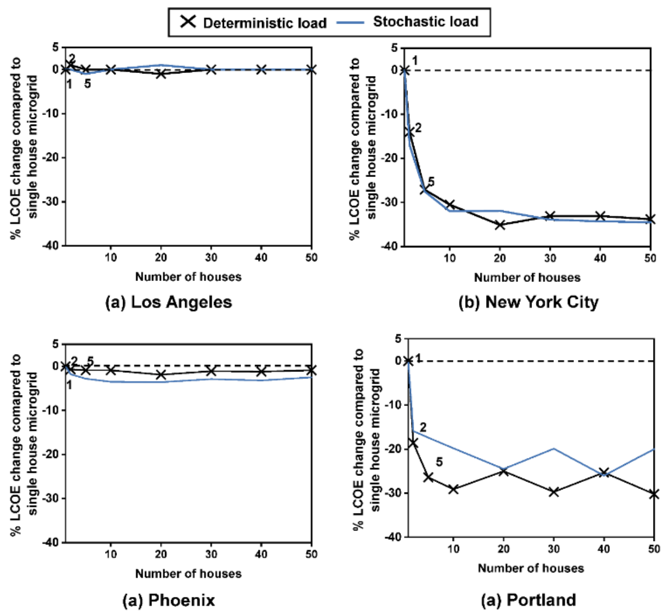

Figure 12. Change in the Levelized cost of electricity (LCOE) for (a) Los Angeles, (b) New York City, (c) Phoenix, and (d) Portland with the number of houses connected in a residential microgrid.

2.4.3 Optimal use conditions of second-life batteries in home energy storage + EV charging applications

With the demonstrated benefits of SLBs in residential applications, the optimal replacement conditions for SLBs were identified for three U.S. locations for home energy storage + EV charging applications because of their high energy demand. Figure 13 shows the change in the carbon footprint of the PV and SLB systems when the SLBs were retired earlier from home energy storage + EV charging applications than 30% degradation in three U.S. locations. There was no difference between the carbon footprint in SLB high-cost and low-cost scenarios in Phoenix and New York City, as the optimized battery capacities in these locations were the same regardless of the SLB cost. However, optimized battery capacities were different in Detroit with different SLB costs due to low PV generation potential and low time-of-use price variation in the grid electricity. 3.2-19.0 metric tonnes CO_2-eq. of the carbon footprint was saved over a project lifetime of 10 years due to a 16-53% reduction in grid purchased electricity when SLBs were retired at 88% state of health instead of 70% state of health from the stationary applications. These carbon footprint savings corresponded to 0.7-4.1 years of running an average light-duty gasoline vehicle in the U.S., thus highlighting the significance of changing the SLB retirement strategy. The difference in carbon footprint reduction among the locations was due to the optimized system capacities and the carbon footprint of the grid electricity. For instance, the battery capacities were smaller in New York City compared to other locations because of the lower off-peak electricity prices and solar generation potential than other locations. Thus, the smaller battery capacities led to the least difference in grid purchases with the early retirement of the SLBs. Therefore, the strategy to save the carbon footprint by the early retirement of SLBs would yield higher benefits in a location with higher off-peak electricity prices.

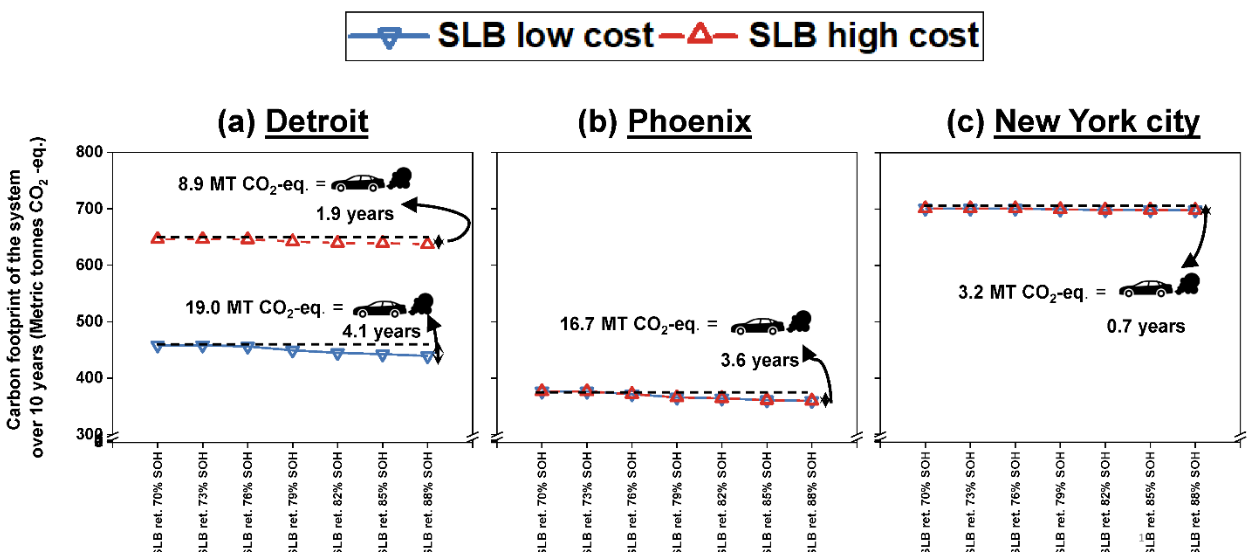

Figure 13. Carbon footprint of a PV and battery system with second-life batteries (SLBs) over 10 years in (a) Detroit, (b) Phoenix, and (c) New York City at different retirement stages based on battery state of health.

Figure 14 shows the LCOE of the home energy storage + EV charging applications does not increase in the three selected locations with the early retirement of SLBs from 70% to 80% state of health point. A minor reduction in the LCOE led to cost savings of 29-94$/year depending on the location, and New York City is the only location with a small (18-28$/year) increase in the cost to consumers with early battery retirement. Thus, the carbon footprint of the home energy storage + EV charging applications can be reduced by early battery retirement with no impact on the cost to the consumers. It should be noted that the minimum replacement time for SLBs was three years; therefore, the potential concerns of consumers about the inconvenience of early battery retirement can also be alleviated.

The additional carbon footprint from reduced useful life of the batteries due to the frequent replacement was not considered in this study. Earlier recycling of the battery after its first life may reduce its overall useful lifetime, but a higher state of health throughout the second life leads to a lower overall carbon footprint of the PV+battery stationary systems. The reduced carbon footprint due to the avoided grid purchase is considerably more than the increased carbon footprint from frequent battery replacement, as most of the carbon footprint of a residential PV+battery is from the grid purchase of electricity [16,17].

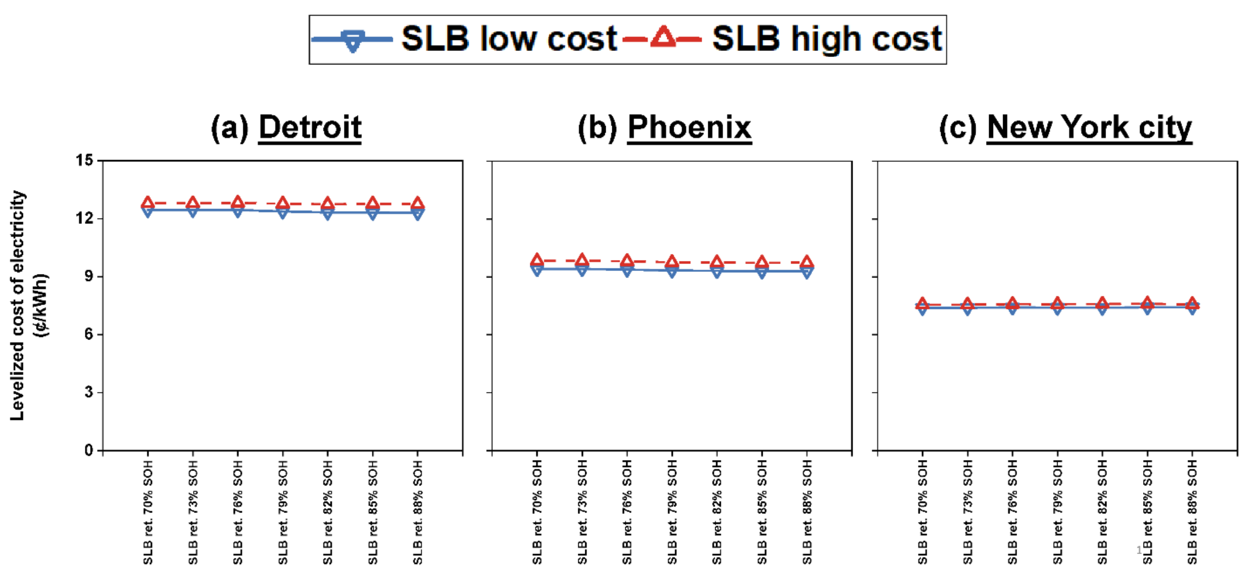

Figure 14. Levelized cost of electricity (LCOE) for PV and battery system with second-life batteries (SLBs) over 10 years in (a) Detroit, (b) Phoenix, and (c) New York City at different retirement stages based on battery state of health.

2.5 Conclusions

Cost and carbon footprint results from the residential microgrids can be considerably different if the PV+battery systems are not designed based on load stochasticity. In most locations, the benefits were overestimated because of the early evening peak load in the individual houses. The early evening peak got delayed by 1-2 hours when the stochastic behavior of the consumers was considered. However, the benefits were underestimated from a PV and battery-based renewable energy system for locations with relatively high loads and low electricity prices like Phoenix. This overestimation was because the optimized PV and battery system capacities insufficient to meet the evening peaks in the deterministic load. However, PV and battery systems contribute more to satisfying the evening loads as the evening peaks widen and get lowered due to stochasticity, thereby reducing the cost and carbon footprint.

As more U.S. locations move towards electrification of water and space heating in future [59] (like Phoenix in our study) the cost and GWP estimates of stationary PV and battery systems are likely to have more wrong estimation. The wrong estimation was due to the erroneous assessment of peak loads' intensity and occurrences. Thus firstly, improved modeling methods need to be employed to estimate the occurrence and intensity of the peaks. Secondly, the PV and battery system capacities need to be designed to satisfy the peaks.

Studies indicate that future residential load peaks may increase up to 10% due to climate change [128]. Apart from using higher battery capacities, the peak loads can be minimized using energy-efficient heat pumps for space and water heating because heating contributes to about 62% of the residential load demand [129]. Similarly, load profile clustering using smart metering can lead to reduced peak load intensity and assigning a higher cost responsibility to customers with higher peaks in residential microgrids [130].

The results in this chapter depend on the residential load profiles which changed significantly for about a year because of the widespread work-from-home during COVID-19 lockdowns [131,132]. The results from this study are likely to change as more employers and employees across the U.S shift towards hybrid work models in the future [133]. However, the conclusions of this study which highlight the importance of stochastic load modeling, will become more important because the energy loads of individual consumers are likely to be more sporadic and unevenly spread throughout the year in hybrid work scenarios. Moreover, the methodology used in this study can be easily modified to account for the changed behavior of residential consumers in the future and determine the cost and carbon footprint benefits of the residential microgrids.

The sensitivity analysis showed that the optimal number of houses connected in a microgrid was ten, regardless of the location. Beyond ten houses, the cost savings to consumers reduce minimally while there may be additional electrical connection costs for bigger microgrids. The results also showed that the dependence of LCOE on the number of houses is more in locations with a higher difference in peak and base electricity prices like New York City and Portland. Thus, accounting for stochastic behavior in the load modeling would be more important as the time-of-use pricing schemes get more complicated in the future.

For home energy storage + EV charging applications, the early retirement of SLBs did not cost extra to the consumers, but it led to increased carbon footprint savings due to avoided grid purchases. The carbon footprint savings shown in these results are from the early retirement of SLBs in one house, so these savings can be significant if the benefits from the early retirements are calculated at a state or the national level.

SLBs' early retirement led to higher carbon footprint savings in locations with higher off-peak electricity prices, as the major portion of the load was from EV charging during off-peak hours [12]. Therefore, as electricity prices increase in the future [134], the early retirement of SLBs can yield more carbon footprint benefits for the PV and SLB systems in all locations. The early retirements can be facilitated by signing contracts between the second-life battery repurposer and the consumers. Such contracts would encourage the consumers to buy SLBs because warranty can be the main concern of the consumers regarding the SLB purchase. Also, with fixed-term contracts, the repurposer can estimate the retired SLB stream that will reach back to them in the future, and recycling facilities can be designed more efficiently based on the certainty in the SLB supply.

Thus, this chapter highlighted the importance of residential energy demand estimation in designing and maintaining PV-based renewable energy solutions. Modeling the load stochasticity was important for the PV+battery systems design. Also, the high peaks during the off-peak prices in home energy storage + EV charging loads can be leveraged to alter the replacement strategies of the SLBs in PV+battery systems. Such changes in the replacement strategies can be beneficial in reducing the carbon footprint of the stationary systems while also benefitting the overall battery recycling supply chain.

Chapter 3 Design and environmental assessment of renewable energy systems for commercial and utility sector

3.1 Background

The commercial sector contributes to 18% of the total U.S. energy demand [135]. Renewable energy solutions like PV and battery systems can reduce this demand and associated cost and environmental impacts [23,24]. However, in addition to the techno-economic and environmental benefits, aesthetic factors like visibility and degree of integration of PV with its surroundings are also becoming an important concern in commercial buildings [25]. An increasing number of studies show that aesthetic and architectural values of renewable energy solutions need to be given importance, especially in commercial spaces and public buildings [25]. Building integrated photovoltaics (BIPVs) is a technology that can produce electricity while preserving the aesthetic and architectural value of the buildings [26]. Previous studies based on expert and non-expert interviews also show that public acceptability of the building integrated PVs is higher than conventional solar modules [136,137]. Due to on-site electricity generation in BIPVs, the transmission losses are also reduced along with the load on the grid [138].

BIPV technologies include opaque, semi-transparent, and transparent photovoltaics that can be used for different parts of building skin [139,140]. Transparent organic photovoltaics (TOPVs) are a special class of BIPVs with high visible transmittance (>60%) and selective absorption of heat or near-infrared (NIR) part of the electromagnetic spectrum [141,142]. TOPVs can be deposited inside the double-paned glass windows and given the desired color to benefit the building in terms of both energy and aesthetics [28,143]. A previous study from our group showed the energy benefits from one type of TOPVs in one type of commercial building [28]. However, the energy benefits from BIPVs can depend on the building's occupancy and characteristics like window-wall ratio and volume [144]. Also, with a change in TOPV donor materials, the energy benefit will change due to a change in the TOPV's NIR absorption, power conversion efficiency, and the required manufacturing energy. Therefore, to bridge this knowledge gap, the energy benefits from TOPVs made from two different donor materials in five types of commercial buildings and four U.S. climates were analyzed. The results provide new insights on whether some buildings are more suitable than others for TOPV applications.

While TOPVs would still be an immature technology for a few years, commercial-based renewable energy solutions need to take advantage of conventional silicon-based PV technology and battery storage. Unlike the residential sector, load leveling generally leads to lesser benefits with PV+battery systems in commercial buildings as their highest load demand and the highest PV generation are both during the daytime. Also, a considerable part of commercial electricity bills can be due to the demand charges levied on commercial buildings by the utilities [31]. Therefore, a building's electricity bill may significantly increase even if they surpass the demand limit for only 15 minutes during a month. PV+battery systems can lead to considerable cost savings in commercial buildings by preventing this peak demand [31]. However, there is little knowledge about the reduction in environmental impacts when the impacts of PV+battery systems are designed to reduce both the energy and demand charges in a commercial building. Thus, we analyzed reduction in the environmental impacts like carbon footprint, photochemical oxidation potential, acidification potential, and abiotic depletion potential when PV+battery systems are used to simultaneously prevent the peak-demand and the reduce overall grid purchase in commercial buildings.

The agriculture sector is another subset of the commercial/industrial sector where the energy demand can be up to 8% of the total energy consumption [145], especially for states like

California, which make up 12.5% of total agricultural production of the U.S. [146]. In the last decade, agriculturally co-located solar PV installations have increased, especially in locations like California [147]. The reason for these increased installations is California's high PV generation potential [148] and net metering scheme that allows the farmers to sell surplus electricity to the grid at the retail price [149].

Although PV installation on agricultural land is possible in the U.S., following land use regulations, such installations can lead to land competition and food-energy-water nexus issues [136,150]. Therefore, a detailed analysis of the current installation practices is required to alleviate the land and food security implications of agriculturally co-locating PVs. Thus, this chapter also deals with energy demand from the agricultural sector by analyzing the energy generated from agriculturally co-located solar PV modules from 2008-2018 in the central valley of California. Further, the energy benefits and the corresponding agricultural land use are compared, and the installation practices of the farmers were analyzed.

Lastly, this chapter moves beyond the behind-the-meter commercial sector demand and focuses on utility-level applications. The output generated from large-scale utility-level PV plants must be stabilized to prevent minutely fluctuations and associated grid instability [151]. Large battery capacities are required for the firming of the PV output from the utility-level plants, which can lead to systems with a high cost and carbon footprint [152]. In this chapter, we explored the capabilities of the second-life Li-ion batteries (SLBs) to firm the output of a utility-level plant. Therefore, the LCOE and carbon footprint of the utility firming was simulated with low-cost SLBs for a 5 MW utility plant across five U.S. climates. The results were compared with the no-firming (baseline) scenario and another scenario where new Li-ion batteries were used for the utility level firming. Essentially, the main goal of this chapter was to analyze how renewable energy systems can reduce the energy and environmental benefits of the commercial and utility sector while satisfying the additional constraints like aesthetics, land use, and cost.

3.2 Methodology

3.2.1 Energy benefits of TOPVs in commercial buildings

The established framework used to calculate the net energy benefit combines building energy simulation, photovoltaic simulation, and LCA (Figure 15(a) and Figure 15(b)) and was previously developed by our group [120]. The system boundary for the LCA is shown in Figure 15(b) and includes TOPV manufacturing and use phase.

The energy consumption for each commercial building was simulated using a double-paned clear glass window baseline and compared with ClAlPc and CyTPFB TOPVs (Figure 15(c)). The building's energy demand (electricity and natural gas), photovoltaic electricity generation, and the TOPV manufacturing energy were combined to get the NEB over time. In addition to the NEB, the EPBT, avoided cost, and avoided GHG emissions were also calculated for two different TOPVs used in the windows of five different commercial buildings in four different climates in the U.S.

The TOPVs were assumed to be deposited inside the glass windows of the commercial buildings. The maximum window size is 2.1 m by 3.7 m, with silver grid covering 11% of the window area [28,153]. The power conversion efficiency practical limit for ClAlPc TOPV was 10%, and 11% for CyTPFB TOPV. The TOPV degrades over time, and its lifetime is expected to be 20 years [154]. The power conversion efficiency degradation was expected to be linear and reached 60% of the original value after 20 years (T_{50}=25 years) [28,155]. The TOPVs consisted of sequentially deposited layers of indium tin oxide (ITO), molybdenum oxide (MoO_3), active layers, bathocuproine (BCP), and ITO, as shown in Figure 15(b). The active layers of the two TOPVs consisted of ClAlPc or CyTPFB with C_{60} (Figure 15(b)). ITO was deposited by sputtering, and all other layers were deposited by vacuum deposition except the CyTPFB active layer, which was deposited using a solution process [140,156]. The thickness of the deposited layers is shown in Figure 15(c). The manufacturing process for the TOPVs was based on previous studies [28,142].

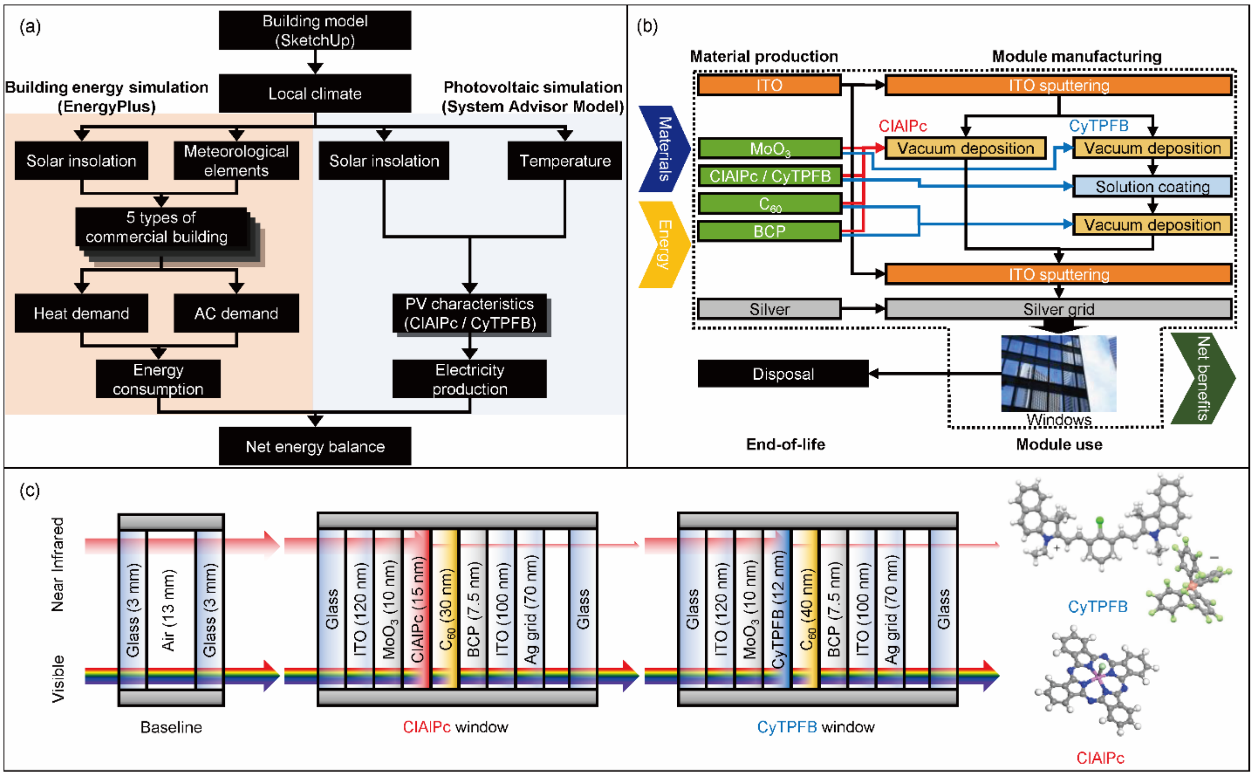

Figure 15. (a) Modeling framework to calculate the net energy benefit using building energy use, photovoltaic generation, and LCA (adapted from [28]). (b) Scope of the LCA for the two types of TOPV materials used in window application and (c) the configuration of the baseline (clear glass), ClAlPc, and CyTPFB TOPVs used in window applications and their chemical structures.

The four locations considered were Detroit (MI), Los Angeles (CA), Phoenix (AZ), and Honolulu (HI) as they represented a broad range of solar insolation, temperature, humidity, and energy mix of the grid. Table 5 summarizes the International Energy Conservation Code (IECC) climate zones [157], electricity eGRID subregions [158], daily average insolation from southern azimuth, and average temperature (1981-2010) for the selected locations [159].

Table 5. Selected locations, their corresponding IECC climate zones, eGRID subregions, daily average insolation (south azimuth, 90°tilt), and average temperature between 1981-2010.

Location	**IECC climate zone** [157]	**eGRID subregion** [158]	**Daily average insolation for south azimuth and 90° tilt (kWh/m^2-day)** [160]	**Average temperature (°C) (1981-2010)** [159]
Detroit, MI	5A	RFCM	2.9	-3.0
Los Angeles, CA	3C	CAMX	3.5	14.0
Phoenix, AZ	2B	AZNM	4.0	14.2
Honolulu, HI	1A	HIOA	2.9	23.1

3.2.1 1 Building energy modeling and electricity generation

The building energy demand was simulated using EnergyPlus 8.9 [161], and the electricity generation was simulated using the System Advisor Model (SAM) [160]. EnergyPlus modeling results have been previously validated using experimental studies conducted on building test cells and research platforms [162,163]. Similarly, previous studies have established the validity of SAM results using experimental data from more than 100 sites [164,165]. Typical meteorological year (TMY 3) weather files from the National Solar Radiation Database (NSRDB) were used to simulate the weather conditions in SAM for each location [166]. The five commercial buildings selected from post-1980 commercial reference building models from the Department of Energy (DoE) are: (1) midrise apartments, (2) medium office, (3) primary school, (4) large hotel, and (5) hospital [167]. The selected buildings had different hourly energy demands because of varied use, structure, and building envelope properties. The structural and thermal envelope properties of the buildings were kept the same as the reference models, and the main entrance of the buildings was assumed to be oriented towards the south. Table 6 summarizes the net conditioned volumes, window areas, window-wall ratios, average weekly occupancy, hourly occupancy schedules, and major heating source of the selected commercial buildings. The net conditioned volume is the volume of building where the temperature and airflow rate are maintained by a heating, ventilation, and air conditioning (HVAC) system. The average weekly occupancy is the average number of occupants per square meter area of building in a typical week. The hourly occupancy schedule is the average of weekly operation hours for each part of the building. The building occupancy schedules and thermal envelope characteristics of the used default DOE commercial buildings are given in appendix B [167].

Table 6. Selected commercial buildings with their net conditioned volumes, window areas in each direction, window-wall ratios (WWR), occupancy, typical operation hours per week and main heating source. The buildings are arranged in increasing order of net conditioned volume from top to bottom.

Building type	**Net conditioned volume (m^3)**	**Windows areas (m^2)**				**WWR (%)**	**Occupancy (Number of people /m^2)**	**Operation hours per week**	**Main heating source**
		N	**E**	**S**	**W**				
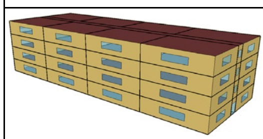 Midrise apartment	9,554	83.2	33.4	83.2	31.2	15	40	163	Natural gas
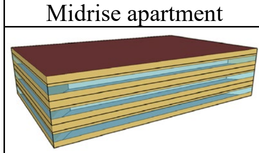 Medium office	13,667	195.8	130.6	195.8	130.6	33	19	98	Electricity
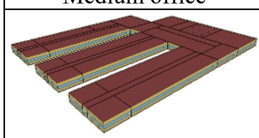 Primary School	27,484	324.8	114.8	324.8	114.8	35	5	62	Natural gas
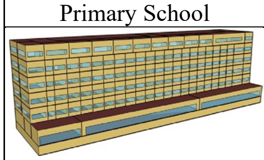 Large Hotel	35,185	432.9	85.8	609.5	85.8	27	8	168	Natural gas
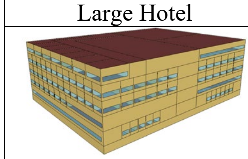 Hospital	88,864	186.2	144.9	220.7	293.7	15	29	160	Natural gas

The spectral properties of the windows were modified in the building models to simulate the building energy saved due to TOPVs in the window applications Figure 16(a) shows the reflectance, transmittance, and absorbance of the incident light by the TOPV film in windows, along with the back reflectance of interior heat from the building. The optical properties of the three types of windows (clear glass, ClAlPc, and CyTPFB) were required to calculate the heat gain/loss in the building simulations. The optical properties of the ClAlPc module are obtained from our previous study (Figure 16(b)) [28]. The front and back optical properties of the CyTPFB module were measured by UV-Vis spectrometer (Figure 16(c)). The corrected front optical properties in Figure 16(c) were calculated based on the methodology from [28] and corresponded to the amount of light that is absorbed and converted to electricity. Corrected front and back optical properties were used for the EnergyPlus simulation. The TOPVs were installed on all four sides of buildings (south, east, west, and north).

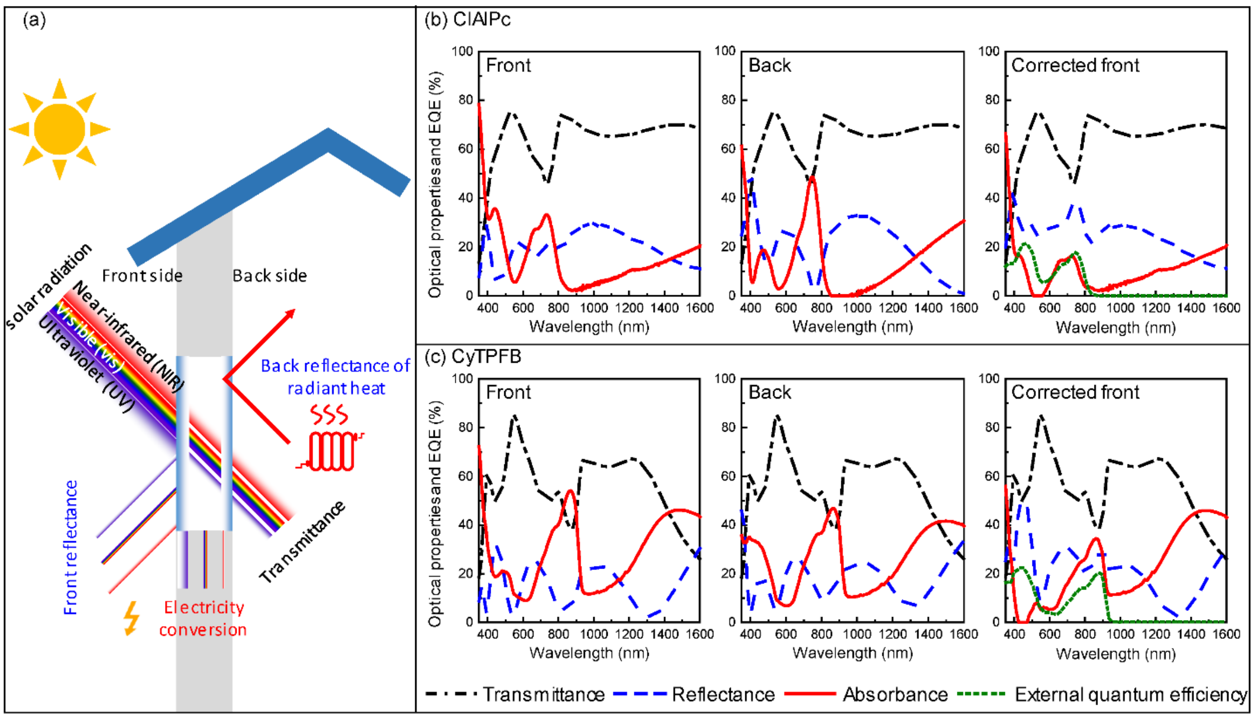

Figure 16. (a) Reflectance, transmittance, and electricity conversion of incident solar radiation on TOPVs incorporated in glass-paned windows (from [28]). The front, back, and corrected front spectral properties for (b) ClAlPc and (c) CyTPFB TOPVs in window applications.

3.2.1 2 Life cycle assessment of TOPV module manufacturing and use

The LCA scope (Figure 16(b)) included material production, module manufacturing, and module use (20 years) but excluded end-of-life. The material and module fabrication for ClAlPc was previously calculated [28]. For CyTPFB, LCA was based on reported synthesis conditions for cyanine heptamethine cation [168], anion [169], and module fabrication [142]. The material deposition efficiency is 30% [170], and the module was assumed to be manufactured in the U.S. The functional unit was *the operation of one commercial building for 20 years*. The changing carbon footprint of the electricity grid over time was taken from [28]. The impact category was CED, which was calculated using the Cumulative Energy Demand Method v 1.09 in SimaPro 8 [112]. The detailed assumptions and upstream processes are summarized in appendix B.

3.2.1 3 Performance metrics

The cumulative energy demand of TOPVs (PV_{CED}) was from the LCA (section 2.2) and combined with saved and generated energy (section 2.1) to calculate the NEB. The saved and generated energy was calculated using the annual PV generation (E_{aPVgen}), avoided electricity consumption (ΔE_{aElec}), and avoided natural gas consumption (ΔE_{aNG}) while accounting for module degradation and changing grid efficiency over the project lifetime (20 years) using Eq. 6 as given by [28].

$$\text{NEB (CED)} = -\ PV_{CED} + \sum \frac{E_{aPVgen}}{\eta_{\text{Grid X}}} \pm \sum \frac{\Delta E_{aElec}}{\eta_{\text{Grid X}}} \pm \sum \frac{\Delta E_{aNG}}{\eta_{NG}} \qquad (6)$$

Here, $\eta_{\text{Grid X}}$ and η_{NG} were the energy conversion efficiency factors to calculate the primary energy requirement for electricity and natural gas production for a given location. An energy conversion efficiency factor of 0.30 for electricity meant that 3.33 MJ of primary energy was required to produce 1 MJ of electricity. $\eta_{\text{Grid X}}$ was calculated for each year and location, based on current and forecasted regional electricity mixes of the respective eGRID subregions, while η_{NG} was assumed to be constant [28,155]. The annual energy conversion efficiency factors used for each location are given in appendix B. The energy payback time (EPBT) represented the time required for the solar panel to produce electricity to compensate for the energy required for its manufacturing. However, TOPVs also saved building energy in addition to electricity production, thus the EPBT was calculated using Eq. (2), using the approach from [28]. The EPBT denoted by $\boldsymbol{t}$ in Equation 7 corresponds to the time when the energy saved or generated by the TOPVs (right-hand side of the equation) becomes equal to the cradle to gate life cycle manufacturing energy for TOPVs (left-hand side of the equation).

$$PV_{CED} = \sum_{1}^{t} \frac{E_{aPVgen}}{\eta_{\mathrm{Grid\ X}}} \pm \sum_{1}^{t} \frac{\Delta E_{aElec}}{\eta_{\mathrm{Grid\ X}}} \pm \sum_{1}^{t} \frac{\Delta E_{aNG}}{\eta_{NG}} \qquad (7)$$

The avoided GHGs were based on the PV generation and the building energy savings and exclude the impact from TOPV manufacturing. The avoided cost is calculated in 2017 dollars and include an annual cost increase of 0.22% per year for electricity and 1.01% for natural gas.

3.2.2 Life cycle assessment of silicon-based PV and Li-ion battery storage in commercial buildings

The following impact categories were considered for behind-the-meter LCA modeling of the four selected commercial buildings in addition to global warming potential or carbon footprint

- **Photochemical oxidation potential (PCOP)**: The photochemical oxidation potential estimates the secondary air pollution, also known as summer smog [171]. It is formed due to the reaction of sunlight in the troposphere with different primary pollutants generated from fossil fuel combustion [172]. The main contributing pollutants to photochemical smog are nitrogen oxides and volatile organic compounds (excluding methane) [173]. Volatile organic compounds include ethane, benzene, ethylene, acetone, etc. Photochemical smog can lead to breathing problems and eye irritations in humans, in addition to the damage to plant and animal life [173,174]. The reference unit for measuring PCOP is kg ethylene (C_2H_4) equivalent.
- **Acidification potential (AP):** The acidification potential evaluates the potential to cause acid rain, e.g., sulfur dioxide (SO_2), nitrogen oxides (NO_x), and reduced nitrogen [175,176]. AP is measured in kg of SO_2 equivalents.

- **Abiotic Depletion Potential (ADP) –** The abiotic depletion potential corresponds to the amount of consumed non-renewable minerals and resources such as copper and iron [175]. In this method, fossil fuels are excluded and abiotic depletion is measured in kg of Antimony (Sb) equivalent [177].

The impacts were calculated using the CML-IA baseline v3.06 method in SimaPro v9.1 software [178]. The inventory data for the manufacturing of Li-ion batteries was taken from [116] and modified for different battery chemistries based on [179]. The life-cycle inventories for all energy generation were from the Ecoinvent 3.6 database [180].

LCA was to calculate the avoided impacts from the grid electricity due to PV + battery systems in behind-the-meter scenarios while considering the manufacturing impacts of PV + battery systems. Four buildings were selected for the LCA of the BTM scenarios: quick-service restaurant, full-service restaurant, supermarket, and hospital. These four buildings were selected because they have a wide range of peak and average electricity demand. LCA of the PV and battery storage system in the buildings for 2020, 2025, and 2030 for electricity rate schedules of both Consumers Energy Electric and DTE Electric with a project lifetime of 25 years. The battery storage in the BTM scenarios was assumed to be Li-ion battery with NMC cathodes. The yearly change in battery chemistry was taken from a 2019 BNEF report [181] and shown in Figure 17.

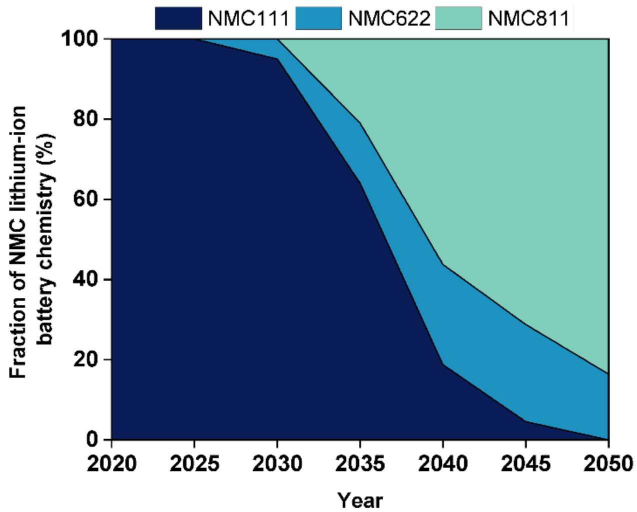

Figure 17. Projected fraction of NMC 111, NMC622 and NMC8111 Li-ion batteries from 2020 to 2050 [1].

The functional unit was the delivery of electricity to meet the demand of behind-the-meter scenarios for 25 years.

3.2.3 Utility-level firming using second-life Lithium-ion batteries

The utility-level PV-firming application considered a 5 MW utility-level PV plant connected to the electric grid. The baseline scenario, denoted as PVF0, consisted of 5 MW of installed PV modules, without energy storage. Energy storage reduce fluctuations in PV generation due to cloud coverage or solar angle and to obtain steady or, in other words, 'firmed' PV output from a PV plant. SLBs or new LIBs were charged when the PV generation was above a preset threshold and discharged when the PV generation fell below the threshold. PVF1 considered the 5 MW PV plant with SLB for firming. PVF1n was a sub-scenario of PVF1 with new lithium-ion batteries (LIBs) instead of SLBs.

The scenarios are illustrated in Figure 18, along with the typical firming operation showing a steady PV output with energy storage. The hourly global horizontal irradiance (GHI) [182] was merged with the 1-second firming duty-cycle (shown in appendix B) from [183] to simulate the fluctuating PV output from a utility-level PV plant. The obtained PV output was converted to a signal with 1-minute averaged interval, since PV firming is characterized by limiting the signal fluctuations in a 1–15 min time interval [183]. The firmed signal was obtained using a 3rd order least squares estimator filter, also known as the Savitzky-Golay filter over a 15-minute moving time window, as proposed in previous literature [184] . Equation 8 represents the general equation used for a Savitzky-Golay filter.

$$(y_k)_s = \frac{\sum_{i=-n}^{n} A_i y_{k+i}}{\sum_{i=-n}^{n} A_i} \tag{8}$$

where A_i is the set of weighted coefficients or convolution integers derived each time from the constituents of the moving window.

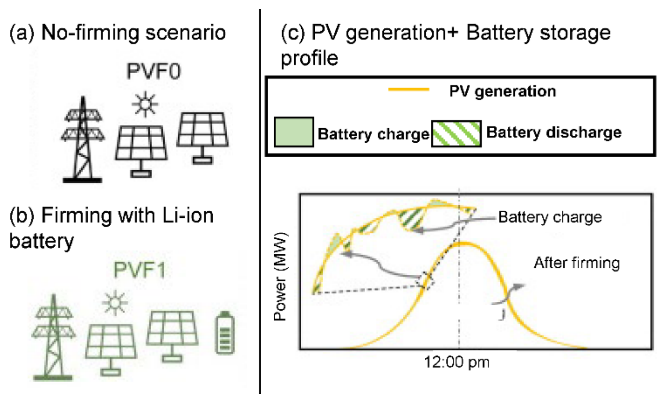

Figure 18. Scenarios (a) without firming, (b) PV firming with Li-ion batteries (both new and SLB) are shown. Also, the PV generation along with battery charge and discharge is shown in (c).

Five locations were selected- Detroit, Los Angeles, New York City, Phoenix, and Portland – due to their diversity in solar radiation, climate, electricity pricing, and electricity grid carbon intensity as shown in the previous sections. The levelized cost of electricity for each location was calculated by minimizing the net present value of system components required to firm the output. Using life-cycle assessment, the carbon emissions for locations were calculated based on a 10-year project lifetime, excluding the first life and transportation of SLBs, and the end-of-life treatment of the system.

3.2.4 Identification and energy benefit analysis of agriculturally co-located PV modules

The PV modules installed in the central valley of California were identified using remote sensed imagery by Jake Stid. Electricity generation was then calculated using the annual commercial installation efficiency data [185] along with weather files from the National Solar Radiation Database [186]. The hourly incident irradiance on fixed and single axis tracker modules was calculated using the *pvlib* python module developed by SANDIA National Laboratory [104]. The maximum rotation for single-axis tracking modules was taken from [187] with PV efficiency degradation from [188]. The soiling loss was taken from [189] while pre-inverter derate losses (DC losses) and inverter efficiency loss (AC losses) were taken from [190]. The energy generation was compared with the energy demand for agricultural purposes in the central valley, California. The comparison was used to analyze the agricultural energy demand that can be offset by the PV generation considering the limited land availability to install PV modules.

3.3 Results and discussion

3.3.1 Net energy benefits, energy payback times, avoided cost and avoided GHGs from TOPVs in commercial buildings[a]

3.3.1 1 Building energy demand and photovoltaic generation

Figure 19(c) shows the difference in the month-by-month heating and cooling energy demand for all the considered buildings and locations, which was dependent on the location's climate (shown in Figure 19(a)) in addition to the building type. The monthly PV electricity generation is shown in Figure 19(b) for each location. For the same building, the energy demand changed with location due to variations in temperature, relative humidity, and solar irradiance. For

[a] Parts of this work has been published as Siddharth Shukla, Eunsang Lee, Richard R. Lunt, Annick Anctil, "Net Energy and cost benefit of phthalocyanine and heptamethine transparent photovoltaics in commercial buildings," Sustainable Energy Technologies and Assessments, Volume 53 part C, 2022, DOI: https://doi.org/10.1016/j.seta.2022.102631

example, the heating demand during winter (December-February) for the large hotel reference building in Detroit was almost seven times the heating demand in Phoenix. However, the cooling demand during summer (June-August) in Detroit was half of the cooling energy demand in Phoenix. The hospital building had the least variation in energy demand with location compared to other buildings. The reason for the lower variation was that the external air needs to be overcooled first (to remove the moisture content) in hospitals and reheated to suit the temperature and humidity requirements of different building sections like patient wings and operating rooms [191]. Therefore, there was a constant heating and cooling energy requirement in hospitals for all types of climatic conditions.

There was considerable variation in energy demand for different buildings in the same climate due to the varied net conditioned volumes, window-wall ratios (WWR), and occupant behaviors, as shown in Table 6. Midrise apartments and medium offices had comparable building energy demands, but the proportion and source of heating energy demand were different, as shown in Figure 19(c). The main heating source for the midrise apartments was natural gas, while it was electricity for the medium office buildings in the selected locations (Figure 19(c)) [167]. Also, due to the different usage hours of the building, the cooling demand was different (Figure 19(c)). For instance, medium offices had a higher cooling energy demand compared to midrise apartments because the offices were generally in operation during the hottest hours of the day.

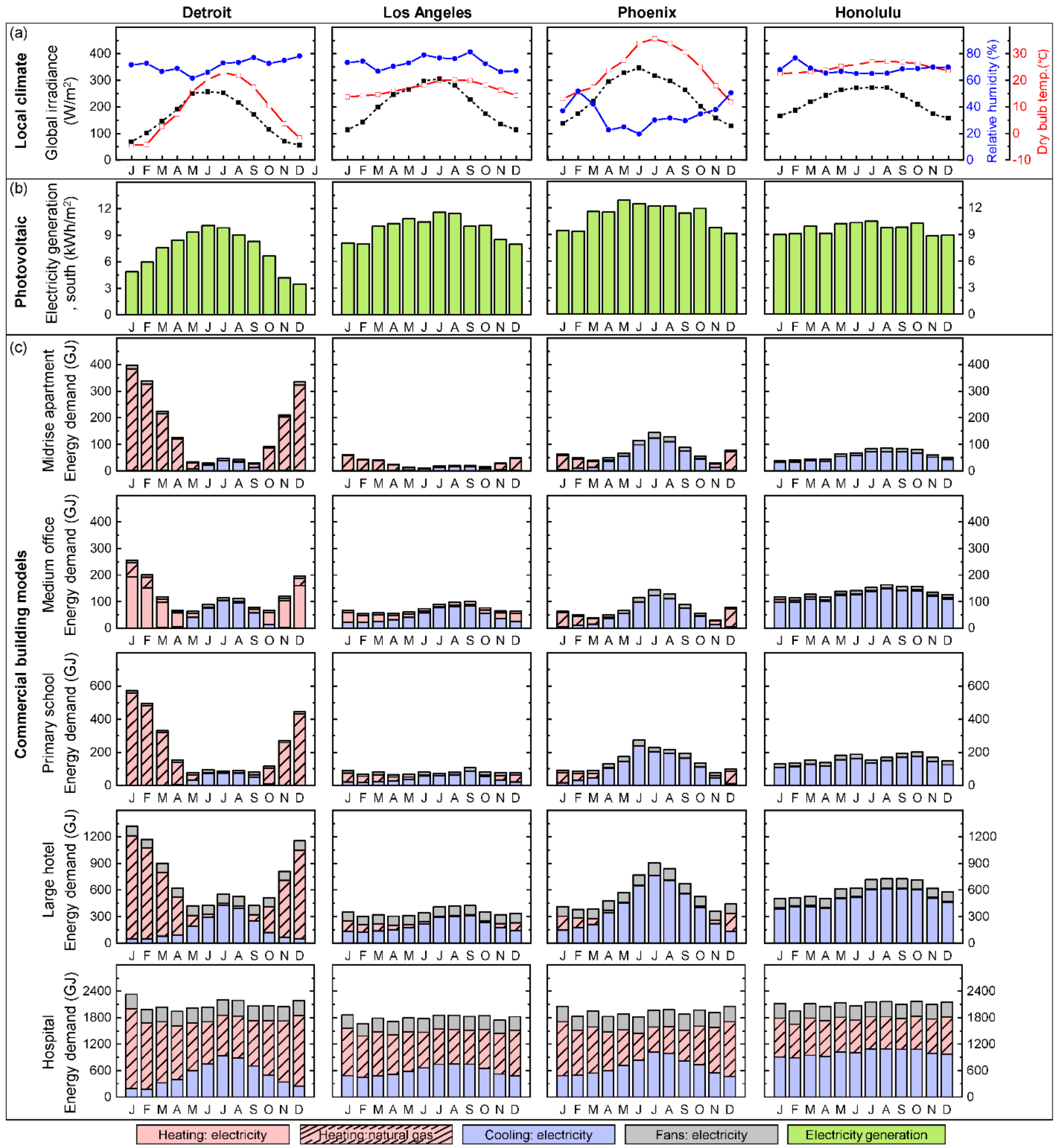

Figure 19. (a) Solar global irradiance, relative humidity, and dry bulb temperature for the four selected locations, with (b) electricity generation from southern azimuth using a typical latitude-tilted photovoltaic module with 20% power conversion efficiency for one year. (c) Month-by-month energy demand in the five commercial buildings for each location broken down into heating and cooling demand components.

3.3.1 2 Life cycle assessment of TOPVs

Figure 20(a) compares the cradle to gate CED of the TOPVs used in this study (ClAlPc and CyTPFB), while Figure 20(b) compares the CED and efficiency of the two TOPVs with other PV technologies. TOPVs' life cycle embodied energy was lower than other types of PV technologies. The cradle to gate CED of CyTPFB was 26.1% higher than ClAlPc (Figure 20(a)). The active layer deposition and ITO (material and deposition), which are unlikely to change in the near future [141], had the highest contribution to CED for both TOPVs. Creating the vacuum condition prior to material deposition was the most energy-intensive stage of small molecules TOPV manufacturing. For CyTPFB, the solution process was preceded and succeeded by vacuum deposition processes (as shown in Figure 15(b)); therefore, the energy required during chamber evacuation was doubled, resulting in a higher CED compared to ClAlPc [170]. Also, the cyanine heptamethine cation was originally paired with an iodide anion (CyI), and the iodide anion was exchanged with TPFB leading to extra energy demand due to material loss [142]. The CED for ClAlPc manufacturing was lower than that of CyI, and the anion exchange further widens the CED gap of active layer materials between the two TOPVs. The CED for the active layer deposition of ClAlPc was 33.4% lower than for CyTPFB (yellow bar in Figure 20(a)). However, Figure 20(b) shows that the CED (MJ/Wp) of both the TOPVs used in this study was lower than other PV technologies (as reviewed in [28]), suggesting that manufacturing TOPV modules was likely to be less energy-intensive compared to other prevalent PV technologies.

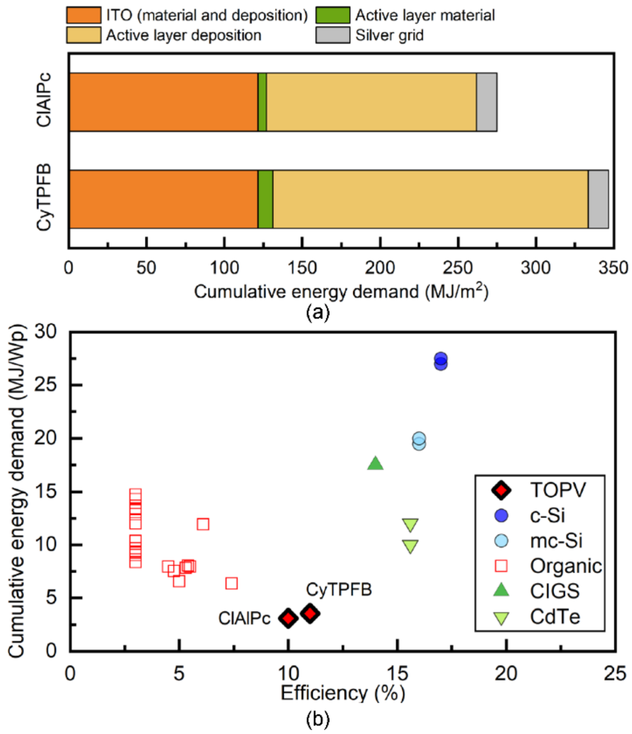

Figure 20. (a) Material and process breakdown of cradle to gate cumulative energy demand (CED) of 1m^2 ClAlPc and CyTPFB TOPVs used in window applications. (b) The CED and practical power conversion efficiency limits of ClAlPc and CyTPFB TOPVs are shown along with other solar technologies (updated from [28]; references given in appendix B).

3.3.1 3 Net energy benefit

The NEB corresponded to the sum of the cradle to gate CED of TOPV manufacturing, electricity generated, and building energy savings and was positive for all cases as shown in Figure 21, meaning that a lot more energy is either saved or produced during the lifetime of the TOPV than used during manufacturing. The PV generation was higher in buildings such as the primary school and medium office due to the large window areas and high window-wall ratios. However, building energy savings were more important in large buildings with small window areas and window-wall ratios, such as a hospital. The heating and cooling energy savings were higher (0.1-10.8%) with ClAlPc than CyTPFB in all the considered scenarios (blue and red bars in Figure 21).

The higher cooling energy savings with ClAlPc TOPVs was because of the lower absorbance of incident heat (short-range NIR), as shown by the corrected front absorbance curve for wavelengths >670 nm in Figure 16(b) and Figure 16(c). ClAlPc TOPVs led to higher conservation of building heat during the winter due to higher back reflectance of longer wavelength NIR from the building interior, as shown by the back reflectance curve for wavelength >900 nm in Figure 16(b) and Figure 16(c)). Therefore, using ClAlPc instead of CyTPFB TOPVs increased energy saving for all the buildings and locations. However, the NEB was higher with CyTPFB (0.4-7.5%) than ClAlPc in 75% of the cases because CyTPFB TOPVs had a higher power conversion efficiency, and the electricity generation contributed more to the NEB in most buildings due to large window areas. The NEB for the medium office (10.23-13.46 TJ) was similar to those obtained in our previous study (10.70 TJ-27.91 TJ) [28]. The slight difference in numbers was due to the higher window-wall ratio in the previous study. The energy consumption for TOPV manufacturing (TOPV manufacturing in Figure 21) was about 0.3-5.5% of total NEB for all cases, which was also comparable to the values from our previous study (1.1-5.0%) [28]. Although, the net energy benefit was a novel metric [28], previous BIPVs studies have shown positive energy benefits using metrics like total electricity savings [192], independence factor [193], and coefficient of performance [29].

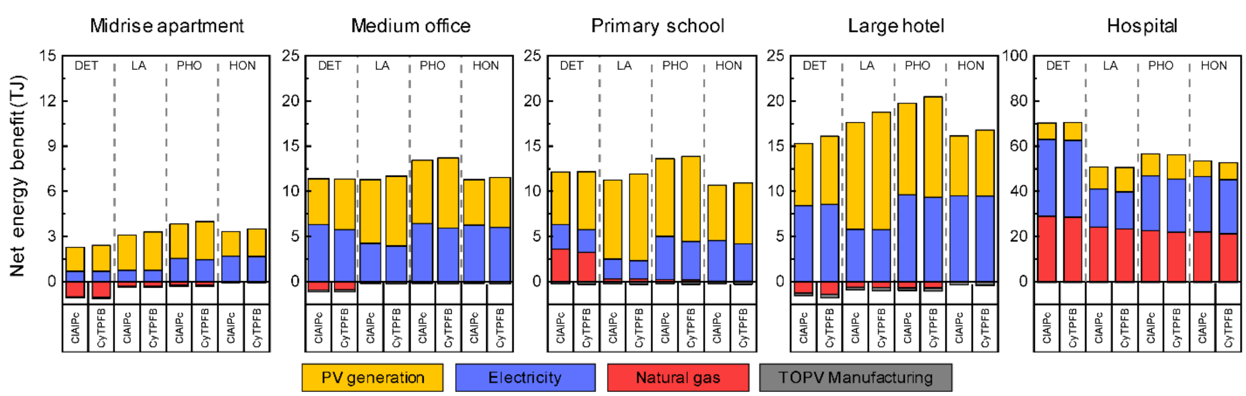

Figure 21. Net cumulative energy benefit for five commercial buildings and four locations (namely Detroit (DET), Los Angeles (LA), Phoenix (PHO), and Honolulu (HON)) using ClAlPc and CyTPFB TOPVs in window applications. The TOPVs in window application are assumed to replace the clear glass windows in all directions (South, East, West, and North).

Figure 22(a) shows the NEB per unit conditioned volume (from smaller to large). The net energy benefit per unit building volume was the highest for the medium office in most locations. However, hospitals had the highest NEB per m^2 of TOPV area in all the locations (Figure 22(b)) because they had higher building energy savings (9-199 times) with a relatively lower difference in window area (4-44%) than other buildings.

The TOPVs in window application reduced the building energy demand in addition to generating electricity as they acted like low emissivity coating [194] that reduced heat transmission in the building during summer and prevented the loss of internal heat during winter. For a building like a hospital, the building energy savings dominated over the PV generation due to the low window area and high building energy demand. PV electricity generation contributed less to net energy benefit in hospitals than in other buildings because the area available for TOPV installation is the least per unit of building volume. However, the prevented heat outflux from the building during winter depended on the building's energy demand, construction, and usage rather than the TOPV area. Essentially, if 1 m^2 of TOPV generated x MJ of energy in a year, a considerably higher amount than x MJ was saved from installing 1 m^2 of TOPV in hospital windows. Therefore, the energy savings component of the TOPVs became more important than electricity generation. ClAlPc had a higher net energy benefit than CyTPFB in most cases for hospitals as ClAlPc led to more savings in cooling energy because of a higher reflectance of incoming short-wavelength NIR (closer to 700 nm) from outside the building, thereby preventing the overheating of building interior during summer. Also, ClAlPc had a higher back reflectance of longer-range NIR (>900 nm), preventing heat loss from building interiors during winter months.

The hospital was different than other buildings because it was divided into separate usage spaces with varying occupancy (appendix B), temperature, and humidity guidelines compared to the other buildings, as explained in section 3.1. Therefore, even with smaller fenestration areas, the TOPVs led to the highest reduction in the building energy demand (especially heating energy demand) in hospitals. The net energy benefit per m^2 of TOPV area was higher in hospitals than in any other building, as shown in Figure 22(b). The choice of TOPVs for window application should consider the building energy saved per area of TOPV in addition to the power conversion efficiency. Among all the cities considered, Phoenix had the highest NEB/m^2 of TOPV area for all buildings (except hospitals) due to a combination of high PV generation and avoided cooling energy demand (Figure 22). However, Detroit was the best location for hospitals as the cooling and heating energy saved/m^2 was more important in hospitals, which was 1-1.2 times higher than other locations.

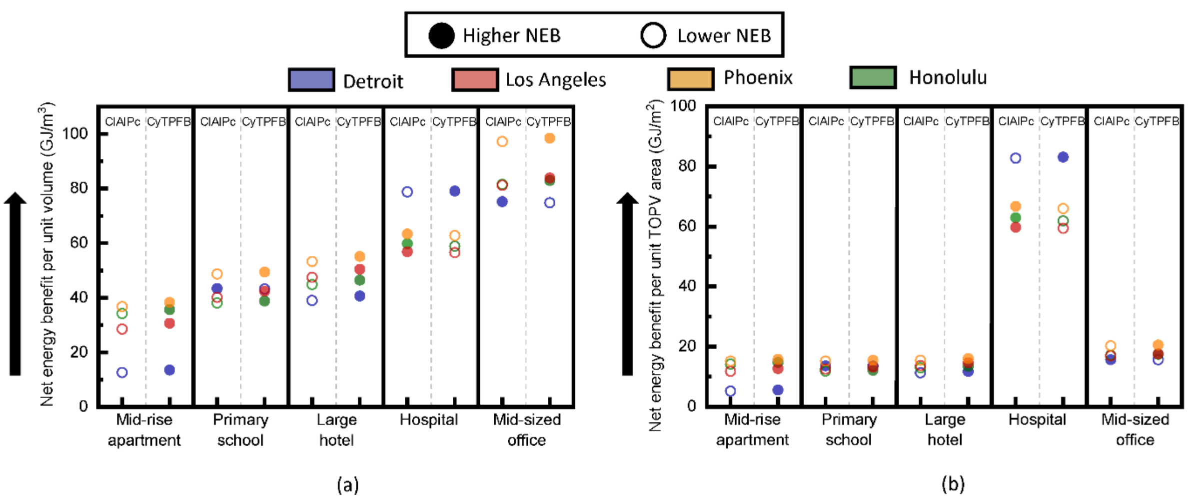

Figure 22. Cumulative net energy benefit for considered buildings and locations with two TOPVs in window applications shown as (a) per unit of building's conditioned volume and (b) per unit of TOPV area. The better option (higher net energy benefit) among the two TOPVs for each building and location is shown with the filled circle.

The analysis did not consider the energy benefits due to the daylighting scheme applications of TOPVs. Previous studies showed that electricity consumption of office buildings can be reduced up to 13% with daylighting applications of semi-transparent BIPVs [195,196].

TOPVs were also expected to show some daylighting scheme benefits but only to a smaller extent than semi-transparent BIPVs, as TOPVs had a higher transmittance of visible light.

3.3.1 4 Energy payback time

Figure 23 shows the energy payback time (EPBT) for all cases. The reason for higher EPBT for CyTPFB was the higher cradle to gate CED compared to ClAlPc as shown in Figure 20(a). The EPBT ranged from 26 to 260 days (0.07-0.71 years) and was smaller than what is reported for silicon-based semi-transparent BIPVs (0.68-16 years) [197–199]. The EPBT range in this study was also lower than other thin-film BIPV technologies like cadmium telluride and copper indium selenide, where EPBT ranged from 1.1-2.8 years [200,201]. Despite the higher materials and energy requirement of the two TOPVs compared to baseline (clear glass), the energy payback times were short as the dual benefit of generating and saving energy from TOPVs (Figure 21) offsets the energy required for the TOPV manufacturing. The payback time was longer in Honolulu (0.10-0.56 years) for most of the buildings because the heating energy savings in Honolulu were lower compared to Detroit, while the PV generation was lower than in Phoenix and Los Angeles. The EPBT was the shortest (0.07-0.12 years) for hospital buildings in all locations due to the high heating and cooling energy savings but lower manufacturing energy for TOPVs due to smaller window areas (Figure 19(b)). For instance, the natural gas savings due to TOPVs in hospitals were 8 to 251 times that of primary school, and the avoided grid electricity in hospitals was two to five times that of primary school, depending on the location. However, the cradle to gate CED of the TOPV installation in hospital was 4% lower than in primary school.

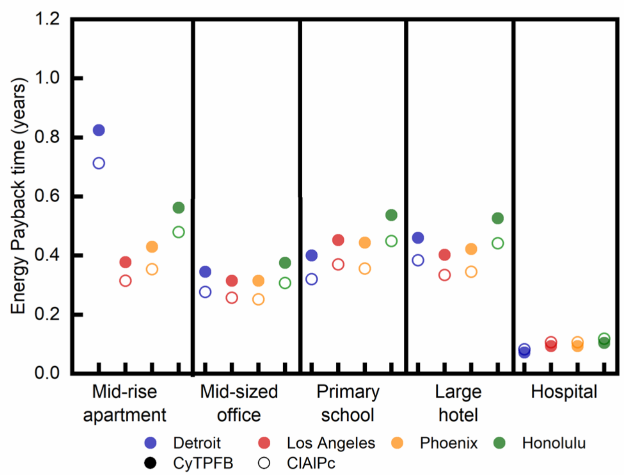

Figure 23. Energy payback time (years) for ClAlPc and CyTPFB TOPVs in window applications for five commercial buildings and four locations over 20 years.

3.3.1 5 Avoided cost and greenhouse gas emissions

The avoided electricity and natural gas consumption in selected buildings and locations due to TOPVs led to avoided cost and greenhouse gas emissions. The electricity and natural gas prices for all the considered locations are given in appendix B. Figure 24 shows the cumulative avoided cost and GHG emissions per unit TOPV area for each building and location over 20 years for CyTPFB TOPVs. The hospital building had the highest cost and carbon footprint savings per unit area of TOPVs in all locations. The highest savings in hospitals was due to the higher net energy benefit (3-58 times) with lower window area (0.8-1.4 times) than other buildings. Figure 24(a) shows that the cumulative avoided costs were higher in locations with higher electricity and natural gas prices, such as Los Angeles and Honolulu.

Detroit had the least PV generation potential of the selected locations (Figure 19(b)), but TOPVs still led to considerable avoided costs because of the high electricity prices. The 20-year cumulative avoided costs in Detroit were 42-101% of the avoided costs in a high PV generation potential location like Phoenix. Figure 24(b) shows that Detroit buildings had high avoided GHG emissions with TOPVs (78-128% of corresponding Phoenix buildings) as Detroit had the highest electricity carbon footprint over 20 years. Therefore, TOPVs can also offset considerable costs and GHG emissions despite the low PV generation potential in locations like Detroit.

The cumulative avoided cost and GHGs in medium office for all locations was about half of what was previously calculated [28] because, in this work, a much smaller window-wall ratio was used in the reference building. Future commercial buildings were likely to have higher window-wall ratios for visual comfort and natural daylighting considerations [199], which will increase the avoided costs and GHGs compared to the values calculated in this study.

The avoided cost/m^2 for most buildings in this study (86.0-603.9 $/$m^2$) was lower than previous studies on cadmium telluride and silicon-based BIPV modules ((575.2-1111.1 $/$m^2$) [202–204]. In previous studies, the higher avoided cost was due to higher power conversion efficiencies, and a longer project life (25 years). However, the avoided cost per area in hospitals with TOPVs was higher (723.8-1816.8 $/$m^2$) due to higher building energy savings. The range of avoided GHG emissions/m^2 was 362.0-1361.6 kgCO_2-eq/m^2 for most buildings and was comparable to previous studies (273-1120 kgCO_2-eq/m^2) [204,205]. However, hospitals had considerably higher GHG savings (3533.1-5736.9 kgCO_2-eq/m^2) due to high building energy savings from TOPVs. Therefore, the high energy savings from TOPVs in buildings like hospitals can lead to higher cost and GHG savings than other prevalent BIPV technologies with higher efficiencies.

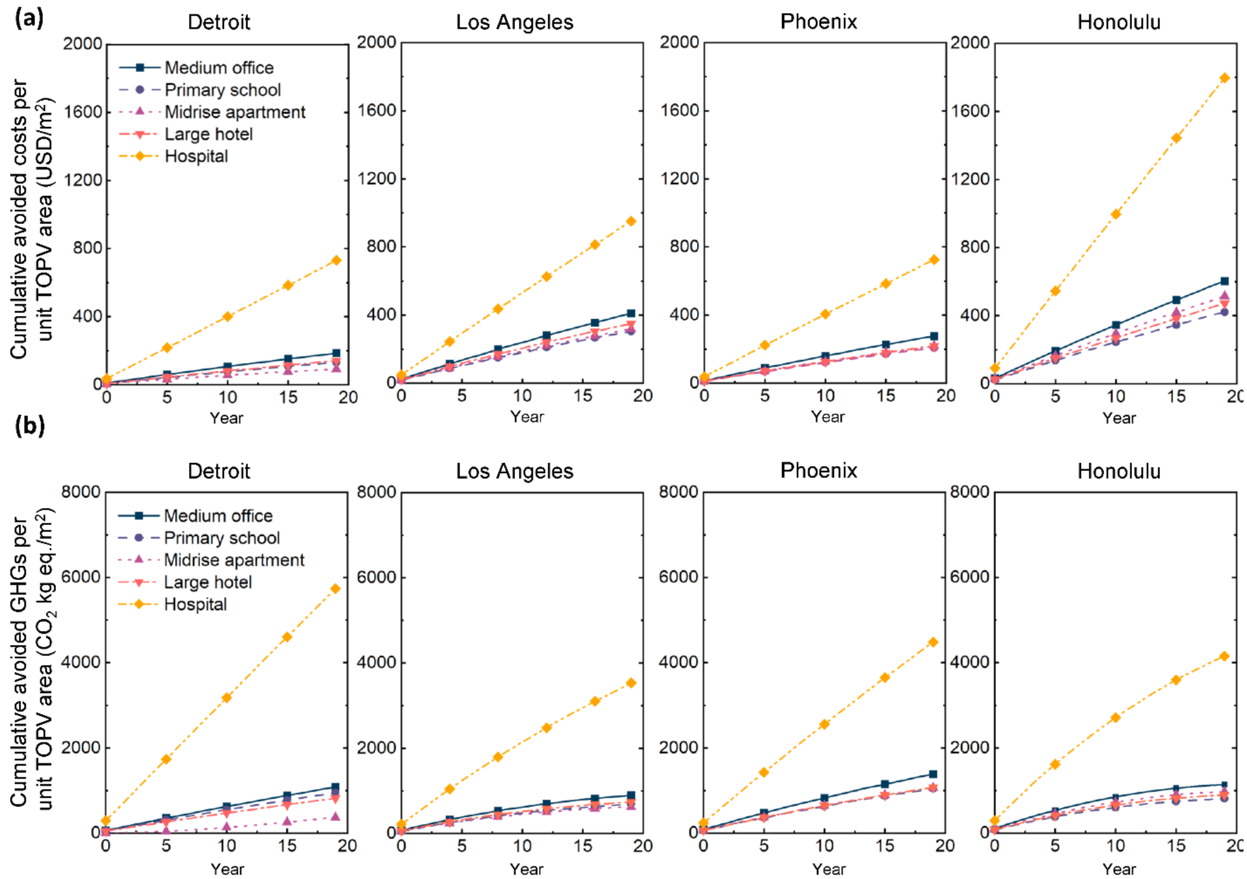

Figure 24. The (a) cumulative avoided cost per unit TOPV area (USD/m^2), and (b) cumulative avoided greenhouse gas (GHG) emissions per unit TOPV area (CO_2 kg eq./m^2) over 20 years in five commercial buildings across four U.S. locations when the clear glass windows are replaced with CyTPFB TOPVs in window application.

The ClAlPc results for each corresponding building and location were within a 2% range of the CyTPFB results, as shown in appendix B. Therefore, even with varying efficiencies and energy savings, both the TOPVs led to similar avoided costs and GHG benefits over 20 years. The cost and GHG emissions of TOPV manufacturing were not included but should be considered in future studies.

3.3.2 Environmental benefits from PV and Li-ion battery storage in commercial buildings[b]

Figure 25 shows the carbon footprint of the electricity was calculated based on the projected energy mix and energy storage goals outlined in [206] after discussion with 5 Lakes Energy team and Michigan Department of Environment, Great Lakes, and Energy. The results showed that the carbon footprint is expected to reduce by 86% by 2050 in Michigan due to considerable increase in Solar PV and wind turbine installations and an energy storage goal of 18,916 MW by 2050.

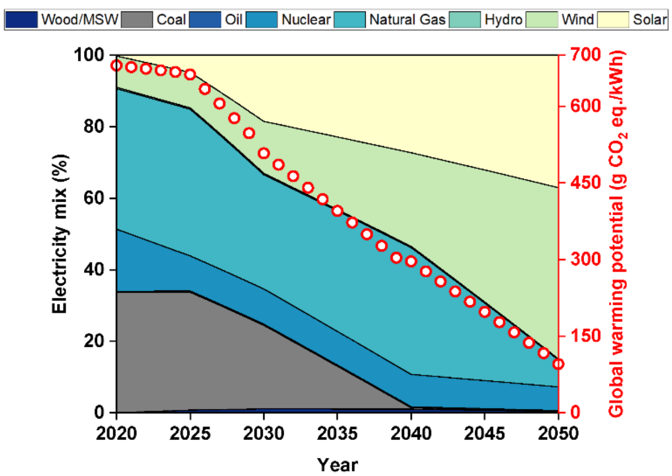

Figure 25. Grid electricity mix over time and global warming potential of electricity generation.

The photochemical oxidation potential (PCOP), acidification potential (AP), and abiotic depletion potential (ADP) corresponding to the planned changes in the grid is shown in Figure 26. Similar to GWP, an 81% reduction in the photochemical oxidation potential and an 87% reduction in the abiotic depletion potential was expected based on Michigan's changing grid by 2050. However, a 528% increase in the abiotic depletion potential was expected due to increased installation of solar PV, wind turbines, and energy storage. These renewable energy solutions and

[b] Parts of this work has been published by Institute for Energy Innovation for the Michigan Department of Environment, Great Lakes, and Energy, "Energy Storage Roadmap for Michigan", Link: https://mieibc.org/reports/iei-releases-energy-storage-roadmap/

energy storage require material inputs like aluminum, lithium, cobalt, silicon and neodymium that exerts a demand on material resources thereby leading to the increased abiotic depletion potential.

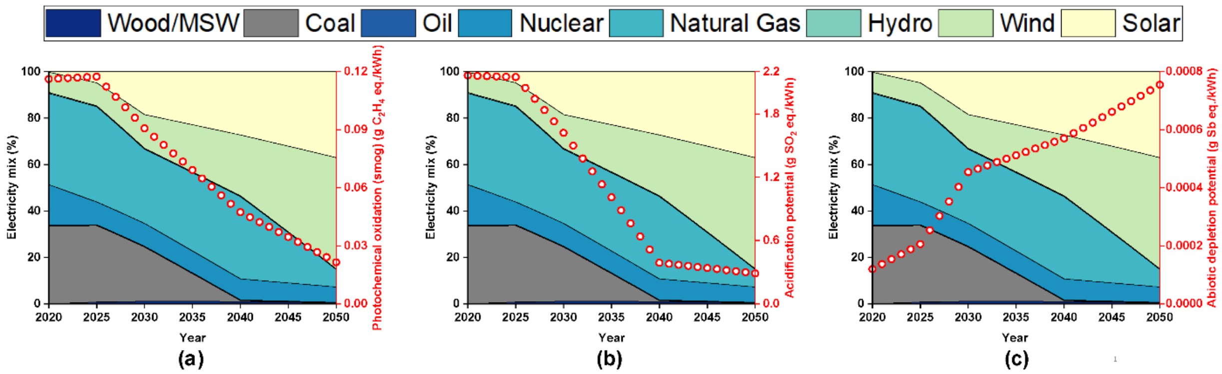

Figure 26. Grid electricity mix over time and associated life cycle impact for (a) photochemical oxidation, (b) acidification potential, and (c) abiotic depletion.

The corresponding reduction in the GWP, PCOP, AP, and ADP with the installation of behind-the-meter (BTM) PV+battery systems were analyzed for four commercial buildings in both Consumers Energy and DTE Energy territories. The selected buildings were quick-service restaurant, full-service restaurant, supermarket, and hospital. These buildings had a wide range of average and peak electricity demand as given in Table 7.

Table 7**.** Average and peak load for quick-service restaurant, full-service restaurant, supermarket, and hospital buildings.

Building	Average load (kW)	Peak load (kW)
Quick service restaurant	22	40
Full-service restaurant	37	71
Supermarket	195	394
Hospital	1063	1553

Additionally, these buildings differ considerably in occupancy per m^2 of floor area, hours of operation per week, and building usage timings. Out of the 16 building types analyzed in the BTM results, these four buildings had the best or second-best net present cost with PV and battery systems for both the utilities in 2020, 2025, and 2030 (apart from the hospital in DTE Energy territory in 2020). The LCA of BTM scenarios depended on the system's (PV, battery, and inverter) capacities as a bigger capacity system would have more upstream environmental impacts, but it would also prevent more purchase of grid electricity, thereby avoiding impacts from the grid. Table 8 lists the PV, inverter, and battery capacities optimized from HOMER grid modeling for the four buildings in the two utility territories in 2020, 2025, and 2030.

Table 8. PV, inverter and battery capacities for PV + battery scenarios for four selected buildings in the two Michigan utilities in 2020, 2025, 2030.

			PV capacity (kW)	Inverter Capacity (kW)	Battery capacity (kWh)	Battery replacements
2020	Consumers Energy	Quick-service restaurant	7.4	0.4	1.0	1
		Full-service restaurant	12.2	0.8	2.0	2
		Supermarket	46.1	14.9	33.0	2
		Hospital	105.0	45.7	95.0	2
	DTE Energy	Quick-service restaurant	4.1	2.6	11.0	2
		Full-service restaurant	8.3	5.0	22.0	2
		Supermarket	23.2	4.7	4.0	2
		Hospital	NA	NA	NA	NA
2025	Consumers Energy	Quick-service restaurant	22.5	2.5	5.0	1
		Full-service restaurant	37.2	6.3	1.0	1
		Supermarket	150	11.8	17.0	4
		Hospital	149	89.0	392.0	2
	DTE Energy	Quick-service restaurant	4.3	3.9	17.0	3
		Full-service restaurant	19.0	9.0	40.0	2
		Supermarket	133.0	12.9	18.0	1
		Hospital	146.0	39.4	65.0	1
2030	Consumers Energy	Quick-service restaurant	22.5	5.6	25.0	2
		Full-service restaurant	37.2	8.7	37.0	2
		Supermarket	150.0	35.2	160.0	2
		Hospital	148.0	139.0	885.0	2
	DTE Energy	Quick-service restaurant	22.2	7.1	33.0	1
		Full-service restaurant	37.2	12.0	53.0	2
		Supermarket	150.0	14.0	28.0	4
		Hospital	149.0	39.4	18.0	4

For each building following two cases are considered in 2020, 2025 and 2030,

a) **Consumers Energy**: PV and battery system installed behind-the meter with Consumers Energy electricity rate schedule.

b) **DTE Energy**: PV and battery system installed behind-the-meter with DTE Energy electricity rate schedule.

The environmental impacts of the above two cases were compared with the impacts of the baseline scenario, i.e., when no PV or battery systems were installed in the selected buildings.

The reduction in the GWP compared to the baseline with the installation of PV + Battery systems in the four selected buildings is given in Figure 27, showing that the GWP always reduced compared to baseline with the installation of PV + Battery systems regardless of the reference year, building type or utility. GWP percentage reduction for quick-service restaurant, full-service restaurant, and supermarket with PV+battery systems ranged between 2-4% in 2020, 7-12% in 2025, and 4-11% in 2030 for Consumers Energy territory. However, for the corresponding three buildings in the DTE Energy territory, the GWP reduction ranged between 2-3% in 2020, 1-8% in 2025, and 5-10% in 2030. Therefore, the GWP benefits in all buildings increased with project reference year as higher capacity PV + battery systems were installed in 2025 and 2030 than in 2020 (as shown in Table 8). Also, the Consumers Energy location had marginally higher GWP benefits with PV+battery systems compared to the DTE Energy location in most cases for quick-service restaurant, full-service restaurant, and supermarket. The higher GWP reduction in Consumers Energy territory was because of the higher optimized system capacities than DTE Energy territory, as shown in Table 8.

The reduction in GWP with PV + battery systems was less than 2% compared to the baseline for hospitals in any year or utility due to the PV capacity limit considered in this study. The upper limit of PV capacity in behind-the-meter scenarios was taken as 150 kW based on Public

Act 342 of 2016 [207]. Therefore, a 150 kW PV capacity could not avoid considerable grid purchases in the hospital buildings due to the high load requirements (as shown in Table 1 in the earlier sections), thus leading to minimal GWP impact reduction in hospitals among the four buildings.

Also, DTE Energy locations had more reduction in GWP with PV+battery systems than Consumers Energy locations for hospitals in 2025 and 2030 and supermarket in 2030. In these three cases, the PV capacity was optimized to the upper limit of 150 kW with a higher inverter and battery capacity in the Consumers Energy territory. Therefore, a higher inverter and battery capacity increased the system's GWP impacts, but the GWP due to avoided electricity purchases could not be reduced considerably because of the limited PV capacity leading to a higher overall GWP in Consumers Energy locations.

The percentage GWP reduction among the two utilities differed more (2-11%) in 2020 and 2025 and considerably lesser (about 1%) in 2030. This progressively narrowing difference between the GWP benefits in the two utilities was because of the similar capacities of the PV systems in 2030 in both utilities due to the declining cost of PV and Battery systems and increasing cost of electricity by 2030.

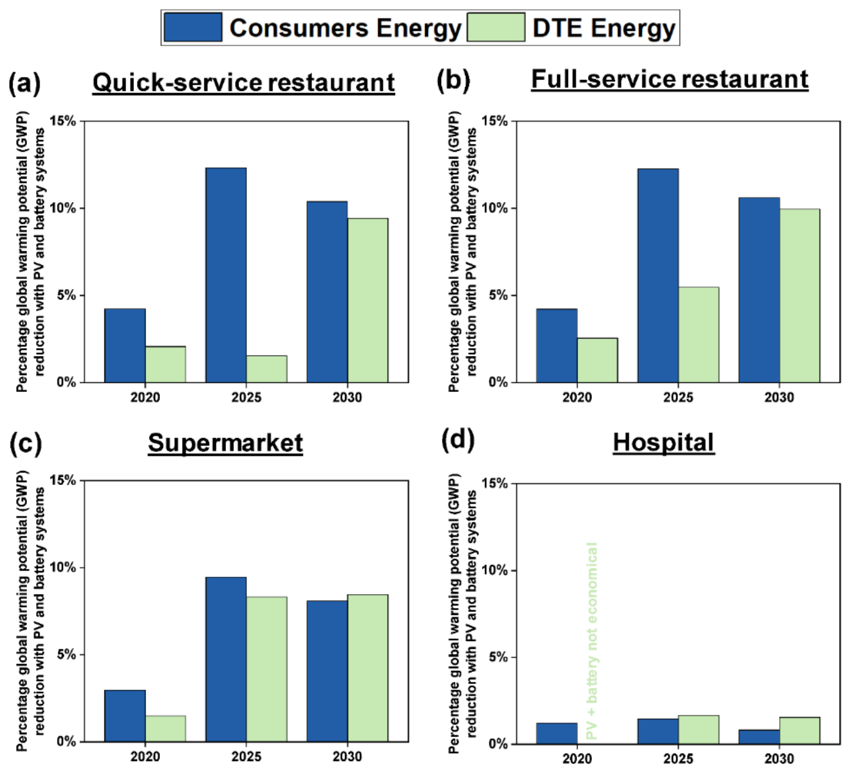

Figure 27. Percentage reduction in global warming potential (GWP) compared to baseline (no PV or battery) when PV + battery systems were installed in the quick-service restaurant, full-service restaurant, supermarket, and hospital in Consumers Energy and DTE Energy territories in 2020, 2025 and 2030.

The PCOP, AP, and ADP impacts of the quick-service restaurant and full-service restaurant are given in Figure 28, showing that the PV + battery storage reduced PCOP, and AP impacts compared to baseline in both the utility territories for all reference years. The PV and Battery systems reduced the PCOP and AP impacts in the range of 2-4% in 2020, 1-11% in 2025, and 5-8% in 2030 for quick-service restaurant and full-service restaurant in both the utilities. The reduction in PCOP and AP impacts with PV + battery systems was marginally higher (up to 9%) in Consumers Energy locations than DTE Energy locations in 2020 and 2025 due to higher system capacities. However, the PCOP and AP benefits were similar in both the utilities by 2030 due to similar optimized system capacities.

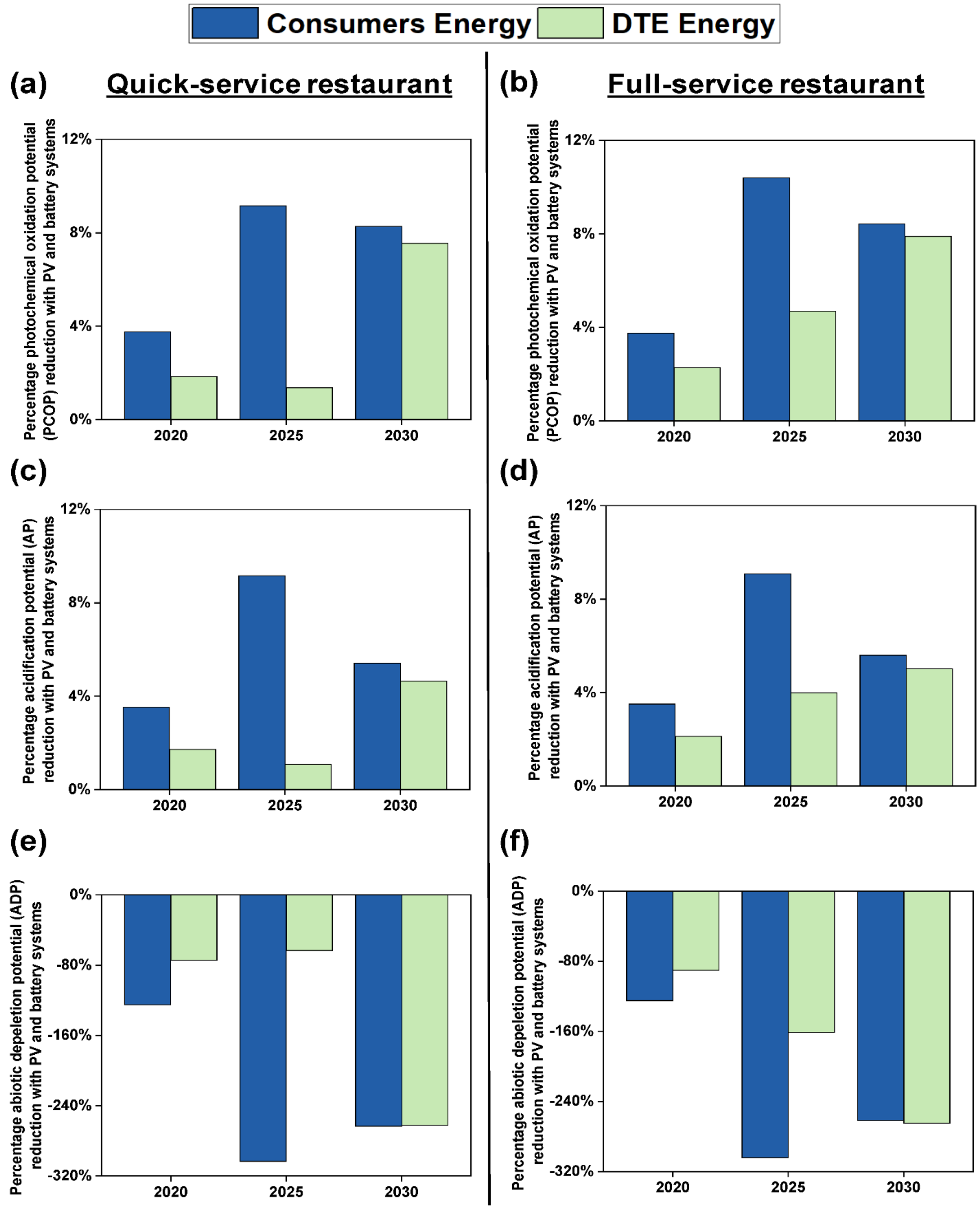

Figure 28. Percentage reduction in photochemical oxidation potential (PCOP) ((a) and (b)), acidification potential (AP) ((c) and (d)), and abiotic depletion potential (ADP) ((e) and(f)) compared to baseline (no PV or battery) when PV + battery systems were installed in the quick-service restaurant and full-service restaurant in Consumers Energy and DTE Energy territories in the years 2020, 2025 and 2030.

Figure 29 presents the percentage reduction in PCOP, AP, and ADP impacts compared to baseline with PV + Battery systems in supermarkets and hospitals, showing that the PV + battery systems reduced the PCOP and AP impacts in both the buildings for all cases. Installing PV and Battery systems reduced the PCOP and AP impacts in the range of 1-3% in 2020, 6-8% in 2025, and 5-7% in 2030 for supermarkets in both the utilities. Similar to Figure 28, the impact reduction was higher in the Consumers Energy locations compared to DTE energy locations due to higher system capacities in 2020 and 2025. Both the utilities had similar PCOP and AP reduction with PV + Battery systems by the reference year 2030 due to similar system capacities. The PCOP and AP reductions in hospitals were less than 1% with installing PV + Battery systems as the PV capacity is restricted to 150 kW.

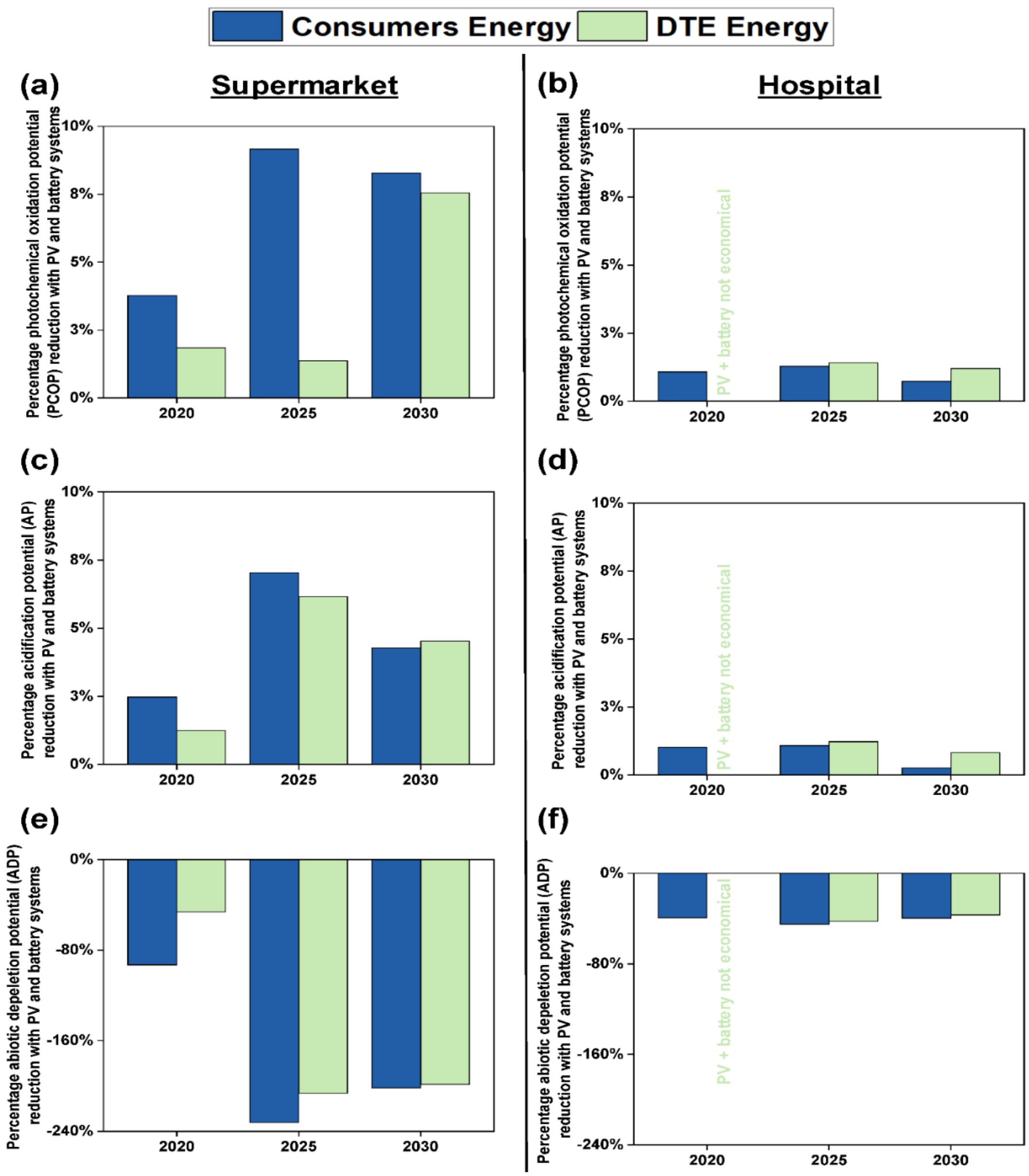

Figure 29. Percentage reduction in photochemical oxidation potential (PCOP) ((a) and (b)) , acidification potential (AP) ((c) and (d)), and abiotic depletion potential (ADP) ((e) and(f)) compared to baseline (no PV or battery) when PV + battery systems were installed in the supermarket and hospitals in Consumers Energy and DTE Energy territories in the years 2020, 2025 and 2030.

Figure 28 and Figure 29 show that all four buildings had an increase in the abiotic depletion potential (0.4-3 times) compared to the baseline due to the addition of PV and battery storage systems because non-renewable resources were required to build these systems. In addition, the abiotic depletion potential of the grid electricity also increased by 46% from 2020 to 2030 because a higher percentage of electricity will come from solar and wind in 2030. However, the abiotic depletion of fossil fuels (not covered in this work) is likely to reduce with PV + Battery systems as these systems avoid grid purchase of electricity, that is expected to be considerably reliant on coal, oil, and natural gas till 2035.

3.3.3 Cost and carbon footprint assessment of utility-level firming applications using second-life batteries[c]

PV firming with energy storage is used to reduce the fluctuations in PV generation. Implementation of PV firming with both SLBs and new Li-ion batteries increased the electricity production in all five locations as shown in the detailed results in appendix B. Production in Phoenix increased the most (~ 18%), whereas it only increased by 8% in Los Angeles. Figure 30 shows the LCOE and life-cycle GWP for utility level firming applications for all considered scenarios in the five selected locations. The results indicate that the LCOE and GWP increased, even though the electricity generation increased with firmed PV output when batteries were used. The LCOE of the baseline was comparable with the results of a previous study on PV firming [208].

[c] Parts of this work has been published as Dipti Kamath, Siddharth Shukla, Renata Arsenault, Hyung Chul Kim Annick Anctil, "Evaluating the cost and carbon footprint of second-life electric vehicle batteries in residential and utility-level applications,", Waste Management , Volume 113, 2020, DOI: https://doi.org/10.1016/j.wasman.2020.05.034

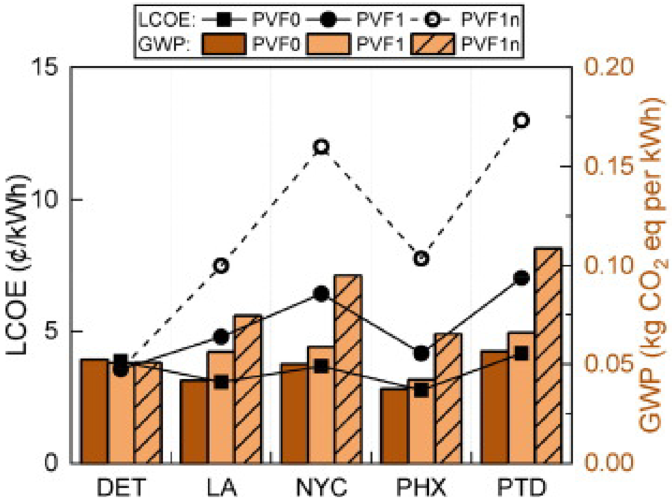

Figure 30. Levelized cost of electricity (LCOE) and the Global warming potential (GWP) for a 5 MW utility-level PV plant over 10 years with new Li-ion batteries (PVF1n) and second-life Li-ion batteries (PVF1). The LCOE and GWP for the corresponding baseline scenario or no-firming scenario is also shown (PVF0).

The LCOE and GWP values were lowered with SLBs compared to new Li-ion batteries in the majority of the locations. The maximum LCOE reduction by adding SLBs compared to new batteries was in Phoenix (46%), with no change in Detroit. The LCOE change depended on the minute-by-minute fluctuation of solar insolation for each location – higher change with higher fluctuation like in New York City and Portland. Using SLBs instead of new batteries reduced the GWP the most in Portland (39%) and the least in Detroit (0.4%). This difference was due to the required battery capacity for PV firming, the changes in the grid electricity needed, and the grid carbon intensity at each location. The detailed results of the utility-level PV firming are provided in appendix B.

3.3.4 Energy benefits from agriculturally co-located PV modules[d]

Figure 31 shows the total installed capacity of the agriculturally co-located PV modules identified in this work. The cumulative capacity of the identified arrays was 3.55 GW. The cumulative generation of all identified arrays through 2018 was 32,656 GWh, 7039 GWh of which was generated in 2018 alone. The average annual electricity generation for single-axis tracking arrays in 2018 was 16.88 GWh per array and for fixed-axis arrays was 1.44 GWh per array.

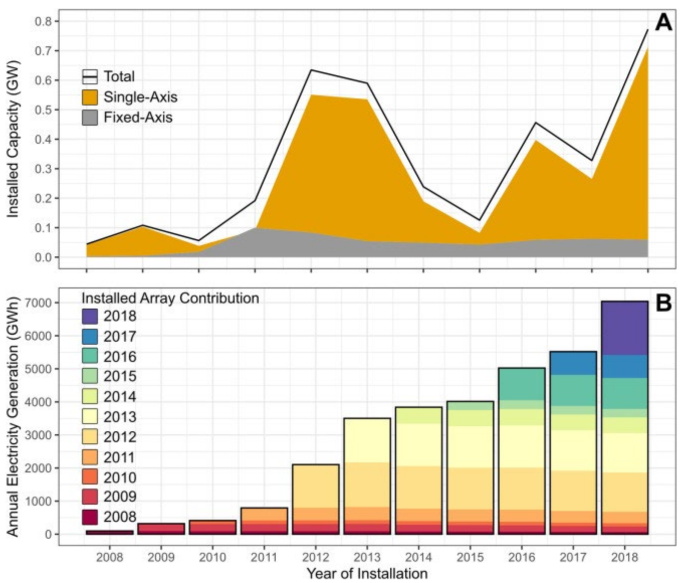

Figure 31. (A) Total installed capacity and (B) modeled annual generation of the remotely sensed arrays in the central valley, California. The values of annual generation represent the contribution of arrays installed in the respective installation year. Colors in (B) delineate the relative contribution of arrays installed in respective years to total annual generation.

The California Energy Statistics and Data portal reported that as of 2018, 731 PV arrays were connected to the grid in all of California accounting for 10.64 GW of capacity and a generation of 24,981 GWh or 12.8% of California's in-state generation in the same year. Note that this excludes the solar thermal arrays (1.2 GW and 2545 GWh reported in 2018) which were not

[d] Parts of this work has been published as Jacob T. Stid, Siddharth Shukla, Annick Anctil, Anthony D. Kendall, Jeremy Rapp, David W. Hyndman, "Solar array placement, electricity generation, and cropland displacement across California's Central Valley," Science of The Total Environment, Volume 835, 2022, DOI: https://doi.org/10.1016/j.scitotenv.2022.155240

the focus of this study because they are primarily located in the Mojave Desert outside of the Central Valley and thus are likely not co-located with agriculture. Therefore, the 7039 GWh and the 3.55 GW from the 1006 identified Central Valley arrays accounted for 28.2% of reported 2018 solar electricity generation and 33.4% of reported solar capacity respectively, and 4% of California's total in-state electricity production in 2018 [209].

Module degradation was primarily responsible for the decreasing trend in electricity generation (Figure 31) in each year's respective contribution to total generation. Annual changes in local solar irradiance included in the generation model, such as the regional drought in 2013 which led to higher solar irradiance, also impacted the annual value. Note that 2013 and 2016 were years of high irradiance, which explains the installed generation increases of all arrays present in those years.

The annual installed capacity peaked in 2012, 2016, and 2018 for single-axis tracking arrays, and 2011 for fixed-axis arrays (Figure 31a). The Federal Emergency Economic Stabilization Act of 2008 [210] included an eight-year extension on the Solar ITC and eliminated the monetary cap of the credit [211]. However, a stipulation to be eligible for the ITC was that projects had to be in service no later than four calendar years after the year in which construction began. It is likely that applications for the credit are concentrated at the end and beginning of each renewal in case the credit is not renewed. Therefore, if there was a surge in applications for the credit and "construction commencement" in the year of the original extension (2008), then the surge in the number of observed installations in 2012 and 2016 was likely indicative of this four-year ITC eligibility requirement repeating itself, and the potential expiration of the extension in 2016. In addition, the ITC has been set to expire every four years since 2016 pending the Congressionally decided extension of the program. The ITC extension along with the end of the four-year construction period requirement (since 2016) would suggest that another peak in the number of solar installations occurred in 2020. Peak installations in 2016 was perhaps also related to the California Public Utilities Commission (CPUC) adoption of the current Net Energy Metering (NEM) 2.0 program early in 2016. The program provides full retail rate credit for overproduced energy exported to the grid [212] and is available to customers in the major utility service providers in the Central Valley (PG&E, SCE, and SDG&E).

It is important to note, however, that the most recent ITC extension projects have decreasing tax incentives over the next four years. A tax credit of 26% will be applied to projects starting construction from 2020 through 2022, 22% through 2023, and 10% from 2024 through 2025.The decreasing credit incentives could drive up early installations over the next four years, with potentially fewer installations at the end of the extension period unless the program incentives change. However, this is also dependent on energy prices (typically increasing), other incentives, and changes in the cost to install solar.

The temporal analysis of mount technologies shows that fixed-axis array installations vastly outnumber single-axis tracking installations over the last decade but tend to be smaller (Figure 31a). Despite the lower proportion of installations, single-axis tracking arrays contributed 82% of co-located installed capacity over the study period. This was mostly due to the median size of co-located single-axis tracking arrays (1.20 MW and 2.1 ha) which was almost four times the median size of fixed-axis arrays (0.34 MW and 0.4 ha). This was likely related to much lower initial cost, ease of installation, and low operation and maintenance costs for fixed-axis arrays ($0.58/kW additional installation and hardware costs and $7.00/kW/year additional O&M costs; [213]). Thus, farmers who are installing smaller capacity arrays are more likely to install fixed-axis arrays. This may also suggest a difference in the installation purpose between the two mount technologies born out of cost and convenience.

California's annual irrigation demand is 10, 159.9 GWh/year [214], a majority of which is from the central valley. Thus, agriculturally co-located solar modules installed in the central valley could satisfy ~69% of the Californian irrigation demand. For fixed-axis modules, the average area of the module was 1% of the agricultural field. Similarly, for the single-axis tracker modules, the average area of the modules was 10% of the agricultural field area. Therefore, the solar modules can reduce a considerable portion of irrigation energy despite occupying disproportionately lower land area. However, this work also showed that current installation practices of agriculturally co-located solar modules are significantly sub-optimal in terms of spacing and spatial field placement of the arrays [215].

The PV generation in this study was calculated using the PVLIB module developed by SANDIA national laboratory [104]. Although PVLIB has been validated through field tests [216], PV generation results have uncertainty because weather files from the nearest weather station were used rather than from the site of the installed PV modules. Similarly, a uniform 20% surface albedo value throughout the central valley and an isotropic irradiance model were assumed to simplify the analysis, possibly leading to uncertainty in the PV generation. Also, for simplicity, the efficiency of all modules installed in a particular year was taken the same based on the median PV efficiency value in that year as given in [217].

3.4 Conclusions

Novel technologies like TOPVs led to net energy benefits in all the commercial buildings and climates despite TOPVs' low power conversion efficiencies. TOPVs can circumnavigate the aesthetic issues with conventional silicon-based PV modules as they are transparent and can be manufactured to have desired color tint. Although the efficiencies of such modules are still significantly low compared to the silicon-based modules, they can be installed on otherwise passive parts of the building skin like windows and facades, providing more installation area. Additionally, the spectral properties of the TOPVs can be tailored corresponding to the type of the building to increase the cooling and heating energy savings. Thus, buildings with smaller window areas like a hospital can also have energy, cost, and carbon footprint benefit from TOPVs.

More and more commercial and public buildings are moving towards the concept of green buildings and zero-net-energy buildings throughout the world. Thus, renewable energy solutions that can preserve the aesthetic value of these buildings are likely to have higher public acceptance in the future. Therefore, TOPVs can be a key technology in reducing the commercial sector's energy demand while preserving the aesthetic and architectural value of the buildings.

Despite their high energy benefits, novel technologies like TOPVs are still at an immature stage and might take a couple of years before an average commercial building owner can install them. Until then, conventional silicon-based modules can still be used to provide considerable cost and environmental benefits in commercial buildings. Unlike residential buildings, the benefits from load leveling can be lesser in commercial buildings as highest demand from commercial buildings is during the daytime. However, buildings with daytime demand peaks like restaurants and supermarkets can benefit if peak demand reduction is primary goal of the Li-ion batteries, thereby saving cost and reducing the environmental impacts of the systems. The peak demand reduction in commercial buildings further highlights the importance of load patterns in the design of renewable energy systems. Thus, a reliable hourly estimate of load data is required to design renewable energy systems to exploit the different parts of the load behavior like peak timing and intensity.

In addition to reducing peak demand in commercial buildings, Li-ion batteries successfully provide services like utility level-frequency regulation. Although, due to the high battery capacities required for such applications, there can be considerable cost and carbon footprint investment in such projects. SLBs can save the cost and carbon footprint associated with such applications while simultaneously prolonging the life of the batteries before they get recycled.

Solar PV-based solutions can also offset considerable energy required from irrigation with disproportionately lesser land requirement for the agriculture sector especially in sunny locations like California. However, better design of such systems, like the presence of trackers, spatial placement, and inter-array spacing, is possible only with a reasonably correct estimate of the energy required patterns on the farms.

Essentially, an array of technologies exists within the broad spectrum of PV-based renewable energy solutions to serve the commercial loads. Each of these solutions can be tailored in terms of materials and design to serve the load and reduce the corresponding environmental impacts appropriately. Thus, this chapter highlights the importance of load determination in selecting the appropriate PV-based solution for commercial loads.

Chapter 4 Feasibility of renewable energy systems to decarbonize transportation sector

4.1 Background

The global temperature is expected to rise by 1.5° C in the next two decades based on the latest IPCC sixth assessment report [3]. The same report states that the global temperature can rise to 4.4° C by the end of this century, leading to a 46-74 cm rise in the sea levels if measures are not taken to reduce the anthropogenic greenhouse gas emissions. One-fifth of the global carbon dioxide emissions come from the transportation sector, with road travel accounting for one-third of total transportation emissions [218]. Similarly, 29 % of the total greenhouse gas emissions in the U.S. come from transportation, and a majority of it is from passenger cars, medium and heavy-duty trucks, including sports utility vehicles, pickup trucks, and minivans [32]. The vehicle miles traveled per year are expected to increase at 0.7% per year till 2049 [33]; therefore, switching the fuel at a massive scale is one of the ways to reduce the greenhouse emissions.

Electrification of vehicle fleet can be one of the ways to reduce the emissions from the transportation sector as suggested by recent scientific and market reports [34,35]. The growth and public acceptance of electric vehicles in the past decade has also shown promising trends, which indicates that electrification can be a viable way to reduce the carbon dioxide emissions from the vehicle fleet [219]. Another way to reduce life-cycle carbon emissions from vehicles is using the fuels made from carbon dioxide captured from ambient air via physical or chemical methods [36]. The resultant carbon dioxide is combined with hydrogen to make conventional hydrocarbon fuels (also known as “e-fuels”) such as diesel and gasoline for vehicles [37]. The e-fuels are advantageous because they can be used without making considerable changes in the vehicle technology or refueling infrastructure [220]. However until recently, e-fuels were considered energy-intensive due to the low efficiency of the involved processes leading to high costs [221]. In future, the increased installation of renewable energy technologies like solar photovoltaic (PV) and wind turbines is expected to solve the issue of the high embodied energy and cost for e-fuels [38]. Thus, making a radical shift to more sustainable fuels for light-duty vehicle fleet is becoming economical at a rapid pace.

The electricity required for both BEV and e-fuels need to come from renewable energy resources like solar PV or wind turbines to reduce the associated CO_2 emissions [38]. Therefore, considerable resources might be required to set up and maintain these renewable energy systems. International and national agencies worldwide have published multiple reports and scientific literature to estimate the required solar PV and wind energy capacity along with the associated land use and materials to achieve various sustainability goals. For instance, an International Energy Agency (IEA) report states that an additional 630 GW of solar PV and 350 GW of wind energy capacity will be required globally to decarbonize the electricity grid by 2050 [222]. Watari et. al, 2019[223] states that total material requirements for solar and wind energy can increase by 200-900% in the electricity sector and 350-700% in the transportation sector based on the scenarios developed by IEA's report [223]. Also, a report from the European commission's Joint Research Center shows a significant increase required in critical and non-critical materials to decarbonize the carbon intensity of the electric grid [224]. However, most of these studies focus on the energy sector, and there is a need for a study that can focus on the material and land-use implications of reducing the greenhouse gas emissions from the transportation sector.

A few studies have focused on the ways to prevent a 2° C rise in temperature by 2050 by preventing carbon footprint from light duty vehicle fleet. Zhu et al., 2021[225], focused on vehicle parameters and electricity decarbonization pathways to prevent the >2° C rise in global temperature. While Milovanoff et al., 2020[226] calculated the energy required by light duty vehicle fleet in the U.S. to prevent >2° C rise in global temperature based on different shared socio-economic pathways. However, none of these studies addressed the land use and material requirement for the accompanying renewable energy systems to power the future light duty vehicle fleet.

In this chapter, the energy required for battery electric vehicles and e-fuels to prevent >2° C global temperature rise by 2050 was estimated from Milovanoff et al., 2020 [226]. Subsequently, the land use and material requirements including aluminum, copper, silicon, neodymium, dysprosium, and praseodymium was calculated to meet this estimated energy demand by 2050.

4.2 Methodology

4.2.1 Energy requirement by 2050

The energy required to prevent a 2° C global temperature rise by 2050 using either BEVs or E-fuels for light-duty vehicles (LDV) was taken from Milovanoff et al., 2020 [226]. Milovanoff et al., 2020 [226] estimated the number of US light-duty vehicle fleet consistent with preventing 2°C temperature rise for different future shared socio-economic pathways (SSPs). For each SSP, the carbon emission was calculated for business-as-usual and vehicle electrification scenarios (EV30@30 campaign[227]). Afterwards, the number of electric vehicles required to meet the temperature target of <2°C were calculated and corresponding required energy was calculated using a backcasting procedure. We took the energy required for electric vehicle from Milovanoff et. al, 2020 for each SSP and calculated the energy required for BEV dominant and e-fuel dominant scenarios accounting for the e-fuel process efficiency, transmission losses and different proportions of long and short-term storage and corresponding losses expected by 2050.

The projected energy required for business as usual (BAU) scenarios in 2050 is taken from two sources: Annual Energy outlook from Energy Information Administration (EIA) [228] and Renewable Electricity futures study by National Renewable Energy Laboratory (NREL) [229]. This study assumed the following three SSPs.

1) SSP-1: Sustainability-Taking the green road.

2) SSP-2: Middle of the road.

3) SSP-5: Fossil-fueled development- Taking the highway.

The key variables that describe these SSPs include population, gross domestic product, environmental awareness, transport energy intensity along with technological development and social acceptance of fossil fuels as given in [226]. The well-to-tank energy required from utility-level PV and wind for each of the above scenarios and pathways is shown in Figure 32.

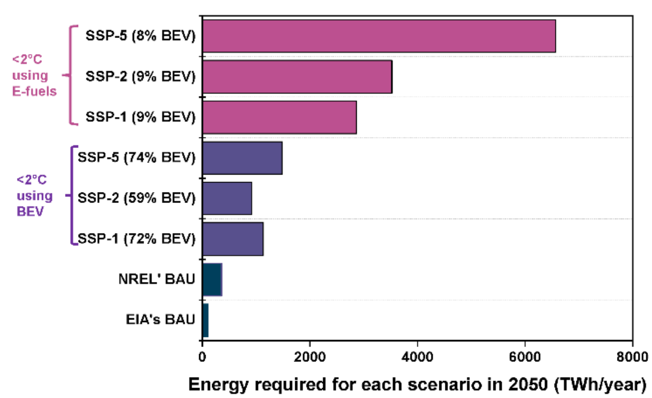

Figure 32. The energy requirement for the business-as-usual scenarios, battery electric vehicle (BEV) dominant scenarios and e-fuel dominant scenarios that can prevent more than 2°C global temperature rise. The y-axis also shows the percentage of BEV required in all scenarios.

The relative proportions of the utility-scale PV, onshore, and offshore wind turbines expected in 2050 were taken from three different future projections: a) North American Renewable Integration Study by NREL [230], b) Annual Energy Outlook 2021 from EIA [228] and, c) Jacobson et al., 2018 [231]. The breakdown of utility-scale PV, onshore and offshore wind from three sources is given in Table 9.

Table 9. Percentage breakdown of projected proportions of utility level solar PV, onshore wind and offshore wind from the three sources.

Projection	**Share of solar PV (%)**	**Share of onshore wind (%)**	**Share of offshore wind (%)**
NREL	55	40.4	4.6
EIA	51.4	42.9	5.7
Jacobson et. al., 2018	33	51.1	15.9

The energy required for e-fuel scenarios was calculated assuming an e-fuel process efficiency of 55% [232]. The energy generated from PV and wind in 2050 was considered to be stored in batteries and hydrogen-based power-to-gas-to-power (PGP) technologies. The battery storage was assumed to contribute to 89.3% of the total energy storage, while PGP contributed 10.7% of the total storage [233]. The efficiency of the battery storage and PGP technology in 2050 was taken as 90% [234] and 49% [235], respectively.

4.2.2 Solar PV requirements

All the solar PV modules were assumed to be utility-level silicon-based ground-mounted modules. The efficiency of the PV modules was assumed to reach 24% by the year 2050 from [236]. Equation (9) is used to calculate the land-use requirement of solar PV modules as given in [236].

$$\rho = I.f_1.f_2.f_3 \tag{9}$$

Where ρ is the yield in terms of energy output per unit of land, f_1 is the average efficiency of a solar power plant, f_2 is the average performance ratio over the lifetime of the solar power plant, f_3 is the land occupation ratio. The land occupation ratio (f_3) is defined by equation (10) where GSR denotes generator to system area, and PF is the packing factor. The packing factor is given by equation (11) where β = ∅ = tilt of the modules or the location's latitude.

$$f_3 = GSR.PF \quad (10)$$

$$PF = (cos\beta + \frac{sin\beta}{\tan\left(66.5°.\frac{\pi}{180°}\right) - \emptyset)})^{-1} \quad (11)$$

The average solar irradiance is taken as 2300 kWh/m^2/year from Fthenakis et. al, 2021[237] assuming that the planned utility scale PV modules are installed in the southwestern and south Atlantic parts of the U.S. [186]. The values of the variables used in equation (9), (10) and (11) are given in Table 10.

Table 10. The values of the different variable as used in equation (9), (10) and (11).

Variable name	**Symbol**	**Value**	**Reference**
Average solar irradiance	I	2300 kWh/m^2/year	[237]
Average efficiency of solar power plant	f_1	24%	[236]
Average performance ratio	f_2	0.65	[236]
Land occupation ratio	f_3	0.35	[236]
Generator to system area	GSR	0.70	[236]
Packing factor	PF	0.50	[236]
Tilt of modules, Latitude of location	$\beta, \emptyset$	39.5°	[238]

The mono-crystalline modules were assumed to be 66% of the total modules[217], and the silicon, aluminum, and copper requirements for mono and poly-crystalline silicon modules were taken from International Energy Agency's Photovoltaic Power Systems Program (PVPS) task-12 report [239]. The silicon, aluminum and copper material requirement assumptions for the mono and multi crystalline silicon modules are given in appendix C.

4.2.3 Wind turbine requirements

The percentage of onshore and offshore turbines assumed for wind power plants is given in Table 9. The land area required for onshore wind power plants includes the total enclosed project area and not just the turbine pad area [240,241]. The enclosed area is usually available for limited anthropogenic activity like agriculture, grazing, etc. The average capacity factor of wind turbines in 2050 was taken as 35.4% [242].

The aluminum and copper required per megawatt for offshore and onshore wind turbines were taken from [243,244]. 68.6% of onshore and 76% of offshore wind turbines were assumed to contain rare earth element (REE) based permanent magnets, which contain neodymium, dysprosium, and praseodymium [245]. The amount of neodymium, dysprosium, and praseodymium per MW in a wind turbine depends on its drivetrain, i.e., direct-drive and geared. The land-based turbines were assumed to have a gearbox drivetrain configuration, while the offshore wind turbines were assumed to have a direct drive configuration [246]. The neodymium, dysprosium, and praseodymium amounts per MW of wind turbines for different drivetrain configurations are given in Table 11.

Table 11. Neodymium, Dysprosium, and Praseodymium requirements for the wind turbines of different direct drive configurations.

Material	Drivetrain configuration	Amount (kg/MW)	Reference
Neodymium	Direct drive	149.8	[246]
Neodymium	Geared	17.5	[247]
Dysprosium	Direct drive	24	[248]
Dysprosium	Geared	1.7	[247]
Praseodymium	Direct drive	53.5	[249]
Praseodymium	Geared	5.8	[247]

4.3 Results and discussion

4.3.1 Solar and Wind capacity requirements

Figure 33 shows the combined PV and wind energy capacity required to meet the <2° C target by 2050, suggesting that e-fuel scenarios required 2.5-4.4 times more capacity than the corresponding BEV dominant scenarios. The figure also shows the installed utility level PV and wind capacity in 2020 on respective figures and the projected capacity by 2050 from EIA [228]. The PV capacity required for most BEV scenarios would be achievable by 2050 if 37-81% projected total PV capacity is used to serve the light duty vehicle fleet. However, the expected PV capacity required for the e-fuel scenarios was more than the projected 2050 PV capacity.

29-72% of the 2050 projected wind capacity can meet the demand for most BEV dominant scenarios. However, the projected 2050 wind capacity in the US cannot satisfy any e-fuel dominant scenario. Figure 33(a) and Figure 33(b) results are interconnected because any shortfall in wind capacity would need to be satisfied with either more PV or other renewable energy sources like biomass, and vice versa. Thus, most BEV dominated scenarios were more likely to be achieved with projected PV and wind capacities by 2050, while e-fuel scenarios requirements were unlikely to be higher than PV and wind capacity projections.

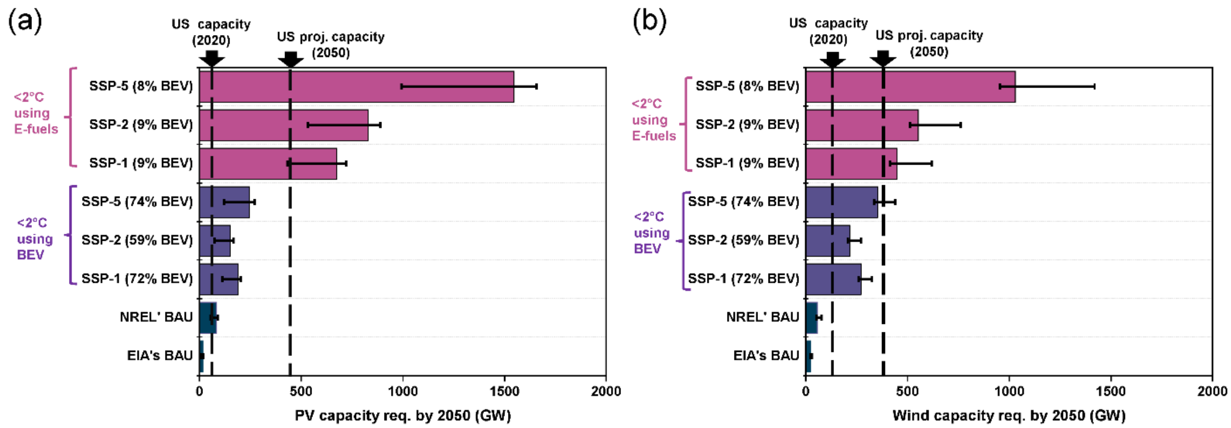

Figure 33. (a)PV capacity and (b)Wind capacity requirement by 2050 to combinedly fulfill energy requirement for all scenarios. The figures also show the utility-level PV and wind capacity for U.S in 2020. and the 2050 projected U.S. capacity from National Renewable Energy Laboratory.

4.3.2 Land use

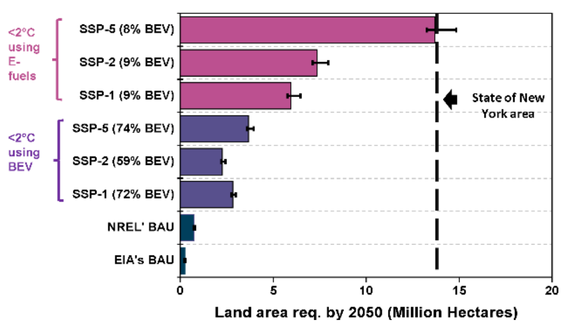

Figure 34. Land required to achieve <2° C target through different BEV and e-fuel scenarios by the year 2050 in addition to the NREL and EIA's business as usual scenarios. The figure also shows the area of the state of New York to put the results in a broader perspective

Figure 34 shows the land-use by the year 2050 for the two BAU scenarios, three BEV scenarios, and the three e-fuel scenarios showing that shortage of land, aluminum, or copper is unlikely to hinder the solar PV and wind energy growth required for either BEV or e-fuel scenarios. The land requirement for BEV scenarios (1.8-3.3 million hectares) was 2.6-10.5 times the BAU scenarios, while the e-fuel scenarios required 9.8-26.5 times the land needed for BAU scenarios. The area of the state of New York is also marked in Figure 34 to put the land-use results in perspective, indicating that the land use requirement for all the scenarios was less than 15 million hectares.

For validation, the energy density of the utility level solar plants in this study was compared to the literature value. The energy density for utility level plants in this study was 503.4 MWh/year/acre, 12 % higher than the value given in Bolinger et al., 2022[250]. A higher energy density was justified in this case because Bolinger et al., 2022 calculates the energy density for modules that were functional up to 2019. However, the current study estimates the expected energy density of modules in 2050 that is expected to be higher due to the rising power conversion efficiencies of solar modules.

Currently. the U.S. has about 1 million hectares of land dedicated to golf courses and about 49 million hectares of land dedicated to major roadways [251]. Therefore, 15 million hectares are likely to be available for solar PV and onshore wind. Moreover, solar PV and on shore wind do not monopolize land use, and the land can be used for other purposes like agriculture, livestock pastures, etc. Therefore, land-use requirements for all the BEV and e-fuel scenarios can be met by 2050.

4.3.3 Aluminum and Copper requirement

Figure 35(a) and Figure 35(b) show the aluminum and copper requirements for all considered eight scenarios with their respective cumulative U.S. production in the last 30 years, indicating that none of the <2° C scenarios were likely to face a shortage of these materials. The amount of aluminum produced in the U.S. from 1987 to 2017 was roughly 9-98 times more than that required for different BEV and e-fuel scenarios [252]. Aluminum is a highly recyclable material (~50% in the U.S.); therefore, more than 75% of aluminum that was ever mined is still in circulation [253]. Thus, the required aluminum for all <2°C scenarios will be available by 2050, although a previous study suggests that secondary aluminum production needs to be rapidly increased to meet such high expected demand[254]. Similarly, copper production from 1987 to 2017 was 35-268 times the copper requirement for BAU, BEV, and e-fuel scenarios [252]. Copper is also a highly recyclable material (~30% in the U.S.) [255], with nearly all mined copper still in circulation [256]. Therefore, the solar PV and wind industry are unlikely to face copper shortage to meet the <2° C targets either via BEV or e-fuel scenarios.

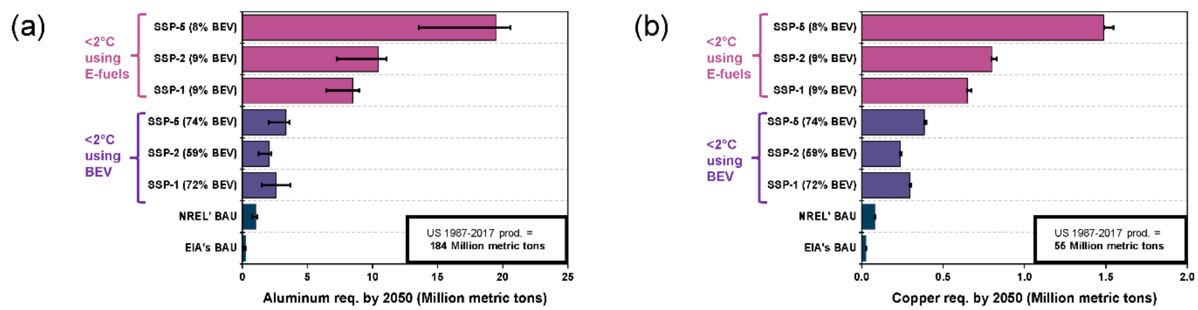

Figure 35. (a) aluminum requirement, and (b) copper requirement to achieve <2° C target through different BEV and e-fuel scenarios by the year 2050 in addition to the NREL and EIA's business as usual scenarios. The figure also shows the U.S. production of aluminum and copper from 1987-2017 to put the results in a broader perspective.

4.3.4 Silicon, Neodymium, Dysprosium, and Praseodymium requirements

Figure 36 shows the silicon, neodymium, dysprosium, and praseodymium requirement for each of the above-stated scenarios, indicating that all these materials apart from praseodymium will likely be insufficient to serve the material demand from e-fuel based <2° C scenarios by 2050. Figure 36(a) shows the silicon required by the eight scenarios compared to the 2021 global production of polysilicon, which is a precursor to solar grade silicon. Similarly, 2021 solar futures study from the U.S Department of Energy stated that 1300-3000 metric tons of silicon will be required by the year 2050 in the U.S. for silicon-based modules [257]. Comparing these estimates with our results indicates that e-fuel dominant scenarios are likely to face shortage of solar grade silicon by 2050.

The BEV-based scenarios are likely to have sufficient silicon based on the global 2021 polysilicon production and future plans to quadruple the polysilicon production in the coming decade [258].

Similarly, Figure 36(b) and Figure 36(c) show the required neodymium, and dysprosium amounts for the considered eight scenarios indicating that both materials were required 2.5-4.4 times more in e-fuel scenarios compared to the BEV scenarios. Currently, most of the neodymium required in the U.S. is imported; however, with the expected opening of mountain pass mine in California, about 15 thousand metric tons of neodymium can be mined by 2050 [246]. Similarly, the domestic production of dysprosium in the U.S. is expected to be 3 thousand metric tons by 2050 [248]. Therefore, the domestic mining and recycling of neodymium and dysprosium are likely to satisfy the demand from the BEV scenarios. However, there would be a shortage of neodymium and dysprosium in case of e-fuel dominant scenarios requiring imports from other countries. Figure 36(d) shows the praseodymium requirement for the considered eight scenarios and its annual global production, which indicated that wind energy industry is unlikely to face shortage of praseodymium. A similar conclusion regarding praseodymium was stated by Binneman et. al, 2018 for the global wind energy market [259]. Therefore, land use and material availability constraints are unlikely to hinder the growth of solar PV and wind required to meet the <2° C target using BEV scenarios. However, most scenarios that use e-fuels to prevent a greater than 2° C rise in temperature are likely to face silicon, neodymium, and dysprosium shortage in the future.

In this study, the required neodymium and dysprosium were calculated only for the wind turbine generators. However, a higher proportion of neodymium and dysprosium-based permanent magnets are used in other applications like electric vehicle motors, laptops, mobile phones, cameras, and medical resonance imaging equipment. A European commission's Joint Research

Center report estimated that electric vehicles may require 2-3 times the rare earth elements needed by wind turbine generators[245]. The same report also states that wind turbines and electric vehicles currently account for only 9% and 30% of neodymium and dysprosium's total global demand, respectively. Therefore, the overall demand of neodymium and dysprosium by 2050 can be higher than stated in this study.

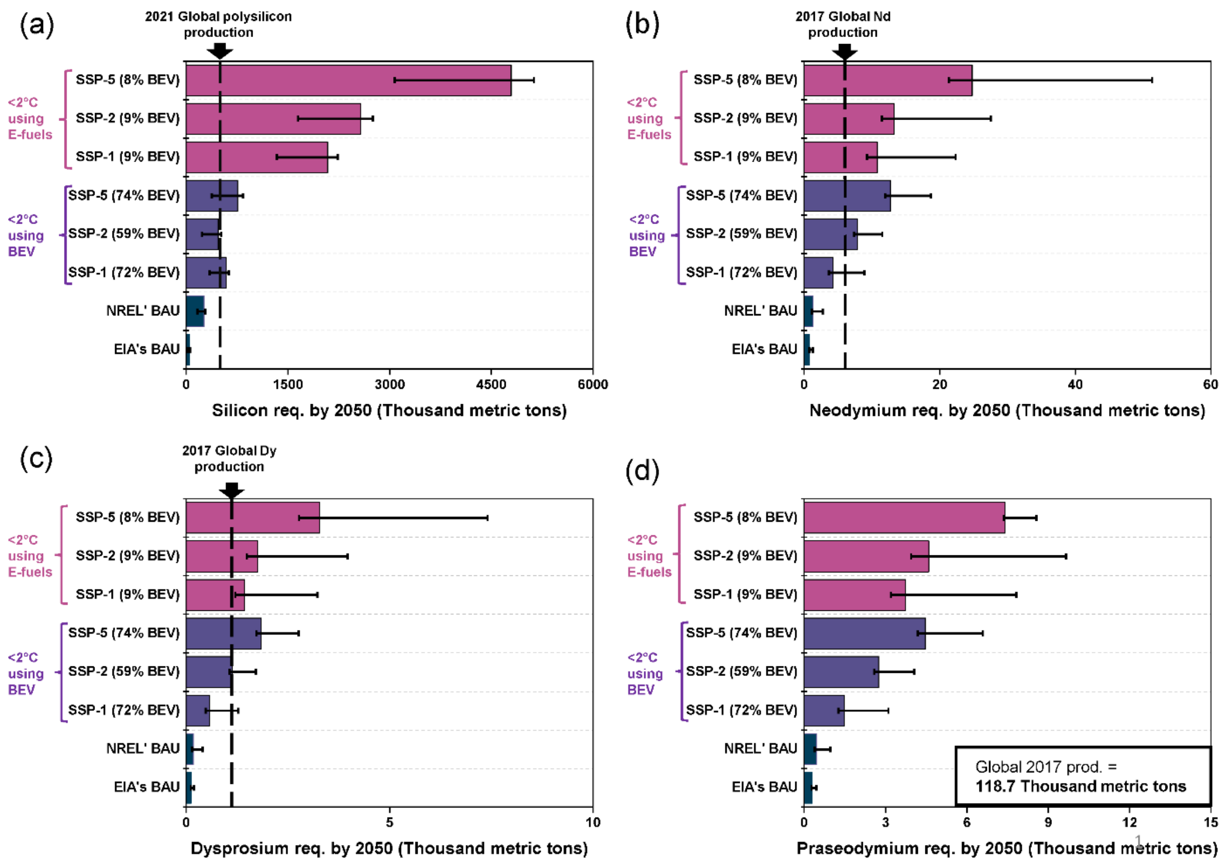

Figure 36. (a) Silicon (b) Neodymium (c) Dysprosium, and (d) Praseodymium requirement business as usual scenarios, battery electric vehicle-based scenarios, and e-fuel based scenarios by the year 2050. The figure also shows 2021 global polysilicon production in addition to 2017 global production of neodymium, dysprosium and praseodymium to put the results into a broader perspective.

4.4 Conclusions

In this chapter, we calculated the land use and materials (aluminum, copper, silicon, neodymium, dysprosium, and praseodymium) required for the renewable energy systems (solar

PV and wind turbines) to power the electricity-based and e-fuel based vehicle fleet that can prevent the rise of global temperature by more than 2°C. Therefore, the results contribute to the growing body of literature related to the supply and demand of rare earth materials and land use required to achieve the sustainability goals.

The results indicated that the electrification of the vehicle fleet needs to play a more prominent role in the transportation sector than e-fuels as the land use and material requirements for e-fuels are considerably higher. Renewable energy industries in the U.S. are likely to face material supply issues in e-fuel dominant scenarios due to limited and geopolitically constrained availability of rare earth elements like neodymium and dysprosium.

This analysis covered a wide range of solar PV and wind energy projections from different sources; however, the results may vary as more recent, and accurate projections are considered. Also, for simplicity, the solar irradiance was taken as 2300 kWh/m^2/year, representing the locations with high solar irradiance in the U.S. Recently, utilities in the states with lower average solar irradiance like Michigan and New York are planning to establish new utility level solar PV plants[260,261]. In such a case, the land use, silicon, aluminum, and copper requirements are expected to increase further than reported in this study. Similarly, wind farms' land use and material requirements are also likely to change with new turbine technologies and material advances in permanent magnet manufacturing.

The rare earth elements required for the motors of electric vehicles were not considered in this study. Therefore, a comprehensive future study is required that accounts for the neodymium and dysprosium needed for the electric vehicles in all the scenarios by 2050. Although electric vehicles may require a considerable amount of rare earth elements for permanent magnets, original equipment manufacturers (OEMs) have made high-performance electric vehicles in the past that do not require any permanent magnets [262,263]. Therefore, the results of this study indicated that more research should extend into such electric vehicle technology so that the supply issues related to neodymium and dysprosium can be alleviated in the future. Also, recent studies indicate that the recovery of rare earth elements from secondary sources is likely to increase in the near future with advances in recycling technologies, which may help in offsetting some demand for the wind turbine permanent magnets[264].

The current study focused on the material requirements of the solar PV and wind power plants but does not consider the material required for energy storage technologies like Li-ion batteries. Installing Li-ion batteries at a large scale might require considerable nickel, manganese, cobalt, and lithium in the future; however, the literature indicates that global battery markets are unlikely to face resource constraint issues for these materials[265].

This chapter highlighted the importance of energy demand estimation at a macroscopic level for renewable energy solutions design. At the micro-level, e-fuels may seem a better technology as ambient air's carbon dioxide capture is possible, and no significant changes would be required in the refueling infrastructure. However, e-fuels will likely face the material supply chain constraints for installing the required renewable energy systems. Therefore, based on the energy demand estimates, battery electric vehicles are a more sustainable way to decarbonize the light-duty vehicle fleet than e-fuels.

It should be noted that this analysis focused on decarbonizing the light-duty vehicle fleet for which electrification options are available. However, electrification options are not available for large vehicle categories like aviation. Therefore, e-fuels might serve towards decarbonization of aviation sector [266,267].

Chapter 5 Conclusions and major contributions

This dissertation focused on underlining the importance of energy demand estimation at the micro and macro-level for better design and economic and environmental assessment of renewable energy solutions. Each chapter of this dissertation deals with a different sector: residential, commercial, utility, and transportation. An array of methods and models were developed and used to show the crucial role played by energy demand estimation in selecting the type of renewable energy systems along with their design, installation strategy, and benefit assessment. The major contributions of this dissertation can be divided into three parts, like the broad energy sectors analyzed in this dissertation.

5.1 Residential sector

Firstly, the results of chapter 2 showed that stochastic considerations in load modeling of residential microgrids led to differences in cost and carbon footprint estimates. The cost and carbon footprint differences were identified in PV+battery systems even with a 1-2 hour lag in the load peaks due to the consumers' stochastic behavior. Depending on the location and the load demand, the cost and carbon footprint estimates from the stochastic load can be higher or lower than the conventional estimates. Results in chapter 2 also showed that as the U.S. moves towards electrification of space and water heating [59], modeling the stochastic behavior of the load would become even more important for designing renewable energy solutions. Chapter-2 results also inform another key aspect regarding the size of a residential microgrid that number of houses in a microgrid should not be more than 10 regardless of the location. With an increasing number of houses in the microgrids, the benefits due to the "economies of scale" diminished after 10 houses. However, for more than 10 houses, there might be difficulties in connecting the entire microgrid as a single electrical entity, incurring more cost.

Chapter 2 also highlights the importance of load patterns in deciding the battery retirement strategy for PV+battery systems. The retirement strategy of the SLBs was changed based on the high peak demand from home energy storage + EV charging applications that might lead to early cyclic degradation. The early retirement strategy led to savings in the carbon footprint of the PV+ battery systems. The results also highlighted the importance of off-peak pricing in PV-based renewable systems design for the applications like home energy storage + EV charging with intense demand during off-peak pricing hours. The conclusions from this part of the thesis are likely to become more relevant and useful as the electricity prices (including off-peak pricing) [134] and the demand for battery manufacturing materials increase [268]. Both the studies in chapter 2 show that PV+battery systems using SLBs always had lower levelized cost of electricity (LCOE), and carbon footprint compared to the systems with new batteries. Thus, second-life batteries can be beneficial for stationary energy storage systems despite their lower roundtrip efficiency and faster degradation compared to the new Li-ion batteries. In addition to benefits for stationary storage applications, using SLBs would also prolong the useful life of the batteries and reduce their associated environmental impacts.

Chapter 2 analyzed the differences in cost and carbon footprint estimates based on novel modeling methodologies at a single house or a single-microgrid level. However, these differences are likely to be significant when analyzed on a national scale. Overall, this chapter contributes towards the design of renewable energy solutions with lesser cost and carbon footprint for the residential sector.

5.2 Commercial and utility sector

Chapter 3 focused on different ways in which renewable energy solutions can reduce the energy demand and the associated environmental impacts from the commercial and utility sectors.

Firstly, the results showed that transparent organic photovoltaics (TOPVs) could lead to energy benefits in commercial buildings despite their low power conversion efficiencies while preserving the aesthetics. The energy benefits consequently lead to avoided GHGs and avoided costs due to avoided grid purchased electricity. Also, TOPVs could compete with conventional PV technologies in terms of manufacturing energy, potentially leading to cheaper commercially available modules.

TOPVs saved building energy in addition to electricity generation due to their spectral properties. Therefore, TOPVs can reduce energy demand even for buildings with small windows or façade areas. The energy benefit results were compared for TOPVs made from two different donor materials, which had different power conversion efficiencies, average visible transmittance, and wavelength ranges for peak absorption. These TOPVs were simulated to be installed on the commercial building windows of five different types of commercial buildings. The results showed that the TOPV with lower power conversion efficiency (ClAlPc) might lead to higher energy benefits than the one with higher power conversion efficiency due to building and load characteristics. Therefore, load characteristics can be an essential determinant in selecting the donor material for the TOPV.

Chapter 3 further showed that Li-ion batteries could also reduce the carbon footprint from commercial buildings. The results showed that considerable carbon footprint reduction (up to 12%) was possible for the commercial PV + battery systems by peak demand prevention using Li-ion batteries, in addition to the reduction in the overall grid purchases. While peak demand prevention can yield better results in buildings with high daytime peaks like restaurants, lesser benefits were observed in commercial buildings with a relatively stable load throughout the day, like hospitals. Therefore, this analysis highlighted the importance of load estimation by showing that PV+

battery-based systems need to be designed to exploit the load characteristics. Thus, due to its load characteristics, a hospital will have higher energy benefits when fitted with TOPVs' windows applications than conventional PV and battery systems despite the low efficiency of the TOPVs.

Chapter 3 also analyzed the agriculture sector's energy demand and the scale at which agriculturally co-located modules can offset this demand. Results showed that a significant portion of energy demand (about 69%) from the most extensively irrigated region of California (central valley) could be met with agriculturally co-located PV modules. However, the consequent land use for these solar modules was disproportionately less (1-10%). Farmers gain cost benefits by selling their additional PV generation to the grid under the net metering schemes [149], in addition to offsetting their own energy demand. These high energy and cost benefits explain the exponential increase in agriculturally co-located installations over the study period (2008-2018). However, significant differences in installation practices were observed based on the size of the PV plant. Installations with higher PV capacity were generally single-axis trackers and had higher deviations from optimal installation practices. Such installations will likely be installed in larger agricultural fields with higher energy demand. Therefore, the energy demand of the agricultural farms also plays a role in considering the optimal design and installation practices for PV. Thus, the results and conclusions from this part of the dissertation might help enforce more stringent land use policies for PV installations on bigger agricultural farms. Stricter land use policies for bigger agricultural farms would prevent wastage of agricultural land and food security issues.

Finally, chapter 4 touched on the utility sector, and the results demonstrated the importance of considering alternates to conventional battery storage in utility level firming systems. SLBs showed cost and carbon footprint savings as higher battery capacities could be used due to the lower cost of SLBs. The benefits of SLBs compared to the new batteries depended on the location and were higher in locations with more minutely variations and higher PV output.

Overall, chapter 4 contributed to suggesting an array of materials and technologies for PV-based renewable energy solutions depending on the load and the application. For each of the commercial sector applications, the different parts/sectors of the commercial loads were targeted to reduce the cost or the environmental impact of the systems. Therefore, the results from this chapter showed that a better estimate of the commercial loads can lead to better design and selection of PV-based systems that can exploit the desired load characteristics for the highest cost and environmental benefits.

5.3 Transportation sector

Chapter 4 of this dissertation focused on the transportation sector by analyzing the material and land use constraints of decarbonizing the light-duty vehicle fleet via multiple future pathways. The analysis focused on the macro-level feasibility of PV and wind turbines by 2050 to set up the refueling infrastructure for a) battery electric vehicle dominant scenarios and b) gasoline vehicle dominant scenarios where the gasoline is obtained from e-fuel processes. The results indicated that the electrification of the vehicle fleet needs to play a more prominent role in the transportation sector than e-fuels as the land use and material requirements for e-fuels were considerably higher.

Renewable energy industries in the U.S. will likely face material supply issues in e-fuel dominant scenarios due to limited and geopolitically constrained availability of rare earth elements like neodymium and dysprosium. This chapter highlighted the importance of energy demand estimation at a macro level for renewable energy systems design. At the micro-level, e-fuels may seem a better technology as atmospheric carbon dioxide capture is possible, and no significant changes would be required in the refueling infrastructure. However, e-fuels will likely face the material supply chain constraints for installing the required capacity of renewable energy solutions. Therefore, based on the energy demand macro-estimates, battery electric vehicles are a more sustainable pathway to decarbonize the light-duty vehicle fleet than e-fuels.

REFERENCES

[1] U.S. energy facts explained - consumption and production - U.S. Energy Information Administration (EIA) n.d. https://www.eia.gov/energyexplained/us-energy-facts/ (accessed August 7, 2022).

[2] Nakolan K, Francis M. U.S. energy-related CO2 emissions rose 6% in 2021 2022. https://www.eia.gov/todayinenergy/detail.php?id=52380 (accessed August 16, 2022).

[3] Sixth Assessment Report — IPCC. 2021.

[4] Akinyele D, Belikov J, Levron Y. Challenges of microgrids in remote communities: A STEEP model application. Energies 2018;11. doi:10.3390/en11020432.

[5] Tawalbeh M, Al-Othman A, Kafiah F, Abdelsalam E, Almomani F, Alkasrawi M. Environmental impacts of solar photovoltaic systems: A critical review of recent progress and future outlook. Sci Total Environ 2021;759:143528. doi:10.1016/j.scitotenv.2020.143528.

[6] Zhou Y, Wu J, Long C. Evaluation of peer-to-peer energy sharing mechanisms based on a multiagent simulation framework. Appl Energy 2018;222:993–1022. doi:10.1016/J.APENERGY.2018.02.089.

[7] Cohn L. Net Metering and Microgrids: Do your Homework 2016. https://microgridknowledge.com/net-metering-and-microgrids/ (accessed July 30, 2022).

[8] Fu R, Feldman D, Margolis R. U . S . Solar Photovoltaic System Cost Benchmark : Q1 2018. Nrel 2018. doi:10.7799/1325002.

[9] Asmus P. Microgrids, Virtual Power Plants and Our Distributed Energy Future. Electr J 2010;23:72–82. doi:10.1016/j.tej.2010.11.001.

[10] Nagapurkar P, Smith JD. Techno-economic optimization and environmental Life Cycle Assessment (LCA) of microgrids located in the US using genetic algorithm. Energy Convers Manag 2019;181:272–91. doi:10.1016/j.enconman.2018.11.072.

[11] Babaee S, Nagpure AS, Decarolis JF. How much do electric drive vehicles matter to future U.S. emissions? Environ Sci Technol 2014. doi:10.1021/es4045677.

[12] Idaho National Laboratory. Plugged In: How Americans Charge Their Electric Vehicles. 2015.

[13] Chen H, Cong TN, Yang W, Tan C, Li Y, Ding Y. Progress in electrical energy storage system: A critical review. Prog Nat Sci 2009;19:291–312. doi:10.1016/j.pnsc.2008.07.014.

[14] Jiao N, Evans S. Business Models for Sustainability: The Case of Second-life Electric

Vehicle Batteries. Procedia CIRP, vol. 40, 2016, p. 250–5. doi:10.1016/j.procir.2016.01.114.

[15] Heymans C, Walker SB, Young SB, Fowler M. Economic analysis of second use electric vehicle batteries for residential energy storage and load-levelling. Energy Policy 2014;71:22–30. doi:10.1016/j.enpol.2014.04.016.

[16] Kamath D, Shukla S, Arsenault R, Kim HC, Anctil A. Evaluating the cost and carbon footprint of second-life electric vehicle batteries in residential and utility-level applications. Waste Manag 2020. doi:10.1016/j.wasman.2020.05.034.

[17] Kamath D, Shukla S, Anctil A. An Economic and Environmental Assessment of Residential Rooftop Photovoltaics with Second Life Batteries in the US. Conf. Rec. IEEE Photovolt. Spec. Conf., 2019.

[18] Ramadass P, Haran B, White R, Popov BN. Mathematical modeling of the capacity fade of Li-ion cells. J Power Sources 2003;123:230–40. doi:10.1016/S0378-7753(03)00531-7.

[19] Swierczynski M, Stroe DI, Laserna EM, Sarasketa-Zabala E, Timmermans JM, Goutam S, et al. The Second Life Ageing of the NMC/C Electric Vehicle Retired Li-Ion Batteries in the Stationary Applications. ECS Trans 2016;74:55–62. doi:10.1149/07401.0055ecst.

[20] Canals Casals L, García B, Aguesse F, Iturrondobeitia A. Second life of electric vehicle batteries: relation between materials degradation and environmental impact. Int J Life Cycle Assess 2015.

[21] Venkatapathy K, Tazelaar E, Veenhuizen B. A Systematic Identification of First to Second Life Shift-Point of Lithium-Ion Batteries. 2015 IEEE Veh Power Propuls Conf VPPC 2015 - Proc 2015. doi:10.1109/VPPC.2015.7352885.

[22] Gohla-Neudecker B, Bowler M, Mohr S. Battery 2nd life: Leveraging the sustainability potential of EVs and renewable energy grid integration. 5th Int Conf Clean Electr Power Renew Energy Resour Impact, ICCEP 2015 2015:311–8. doi:10.1109/ICCEP.2015.7177641.

[23] Mariaud A, Acha S, Ekins-Daukes N, Shah N, Markides CN. Integrated optimisation of photovoltaic and battery storage systems for UK commercial buildings. Appl Energy 2017;199:466–78. doi:10.1016/J.APENERGY.2017.04.067.

[24] Ceran B, Jurasz J, Mielcarek A, Campana PE. PV systems integrated with commercial buildings for local and national peak load shaving in Poland. J Clean Prod 2021;322:129076. doi:10.1016/J.JCLEPRO.2021.129076.

[25] Sánchez-Pantoja N, Vidal R, Pastor MC. Aesthetic impact of solar energy systems. Renew Sustain Energy Rev 2018;98:227–38. doi:10.1016/J.RSER.2018.09.021.

[26] Shukla AK, Sudhakar K, Baredar P. Recent advancement in BIPV product technologies: A review. Energy Build 2017. doi:10.1016/j.enbuild.2017.02.015.

[27] Yang C, Liu D, Bates M, Barr MC, Lunt RR. How to Accurately Report Transparent Solar Cells. Joule 2019;3:1803–9. doi:10.1016/J.JOULE.2019.06.005.

[28] Anctil A, Lee E, Lunt RR. Net energy and cost benefit of transparent organic solar cells in building-integrated applications. Appl Energy 2020. doi:10.1016/j.apenergy.2019.114429.

[29] Jayathissa P, Luzzatto M, Schmidli J, Hofer J, Nagy Z, Schlueter A. Optimising building net energy demand with dynamic BIPV shading. Appl Energy 2017;202:726–35. doi:10.1016/J.APENERGY.2017.05.083.

[30] Power generation you can see through | MSUToday | Michigan State University n.d. https://msutoday.msu.edu/news/2021/solar-glass-panels-installed (accessed August 7, 2022).

[31] Davidson C, Gagnon P, Denholm P, Margolis R. Nationwide Analysis of U.S. Commercial Building Solar Photovoltaic (PV) Breakeven Conditions 2015.

[32] Sources of Greenhouse Gas Emissions | US EPA n.d. https://www.epa.gov/ghgemissions/sources-greenhouse-gas-emissions (accessed January 1, 2022).

[33] FHWA Forecasts of Vehicle Miles Traveled (VMT): Spring 2021. 2021.

[34] Birol F. World Energy Outlook 2018 – Analysis - IEA. 2018.

[35] Cornet A, Conzade J, Schaufuss P, Schenk S, Tschiesner A, Hensley R, et al. Why the future involves e-mobility | McKinsey 2021. https://www.mckinsey.com/industries/automotive-and-assembly/our-insights/why-the-automotive-future-is-electric (accessed January 1, 2022).

[36] Liu CM, Sandhu NK, McCoy ST, Bergerson JA. A life cycle assessment of greenhouse gas emissions from direct air capture and Fischer-Tropsch fuel production. Sustain Energy Fuels 2020;4:3129–42. doi:10.1039/c9se00479c.

[37] Zeman FS, Keith DW. Carbon neutral hydrocarbons n.d. doi:10.1098/rsta.2008.0143.

[38] Ueckerdt F, Bauer C, Dirnaichner A, Everall J, Sacchi R, Luderer G. Potential and risks of hydrogen-based e-fuels in climate change mitigation. Nat Clim Chang 2021 115 2021;11:384–93. doi:10.1038/s41558-021-01032-7.

[39] Sigrin B, Mooney M. Rooftop Solar Technical Potential for Low-to-Moderate Income Households in the United States. 2018.

[40] Sonnichsen N. PV capacity installations: U.S. residential sector 2019 | Statista 2020. https://www.statista.com/statistics/185694/us-residential-annual-pv-installed-capacity-since-2005/ (accessed November 2, 2020).

[41] Michelle D, White B, Goldstein R, Martinez SL, Chopra S, Gross K, et al. Solar Market Insight Report 2022 Q2 2020. https://www.seia.org/research-resources/solar-market-insight-report-2022-q2 (accessed July 31, 2022).

[42] Ground Mounted Solar: Top 3 Things You Should Know | EnergySage n.d. https://news.energysage.com/ground-mounted-solar-panels-top-3-things-you-need-to-know/ (accessed April 5, 2021).

[43] Ton DT, Smith MA. The U.S. Department of Energy's Microgrid Initiative. Electr J 2012;25:84–94. doi:10.1016/j.tej.2012.09.013.

[44] Berkeley Labs. Types of Microgrids | Building Microgrid 2018. https://building-microgrid.lbl.gov/types-microgrids (accessed July 16, 2018).

[45] Hirsch A, Parag Y, Guerrero J. Microgrids: A review of technologies, key drivers, and outstanding issues. Renew Sustain Energy Rev 2018;90:402–11. doi:10.1016/j.rser.2018.03.040.

[46] Said M, EL-Shimy M, Abdelraheem MA. Photovoltaics energy: Improved modeling and analysis of the levelized cost of energy (LCOE) and grid parity – Egypt case study. Sustain Energy Technol Assessments 2015;9:37–48. doi:10.1016/j.seta.2014.11.003.

[47] Rahmann C, Núñez O, Valencia F, Arrechea S, Sager J, Kammen D. Methodology for monitoring sustainable development of isolated microgrids in rural communities. Sustain 2016. doi:10.3390/su8111163.

[48] Kannan R, Leong KC, Osman R, Ho HK, Tso CP. Life cycle assessment study of solar PV systems: An example of a 2.7 kWp distributed solar PV system in Singapore. Sol Energy 2006. doi:10.1016/j.solener.2005.04.008.

[49] Rojas-Zerpa JC, Yusta JM. Application of multicriteria decision methods for electric supply planning in rural and remote areas. Renew Sustain Energy Rev 2015. doi:10.1016/j.rser.2015.07.139.

[50] Bilich A, Langham K, Geyer R, Goyal L, Hansen J, Krishnan A, et al. Life Cycle Assessment of Solar Photovoltaic Microgrid Systems in Off-Grid Communities. Environ Sci Technol 2017;51:1043–52. doi:10.1021/acs.est.6b05455.

[51] Smith C, Burrows J, Scheier E, Young A, Smith J, Young T, et al. Comparative Life Cycle Assessment of a Thai Island's diesel/PV/wind hybrid microgrid. Renew Energy 2015;80:85–100. doi:10.1016/j.renene.2015.01.003.

[52] Üçtuğ FG, Azapagic A. Environmental impacts of small-scale hybrid energy systems: Coupling solar photovoltaics and lithium-ion batteries. Sci Total Environ 2018. doi:10.1016/j.scitotenv.2018.06.290.

[53] Akter MN, Mahmud MA, Oo AMT. A Hierarchical Transactive Energy Management System for Energy Sharing in Residential Microgrids. Energies 2017, Vol 10, Page 2098 2017;10:2098. doi:10.3390/EN10122098.

[54] Mohan V, Singh JG, Ongsakul W, Unni AC, Sasidharan N. Stochastic Effects of Renewable Energy and Loads on Optimizing Microgrid Market Benefits. Procedia Technol 2015;21:15–23. doi:10.1016/j.protcy.2015.10.004.

[55] Silani A, Yazdanpanah MJ. Distributed Optimal Microgrid Energy Management With Considering Stochastic Load. IEEE Trans Sustain Energy 2019;10:729–37. doi:10.1109/TSTE.2018.2846279.

[56] Giaouris D, Papadopoulos AI, Patsios C, Walker S, Ziogou C, Taylor P, et al. A systems approach for management of microgrids considering multiple energy carriers, stochastic loads, forecasting and demand side response. Appl Energy 2018;226:546–59. doi:10.1016/J.APENERGY.2018.05.113.

[57] Kumar M, Tyagi B. Multi-variable constrained non-linear optimal planning and operation problem for isolated microgrids with stochasticity in wind, solar, and load demand data. IET Gener Transm Distrib 2020;14:2181–90. doi:10.1049/IET-GTD.2019.0643.

[58] Cingoz F, Elrayyah A, Sozer Y. Optimized Settings of Droop Parameters Using Stochastic Load Modeling for Effective DC Microgrids Operation. IEEE Trans Ind Appl 2017;53:1358–71. doi:10.1109/TIA.2016.2633538.

[59] Nadal S. Programs to Electrify Space Heating Are Growing 2020. https://www.aceee.org/blog-post/2020/06/programs-electrify-space-heating-are-growing (accessed July 29, 2022).

[60] Casals LC, Amante García B, Canal C. Second life batteries lifespan: Rest of useful life and environmental analysis. J Environ Manage 2019. doi:10.1016/j.jenvman.2018.11.046.

[61] Tong S, Fung T, Klein MP, Weisbach DA, Park JW. Demonstration of reusing electric vehicle battery for solar energy storage and demand side management. J Energy Storage 2017. doi:10.1016/j.est.2017.03.003.

[62] Strickland D, Chittock L, Stone DA, Foster MP, Price B. Estimation of transportation battery second life for use in electricity grid systems. IEEE Trans Sustain Energy 2014;5:795–803. doi:10.1109/TSTE.2014.2303572.

[63] HOMER PRO Version 3.7 User Manual. 2016.

[64] Youli S. Economic and Environmental Impact Assesment of Micro Grid. Proc. Int. MultiConference Eng. Comput. Sci. Vol II, IMECS, 2015, p. 4.

[65] Zia Z, Ali F. Economic and Environmental Impact Assessment of Microgrid for Rural Areas of Pakistan. 10th Int. Conf. Sustain. Energy Environ. Prot., Bled, Slovenia: 2017. doi:10.18690/978-961-286-053-0.6.

[66] Northwest Energy Efficiency Alliance. Oregon single-family homes 2014. http://neea.org/docs/default-source/rbsa/oregon-state-report-final.pdf (accessed November 25, 2017).

[67] Energy Information Administration. Household Energy Use in Michigan 2009. https://www.eia.gov/consumption/residential/reports/2009/state_briefs/pdf/mi.pdf (accessed November 25, 2017).

[68] Energy Information Administration. Household Energy use in California 2009. https://www.eia.gov/consumption/residential/reports/2009/state_briefs/pdf/ca.pdf (accessed November 25, 2017).

[69] Energy Information Administration. Household Energy Use in New York 2009.

[70] Energy Information Administration. Household Energy use in Arizona 2009. https://www.eia.gov/consumption/residential/reports/2009/state_briefs/pdf/az.pdf (accessed November 25, 2017).

[71] Solar Maps | Geospatial Data Science | NREL 2018. https://www.nrel.gov/gis/solar.html (accessed November 22, 2018).

[72] U.S. Energy Information Administration. Electricity: End-Use Prices: Residential. Annu Energy Outlook 2018 With Proj to 2050 2018.

[73] Kneifel J. Benefits and Costs of Energy Standard Adoption in New Commercial Buildings: State-by-State Summaries. NIST Spec Publ 1165 2013.

[74] Los Angeles County, California: Energy Resources | Open Energy Information 2010. https://openei.org/wiki/Los_Angeles_County,_California (accessed May 21, 2019).

[75] Wright GS, Klingenberg K. Climate-Specific Passive Building Standards. 2015.

[76] IECC compliance guide for homes in Arizona. International Energy Conservation code; 2012.

[77] Christensen C, Anderson R, Horowitz S, Courtney A, Spencer J. BEopt Software for Building Energy Optimization: Features and Capabilities. Build Am US Deparment Energy 2006:21. doi:10.2172/891598.

[78] Bureau USC. Average number of people per family in the United States from 1960 to 2018. 2019 2019. https://www.statista.com/statistics/183657/average-size-of-a-family-in-the-us/ (accessed December 2, 2019).

[79] Energy Information Administration. About the Residential Energy Consumption Survey (RECS): Fuels used and end uses in U.S. homes by housing unit type, 2015 2015. https://www.eia.gov/consumption/residential/data/2015/hc/php/hc8.7.php (accessed December 24, 2017).

[80] Heating and cooling no longer majority of U.S. home energy use - Today in Energy - U.S. Energy Information Administration (EIA) 2013. https://www.eia.gov/todayinenergy/detail.php?id=10271 (accessed August 6, 2018).

[81] Home Cooling Systems | Department of Energy 2017. https://www.energy.gov/energysaver/heat-and-cool/home-cooling-systems (accessed November 22, 2020).

[82] Jenkins DP, Patidar S, Simpson SA. Synthesising electrical demand profiles for UK dwellings. Energy Build 2014;76:605–14. doi:10.1016/j.enbuild.2014.03.012.

[83] National Grid. Operating the Electricity Transmssion Networks in 2020. 2011.

[84] Viswanathan V V., Kintner-Meyer M. Second use of transportation batteries: Maximizing the value of batteries for transportation and grid services. IEEE Trans Veh Technol 2011. doi:10.1109/TVT.2011.2160378.

[85] Cready E, Lippert J, Pihl J, Weinstock I, Symons P. Technical and Economic Feasibility of Applying Used EV Batteries in Stationary Applications. Other Inf PBD 1 Mar 2003 2003:Medium: ED; Size: 130 pages. doi:SAND2002-4084.

[86] DOE Global Energy Storage Database n.d. http://www.energystorageexchange.org/ (accessed June 21, 2018).

[87] Fu R, Feldman D, Margolis R, Woodhouse M, Ardani K. U.S. Solar Photovoltaic System Cost Benchmark: Q1 2017. 2017. doi:NREL/TP-6A20-68925.

[88] Melius J, Margolis R, Ong S. Estimating Rooftop Suitability for PV: A Review of Methods, Patents, and Validation Techniques 2013.

[89] O'Connor B. Residential Energy Storage System Regulations | NFPA | NFPA 2021. https://www.nfpa.org/News-and-Research/Publications-and-media/Blogs-Landing-Page/NFPA-Today/Blog-Posts/2021/10/01/Residential-Energy-Storage-System-Regulations (accessed August 11, 2022).

[90] Wilcox S, Marion W. Innovation for Our Energy Future Users Manual for TMY3 Data Sets. 1994.

[91] Falk J, Nedjalkov · Antonio, Angelmahr M, Schade W. Applying Lithium-Ion Second Life Batteries for Off-Grid Solar Powered System—A Socio-Economic Case Study for Rural Development. Zeitschrift Für Energiewirtschaft 2020 441 2020;44:47–60. doi:10.1007/S12398-020-00273-X.

[92] Mathews I, Xu B, He W, Barreto V, Buonassisi T, Peters IM. Technoeconomic model of second-life batteries for utility-scale solar considering calendar and cycle aging. Appl Energy 2020;269:115127. doi:10.1016/J.APENERGY.2020.115127.

[93] Feldman D, Ramasamy V, Fu R, Ramdas A, Desai J, Margolis R. U.S. Solar Photovoltaic System and Energy Storage Cost Benchmark: Q1 2020. 2020.

[94] Kamath D, Shukla S, Arsenault R, Kim HC, Anctil A. Evaluating the cost and carbon footprint of second-life electric vehicle batteries in residential and utility-level applications. Waste Manag 2020. doi:10.1016/j.wasman.2020.05.034.

[95] Kamath D, Arsenault R, Kim HC, Anctil A. Economic and Environmental Feasibility of Second-Life Lithium-Ion Batteries as Fast-Charging Energy Storage. Environ Sci Technol 2020:acs.est.9b05883. doi:10.1021/acs.est.9b05883.

[96] Pavan Kumar Y V., Bhimsingu R. Renewable energy based microgrid system sizing and energy management for green buildings. J Mod Power Syst Clean Energy 2015;3:1–13. doi:10.1007/s40565-015-0101-7.

[97] National Renewable Energy Laboratory. Simple Levelized Cost of Energy (LCOE) Calculator Documentation. Natl Renew Energy Lab 2018.

[98] Hor C-L, Watson SJ, Majithia S. Analyzing the Impact of Weather Variables on Monthly Electricity Demand. IEEE Trans Power Syst 2005;20:2078–85. doi:10.1109/TPWRS.2005.857397.

[99] Solar Investment Tax Credit (ITC) | SEIA 2020. https://www.seia.org/initiatives/solar-investment-tax-credit-itc (accessed January 18, 2021).

[100] Blank J, Deb K. Pymoo: Multi-Objective Optimization in Python. IEEE Access 2020;8:89497–509.

[101] Versaw N. How Long Do Electric Cars Last Compared to Conventional Cars? 2022. https://www.compare.com/electric-cars/guides/how-long-do-electric-cars-last (accessed July 7, 2022).

[102] Jerew B. EV Lifespan: Do They Last as Long as Gasoline Cars? 2021. https://www.lifewire.com/do-evs-last-as-long-as-gasoline-cars-5202392 (accessed July 7, 2022).

[103] National Renewable Energy Laboratory (NREL). National Solar Radiation DataBase 1991-2005: Typical Meterological Year 3. 2015 2015. https://rredc.nrel.gov/solar/old_data/nsrdb/1991-2005/tmy3/ (accessed January 10, 2017).

[104] F. Holmgren W, W. Hansen C, A. Mikofski M. pvlib python: a python package for modeling solar energy systems. J Open Source Softw 2018. doi:10.21105/joss.00884.

[105] Gilman P, Dobos A, Diorio N, Freeman J, Janzou S, Ryberg D. SAM Photovoltaic Model Technical Reference Update. 2016.

[106] Battery Second-Use Repurposing Cost Calculator 2020. https://www.nrel.gov/transportation/b2u-calculator.html (accessed July 28, 2022).

[107] Schmalstieg J, Käbitz S, Ecker M, Sauer DU. A holistic aging model for Li(NiMnCo)O2 based 18650 lithium-ion batteries. J Power Sources 2014. doi:10.1016/j.jpowsour.2014.02.012.

[108] IEC. IEC 61427-1: Secondary Cells and Batteries for Renewable Energy Storage- General Requirements and Methods of Test. Geneva, Switzerland: 2013.

[109] Uddin K, Gough R, Radcliffe J, Marco J, Jennings P. Techno-economic analysis of the viability of residential photovoltaic systems using lithium-ion batteries for energy storage in the United Kingdom. Appl Energy 2017. doi:10.1016/j.apenergy.2017.08.170.

[110] Bare J. TRACI 2.0: The tool for the reduction and assessment of chemical and other environmental impacts 2.0. Clean Technol Environ Policy 2011. doi:10.1007/s10098-010-0338-9.

[111] Frischknecht R, Jungbluth N. Implementation of Life Cycle Impact Assessment Methods. Dubendorf: 2007.

[112] Pre Sustainability. SimaPro Database Manual. 2014. doi:10.1017/CBO9781107415324.004.

[113] Wernet G, Bauer C, Steubing B, Reinhard J, Moreno-Ruiz E, Weidema B. The ecoinvent database version 3 (part I): overview and methodology. Int J Life Cycle Assess 2016;21:1218–30. doi:10.1007/s11367-016-1087-8.

[114] LTS. DATASMART LCI Package (US-EI SimaPro® Library) 2016.

[115] eGRID2019 Summary Tables. 2021.

[116] Kim HC, Wallington TJ, Arsenault R, Bae C, Ahn S, Lee J. Cradle-to-Gate Emissions from a Commercial Electric Vehicle Li-Ion Battery: A Comparative Analysis. Environ Sci Technol 2016;50:7715–22. doi:10.1021/acs.est.6b00830.

[117] Frischknecht R, Jungbluth N. Cumulative energy demand. 2007.

[118] PRé Sustainability. About SimaPro. Https://SimaproCom/About/ 2018.

[119] Moreno Ruiz E, Valsasina L, Brunner F, Symeonidis A, FitzGerald D, Treyer K, et al. Documentation of changes implemented in ecoinvent database v3. 5. Ecoinvent Zürich, Switz 2018.

[120] Kamath D, Arsenault R, Kim HC, Anctil A. Economic and Environmental Feasibility of Second-Life Lithium-Ion Batteries as Fast-Charging Energy Storage. Environ Sci Technol 2020;54. doi:10.1021/acs.est.9b05883.

[121] U.S. Energy Information Administration. Annual Energy Outlook 2019: With projections to 2050. Washington, D. C.: U.S. Energy Information Administration; 2019.

[122] Murphy P. As contentious net metering debates persist across the US, Connecticut and Hawaii show a way forward | Utility Dive 2022. https://www.utilitydive.com/news/as-contentious-net-metering-debates-persist-across-the-us-connecticut-and/624658/ (accessed July 25, 2022).

[123] Mauler L, Duffner F, Zeier WG, Leker J. Battery cost forecasting: a review of methods and results with an outlook to 2050. Energy Environ Sci 2021;14:4712–39. doi:10.1039/D1EE01530C.

[124] Weaver JF. Holistic solar modeling predicts even lower future pricing – pv magazine USA 2022. https://pv-magazine-usa.com/2022/06/07/holistic-solar-modeling-predicts-even-lower-future-pricing/ (accessed September 12, 2022).

[125] Fields S. Are Electricity Prices Going Up or Down? | EnergySage 2022. https://news.energysage.com/residential-electricity-prices-going-up-or-down/ (accessed September 12, 2022).

[126] Houghton B, Salovaara J, Tai H. The future of electricity rate design 2019. https://www.mckinsey.com/industries/electric-power-and-natural-gas/our-insights/solving-the-rate-puzzle-the-future-of-electricity-rate-design (accessed September 12, 2022).

[127] Michigan EIBC Newsletter: New Electrification/Efficiency Tax Credits and More 2022. https://mieibc.org/michigan-eibc-newsletter-new-electrification-efficiency-tax-credits-and-more/ (accessed September 19, 2022).

[128] Lu N, Taylor ZT, Jiang W, Xie Y, Leung LR, Correia J, et al. Climate Change Impacts on Residential and Commercial Loads in the Western U.S. Grid 2008.

[129] Berry C. Space heating and water heating account for nearly two thirds of U.S. home energy use 2018. https://www.eia.gov/todayinenergy/detail.php?id=37433 (accessed September 8,

2022).

[130] Azaza M, Wallin F. Smart meter data clustering using consumption indicators: Responsibility factor and consumption variability. Energy Procedia 2017;142:2236–42. doi:10.1016/j.egypro.2017.12.624.

[131] Chinthavali S, Tansakul V, Lee S, Whitehead M, Tabassum A, Bhandari M, et al. COVID-19 pandemic ramifications on residential Smart homes energy use load profiles. Energy Build 2022;259:111847. doi:10.1016/J.ENBUILD.2022.111847.

[132] Burleyson CD, Rahman A, Rice JS, Smith AD, Voisin N. Multiscale effects masked the impact of the COVID-19 pandemic on electricity demand in the United States. Appl Energy 2021;304:117711. doi:10.1016/J.APENERGY.2021.117711.

[133] Kelly J. Hybrid Will Be The New Work Style, But 72% Of Businesses Lack A Strategy, AT&T's 'Future Of Work' Study Shows n.d. https://www.forbes.com/sites/jackkelly/2022/03/16/hybrid-will-be-the-new-work-style-but-72-of-businesses-lack-a-strategy-atts-future-of-work-study-shows/?sh=1d4392fa3989 (accessed September 15, 2022).

[134] Are Electricity Prices Going Up or Down? 2022. https://news.energysage.com/residential-electricity-prices-going-up-or-down/ (accessed July 29, 2022).

[135] Use of energy explained - U.S. Energy Information Administration (EIA) n.d. https://www.eia.gov/energyexplained/use-of-energy/ (accessed August 5, 2022).

[136] Naspetti S, Mandolesi S, Zanoli R. Using visual Q sorting to determine the impact of photovoltaic applications on the landscape. Land Use Policy 2016;57:564–73. doi:10.1016/J.LANDUSEPOL.2016.06.021.

[137] Strazzera E, Statzu V. Fostering photovoltaic technologies in Mediterranean cities: Consumers' demand and social acceptance. Renew Energy 2017;102:361–71. doi:10.1016/J.RENENE.2016.10.056.

[138] Strong S. Building Integrated Photovoltaics (BIPV) | WBDG - Whole Building Design Guide 2016. https://www.wbdg.org/resources/building-integrated-photovoltaics-bipv (accessed August 5, 2022).

[139] Zhang T, Wang M, Yang H. A review of the energy performance and life-cycle assessment of building-integrated photovoltaic (BIPV) systems. Energies 2018;11. doi:10.3390/en11113157.

[140] Traverse CJ, Pandey R, Barr MC, Lunt RR. Emergence of highly transparent photovoltaics for distributed applications. Nat Energy 2017;2:849–60. doi:10.1038/s41560-017-0016-9.

[141] Lunt RR, Bulovic V. Transparent, near-infrared organic photovoltaic solar cells for window

and energy-scavenging applications. Appl Phys Lett 2011;98:3–5. doi:10.1063/1.3567516.

[142] Suddard-Bangsund J, Traverse CJ, Young M, Patrick TJ, Zhao Y, Lunt RR. Organic Salts as a Route to Energy Level Control in Low Bandgap, High Open-Circuit Voltage Organic and Transparent Solar Cells that Approach the Excitonic Voltage Limit. Adv Energy Mater 2016;6:1501659. doi:10.1002/aenm.201501659.

[143] Organic Photovoltaics Research | Department of Energy n.d. https://www.energy.gov/eere/solar/organic-photovoltaics-research (accessed June 21, 2022).

[144] Feng X, Yan D, Hong T. Simulation of occupancy in buildings. Energy Build 2015. doi:10.1016/j.enbuild.2014.11.067.

[145] Water & Energy – California Agricultural Water Stewardship Initiative n.d. http://agwaterstewards.org/practices/water_energy/ (accessed August 5, 2022).

[146] Manley T. California Agriculture – A State of Abundance - Northern California Water Association 2017. https://norcalwater.org/2017/08/04/california-agriculture-a-state-of-abundance/ (accessed August 5, 2022).

[147] Kasler D. More California farmland could vanish as water shortages loom beyond drought. Sacramento Bee 2015.

[148] Comparison of Solar Power Potential by State n.d. https://neo.ne.gov/programs/stats/inf/201.htm (accessed August 5, 2022).

[149] Net Energy Metering n.d. https://www.cpuc.ca.gov/industries-and-topics/electrical-energy/demand-side-management/net-energy-metering (accessed August 5, 2022).

[150] Barron-Gafford GA, Pavao-Zuckerman MA, Minor RL, Sutter LF, Barnett-Moreno I, Blackett DT, et al. Agrivoltaics provide mutual benefits across the food–energy–water nexus in drylands. Nat Sustain 2019 29 2019;2:848–55. doi:10.1038/s41893-019-0364-5.

[151] Karandeh R, Prendergast W, Cecchi V. Optimal Scheduling of Battery Energy Storage Systems for Solar Power Smoothing. Conf Proc - IEEE SOUTHEASTCON 2019;2019-April. doi:10.1109/SOUTHEASTCON42311.2019.9020340.

[152] Saez-De-Ibarra A, Martinez-Laserna E, Stroe DI, Swierczynski M, Rodriguez P. Sizing Study of Second Life Li-ion Batteries for Enhancing Renewable Energy Grid Integration. IEEE Trans. Ind. Appl., vol. 52, 2016, p. 4999–5007. doi:10.1109/TIA.2016.2593425.

[153] Patil BR, Mirsafaei M, Cielecki PP, Cauduro ALF, Fiutowski J, Rubahn HG, et al. ITO with embedded silver grids as transparent conductive electrodes for large area organic solar cells. Nanotechnology 2017. doi:10.1088/1361-6528/aa820a.

[154] DeForest N, Shehabi A, O'Donnell J, Garcia G, Greenblatt J, Lee ES, et al. United States energy and CO2 savings potential from deployment of near-infrared electrochromic window glazings. Build Environ 2015;89:107–17. doi:10.1016/j.buildenv.2015.02.021.

[155] Shukla S, Lee E, Lunt RR, Anctil A. Evaluating the Electricity Production and Energy Saving from Transparent Photovoltaics for Windows in Commercial Buildings. 2019 IEEE 46th Photovolt. Spec. Conf., IEEE; 2019, p. 0567–71. doi:10.1109/PVSC40753.2019.8980609.

[156] Traverse CJ, Chen P, Lunt RR. Lifetime of Organic Salt Photovoltaics. Adv Energy Mater 2018;8:1703678. doi:10.1002/aenm.201703678.

[157] Mendon V V, Taylor ZT, Rao SU, Xie YL. 2015 IECC Determination of Energy Savings: Preliminary Technical Analysis. 2014.

[158] United States Environmental Protection Agency. Emissions & Generation Resource Integrated Database (eGRID) 2020. https://www.epa.gov/energy/emissions-generation-resource-integrated-database-egrid (accessed March 3, 2020).

[159] Climate at a Glance | National Centers for Environmental Information (NCEI) 2019. https://www.ncdc.noaa.gov/cag/statewide/time-series (accessed November 6, 2019).

[160] Blair N, Dobos AP, Freeman J, Neises T, Wagner M, Ferguson T, et al. System Advisor Model, SAM 2014.1.14: General Description. Golden, CO (United States): 2014. doi:10.2172/1126294.

[161] Energy Plus Version 8.9.0 Documentation. 2018.

[162] Mateus NM, Pinto A, Da Graça GC. Validation of EnergyPlus thermal simulation of a double skin naturally and mechanically ventilated test cell. Energy Build 2014;75:511–22. doi:10.1016/J.ENBUILD.2014.02.043.

[163] Im P, New JR, Joe J. Empirical Validation of Building Energy Modeling using Flexible Research Platform n.d. doi:10.26868/25222708.2019.210263.

[164] Rudié E, Thornton A, Rajendra N, Kerrigan S. System Advisor Model Analysis of 100 sites 2014.

[165] Blair N, Dobos A, Sather N. Case Studies Comparing System Advisor Model (SAM) Results to Real Performance Data: Preprint 2012.

[166] National Renewable Energy Laboratory. National Solar Radiation Data Base 1991- 2005 Update: Typical Meteorological Year 3 n.d.

[167] Deru M, Field K, Studer D, Benne K, Griffith B, Torcellini P, et al. U.S. Department of Energy Commercial Reference Building Models of the National Building Stock. 2011.

[168] Han C, Yang H, Chen M, Su Q, Feng W, Li F. Mitochondria-Targeted Near-Infrared Fluorescent Off–On Probe for Selective Detection of Cysteine in Living Cells and in Vivo. ACS Appl Mater Interfaces 2015;7:27968–75. doi:10.1021/acsami.5b10607.

[169] Romanato P, Duttwyler S, Linden A, Baldridge KK, Siegel JS. Intramolecular Halogen Stabilization of Silylium Ions Directs Gearing Dynamics. J Am Chem Soc 2010;132:7828–9. doi:10.1021/ja9109665.

[170] Anctil A, Babbitt CW, Raffaelle RP, Landi BJ. Cumulative energy demand for small molecule and polymer photovoltaics. Prog Photovoltaics Res Appl 2013;21:1541–54. doi:10.1002/pip.2226.

[171] Photochemical oxidation potential. n.d.

[172] Klöpffer W. The Hitch Hiker´s Guide to LCA - An orientation in LCA methodology and application. Int J Life Cycle Assess 2006;11:142–142. doi:10.1065/LCA2006.02.008.

[173] Manahan S. Fundamentals of Environmental Chemistry, Third Edition - Stanley E. Manahan - Google Books. Third. Taylor and Francis; 1994.

[174] Adeeb F, Shooter D. Ozone highs and lows in Auckland. NIWA Water Atmos 2002;10.

[175] Dincer I, Abu-Rayash A. Sustainability modeling. Energy Sustain 2020:119–64. doi:10.1016/B978-0-12-819556-7.00006-1.

[176] Farinha C, Brito J de, Veiga M Do. Life cycle assessment. Eco-Efficient Render Mortars 2021:205–34. doi:10.1016/B978-0-12-818494-3.00008-8.

[177] Van Oers L, Guinée J, Giurco D, Schmidt M. The Abiotic Depletion Potential: Background, Updates, and Future. Resour 2016, Vol 5, Page 16 2016;5:16. doi:10.3390/RESOURCES5010016.

[178] Simapro from PreSustainability n.d. https://simapro.com/about/ (accessed January 31, 2022).

[179] Accardo A, Dotelli G, Musa ML, Spessa E. Life cycle assessment of an NMC battery for application to electric light-duty commercial vehicles and comparison with a sodium-nickel-chloride battery. Appl Sci 2021;11:1–32. doi:10.3390/app11031160.

[180] Wernet G, Bauer C, Steubing B, Reinhard J, Moreno-Ruiz E, Weidema B. The ecoinvent database version 3 (part I): overview and methodology. Int J Life Cycle Assess 2016. doi:10.1007/s11367-016-1087-8.

[181] Bloomberg New Energy Finance. Lithium-Ion Battery Recycling : 2 Million Tons by 2030. 2019.

[182] Wilcox S, Marion W. Users manual for TMY3 data sets. Renew Energy 2008. doi:NREL/TP-581-43156.

[183] Schoenwald D, Ellison J. Determination of Duty Cycle for Energy Storage Systems in a Renewables (Solar) Firming Application 2016.

[184] Atif A, Khalid M. Saviztky-Golay Filtering for Solar Power Smoothing and Ramp Rate Reduction Based on Controlled Battery Energy Storage. IEEE Access 2020;8:33806–17. doi:10.1109/ACCESS.2020.2973036.

[185] Barbose GL, Darghouth N, O'shaughnessy E. Distributed Solar 2020 Data Update. 2020.

[186] Sengupta M, Xie Y, Lopez A, Habte A, Maclaurin G, Shelby J. The National Solar Radiation Data Base (NSRDB). Renew Sustain Energy Rev 2018. doi:10.1016/j.rser.2018.03.003.

[187] Schneider D. Control algorithms for large-scale single-axis photovoltaic trackers. Acta Polytech 2012. doi:10.14311/1648.

[188] Jordan DC, Kurtz SR, VanSant K, Newmiller J. Compendium of photovoltaic degradation rates. Prog Photovoltaics Res Appl 2016. doi:10.1002/pip.2744.

[189] Photovoltaic Module Soiling Map | Photovoltaic Research | NREL 2017. https://www.nrel.gov/pv/soiling.html (accessed July 29, 2020).

[190] Feldman D, Margolis R. Q4 2019/Q1 2020 Solar Industry Update. 2019.

[191] Bawaneh K, Nezami FG, Rasheduzzaman M, Deken B. Energy Consumption Analysis and Characterization of Healthcare Facilities in the United States. Energies 2019, Vol 12, Page 3775 2019;12:3775. doi:10.3390/EN12193775.

[192] Hu Z, He W, Ji J, Hu D, Lv S, Chen H, et al. Comparative study on the annual performance of three types of building integrated photovoltaic (BIPV) Trombe wall system. Appl Energy 2017;194:81–93. doi:10.1016/J.APENERGY.2017.02.018.

[193] Mandalaki M, Zervas K, Tsoutsos T, Vazakas A. Assessment of fixed shading devices with integrated PV for efficient energy use. Sol Energy 2012;86:2561–75. doi:10.1016/J.SOLENER.2012.05.026.

[194] Ding G, Clavero C. Silver-Based Low-Emissivity Coating Technology for Energy- Saving Window Applications. Mod Technol Creat Thin-Film Syst Coatings 2017. doi:10.5772/67085.

[195] Miyazaki T, Akisawa A, Kashiwagi T. Energy savings of office buildings by the use of semi-transparent solar cells for windows. Renew Energy 2005;30:281–304.

doi:10.1016/j.renene.2004.05.010.

[196] Lam JC, Li DHW. An analysis of daylighting and solar heat for cooling-dominated office buildings. Sol Energy 1999;65:251–62. doi:10.1016/S0038-092X(98)00136-4.

[197] Ng PK, Mithraratne N. Lifetime performance of semi-transparent building-integrated photovoltaic (BIPV) glazing systems in the tropics. Renew Sustain Energy Rev 2014. doi:10.1016/j.rser.2013.12.044.

[198] Radhi H. Energy analysis of façade-integrated photovoltaic systems applied to UAE commercial buildings. Sol Energy 2010;84:2009–21. doi:10.1016/J.SOLENER.2010.10.002.

[199] Harris C, LaFrance M, Sawyer K. Emerging Technologies Research and Development - Research and Development Opportunities Report for Windows. 2020.

[200] Raugei M, Bargigli S, Ulgiati S. Life cycle assessment and energy pay-back time of advanced photovoltaic modules: CdTe and CIS compared to poly-Si. Energy 2007;32:1310–8. doi:10.1016/J.ENERGY.2006.10.003.

[201] Alsema EA. Environmental Impacts of PV Electricity Generation-A Critical Comparison of Energy Supply Options. 21st Euopean Photovolt. Sol. Energy Conf., 2006.

[202] Sorgato MJ, Schneider K, Rüther R. Technical and economic evaluation of thin-film CdTe building-integrated photovoltaics (BIPV) replacing façade and rooftop materials in office buildings in a warm and sunny climate. Renew Energy 2018;118:84–98. doi:10.1016/J.RENENE.2017.10.091.

[203] Aste N, Del Pero C, Leonforte F. The first Italian BIPV project: Case study and long-term performance analysis. Sol Energy 2016;134:340–52. doi:10.1016/J.SOLENER.2016.05.010.

[204] Wang W, Liu Y, Wu X, Xu Y, Yu W, Zhao C, et al. Environmental assessments and economic performance of BAPV and BIPV systems in Shanghai. Energy Build 2016;130:98–106. doi:10.1016/J.ENBUILD.2016.07.066.

[205] Hammond GP, Harajli HA, Jones CI, Winnett AB. Whole systems appraisal of a UK Building Integrated Photovoltaic (BIPV) system: Energy, environmental, and economic evaluations. Energy Policy 2012;40:219–30. doi:10.1016/J.ENPOL.2011.09.048.

[206] Energy Storage Roadmap for Michigan. 2022.

[207] State of Michigan 98th Legislature Regular Session of 2016. https://www.legislature.mi.gov/documents/2015-2016/publicact/pdf/2016-PA-0342.pdf; 2016.

[208] Perez M, Perez R, Rábago KR, Putnam M. Overbuilding & curtailment: The cost-effective enablers of firm PV generation. Sol Energy 2019;180:412–22. doi:10.1016/J.SOLENER.2018.12.074.

[209] Nyberg M. California Solar Energy Statistics and Data n.d. https://ww2.energy.ca.gov/almanac/renewables_data/solar/index_cms.php#pvThermal (accessed June 8, 2022).

[210] Shah A. Emergency Economic Stabilization Act of 2008. Harvard J Legis 2009;46.

[211] " Solar Investment Tax Credit (ITC) 2019.

[212] Decision adopting successor to net energy metering tariff. 2014.

[213] Drury E, Lopez A, Denholm P, Margolis R. Relative performance of tracking versus fixed tilt photovoltaic systems in the USA. Prog Photovoltaics Res Appl 2014;22:1302–15. doi:10.1002/PIP.2373.

[214] Marks G, Wilcox E, Olsen D, Goli S. Opportunities for Demand Response in California Agricultural Irrigation: A Scoping Study 2013:82.

[215] Stid JT, Shukla S, Anctil A, Kendall AD, Rapp J, Hyndman DW. Solar array placement, electricity generation, and cropland displacement across California's Central Valley. Sci Total Environ 2022:155240. doi:10.1016/J.SCITOTENV.2022.155240.

[216] Stein J. 2021 Q1 Project Report: PV Performance Modeling and Stakeholder Engagement. 2021.

[217] Barbose G, Darghouth N, Elmallah S, Forrester S, Lacommare K, Millstein D, et al. Tracking the Sun Primary -Pricing and Design Trends for Distributed Photovoltaic Systems in the United States 2019 Edition. 2019.

[218] Data Explorer | Climate Watch 2022. https://www.climatewatchdata.org/data-explorer/historical-emissions?historical-emissions-data-sources=cait&historical-emissions-gases=co2&historical-emissions-regions=All Selected&historical-emissions-sectors=total-including-lucf%2Ctransportation&page=1&sort_col=country&sort_dir=ASC (accessed January 1, 2022).

[219] Skidmore Z. Electric vehicle sales surge in 2021 - Power Technology 2021. https://www.power-technology.com/news/electric-vehicle-sales-surge-in-2021/ (accessed January 1, 2022).

[220] Petroni G, Holger D. Can E-Fuels Save the Combustion Engine? - WSJ. Wall Str J 2021.

[221] Searle S. E-fuels won't save the internal combustion engine | International Council on Clean

Transportation. Int Counc Clean Transp 2020. https://theicct.org/blog/staff/e-fuels-will-not-save-ice (accessed January 1, 2022).

[222] Birol F. Net Zero by 2050 - A Roadmap for the Global Energy Sector. 2021.

[223] Watari T, McLellan BC, Giurco D, Dominish E, Yamasue E, Nansai K. Total material requirement for the global energy transition to 2050: A focus on transport and electricity. Resour Conserv Recycl 2019;148:91–103. doi:10.1016/J.RESCONREC.2019.05.015.

[224] Carrara S, Dias A, Plazotta B, Pavel C. Raw materials demand for wind and solar PV technologies in the transition towards a decarbonised energy system 2020. doi:10.2760/160859.

[225] Zhu Y, Skerlos S, Xu M, Cooper DR. Reducing Greenhouse Gas Emissions from U.S. Light-Duty Transport in Line with the 2 °C Target. Environ Sci Technol 2021;55:9326–38. doi:10.1021/acs.est.1c00816.

[226] Milovanoff A, Posen ID, MacLean HL. Electrification of light-duty vehicle fleet alone will not meet mitigation targets. Nat Clim Chang 2020 1012 2020;10:1102–7. doi:10.1038/s41558-020-00921-7.

[227] Global EV Outlook 2019 – Analysis - IEA n.d. https://www.iea.org/reports/global-ev-outlook-2019 (accessed May 27, 2022).

[228] Annual Energy Outlook 2021. 2021.

[229] National Renewable Energy Laboratory (NREL). Renewable Electricity Futures Study. US Dep Energy 2012.

[230] Brinkman G, Bain D, Buster G, Draxl C, Das P, Ho J, et al. North American Renewable Integration Study- A U.S. perspective. Denver, CO: 2021. doi:NREL/TP-6A20-79224.

[231] Jacobson MZ, Delucchi MA, Cameron MA, Mathiesen B V. Matching demand with supply at low cost in 139 countries among 20 world regions with 100% intermittent wind, water, and sunlight (WWS) for all purposes. Renew Energy 2018;123:236–48. doi:10.1016/J.RENENE.2018.02.009.

[232] Why adding fuel credits to vehicle standards is a bad idea | Transport & Environment n.d. https://www.transportenvironment.org/publications/why-adding-fuel-credits-vehicle-standards-bad-idea (accessed August 15, 2021).

[233] Long-Duration Energy Storage to Support the Grid of the Future | Department of Energy n.d. https://www.energy.gov/articles/long-duration-energy-storage-support-grid-future (accessed August 15, 2021).

[234] Raugei M, Leccisi E, Fthenakis VM. What Are the Energy and Environmental Impacts of

Adding Battery Storage to Photovoltaics? A Generalized Life Cycle Assessment. Energy Technol 2020;8:1901146. doi:10.1002/ENTE.201901146.

[235] Rinaldi KZ, Dowling JA, Ruggles TH, Caldeira K, Lewis NS. Wind and Solar Resource Droughts in California Highlight the Benefits of Long-Term Storage and Integration with the Western Interconnect. Environ Sci Technol 2021;55:6214–26. doi:10.1021/ACS.EST.0C07848.

[236] van de Ven DJ, Capellan-Peréz I, Arto I, Cazcarro I, de Castro C, Patel P, et al. The potential land requirements and related land use change emissions of solar energy. Sci Rep 2021;11:2907. doi:10.1038/s41598-021-82042-5.

[237] Fthenakis V, Leccisi E. Updated sustainability status of crystalline silicon-based photovoltaic systems: Life-cycle energy and environmental impact reduction trends. Prog Photovoltaics Res Appl 2021. doi:10.1002/PIP.3441.

[238] GeoHack - Geographic Center of the Contiguous United States n.d. https://geohack.toolforge.org/geohack.php?pagename=Geographic_center_of_the_United_States&params=39_50_N_98_35_W_region:US-KS_type:landmark&title=Geographic+Center+of+the+Contiguous+United+States (accessed May 30, 2022).

[239] Frischknecht R, Stolz P, Krebs L, Wild-Scholten M, Sinha P. Life Cycle Inventories and Life Cycle Assessments of Photovoltaic Systems - IEA-PVPS. 2020. doi:978-3-907281-14-7.

[240] Fthenakis V, Kim HC. Land use and electricity generation: A life-cycle analysis. Renew Sustain Energy Rev 2009;13:1465–74. doi:10.1016/J.RSER.2008.09.017.

[241] Wachs E, Engel B. Land use for United States power generation: A critical review of existing metrics with suggestions for going forward. Renew Sustain Energy Rev 2021;143:110911. doi:10.1016/J.RSER.2021.110911.

[242] Electric Power Monthly - U.S. Energy Information Administration (EIA) n.d. https://www.eia.gov/electricity/monthly/epm_table_grapher.php?t=epmt_6_07_b (accessed August 15, 2021).

[243] Alsaleh A, Sattler M. Comprehensive life cycle assessment of large wind turbines in the US. Clean Technol Environ Policy 2019 214 2019;21:887–903. doi:10.1007/S10098-019-01678-0.

[244] Haapala KR, Prempreeda P. Comparative life cycle assessment of 2.0 MW wind turbines. Int J Sustain Manuf 2014;3:170–85. doi:10.1504/IJSM.2014.062496.

[245] Alves Dias P, Bobba S, Carrara S, Plazzotta B, European Commission. Joint Research Centre. The role of rare earth elements in wind energy and electric mobility : an analysis of

future supply/demand balances. n.d.

[246] Fishman T, Graedel TE. Impact of the establishment of US offshore wind power on neodymium flows. Nat Sustain 2019 24 2019;2:332–8. doi:10.1038/s41893-019-0252-z.

[247] Ballinger B, Schmeda-Lopez D, Kefford B, Parkinson B, Stringer M, Greig C, et al. The vulnerability of electric-vehicle and wind-turbine supply chains to the supply of rare-earth elements in a 2-degree scenario. Sustain Prod Consum 2020;22:68–76. doi:10.1016/J.SPC.2020.02.005.

[248] Hoenderdaal S, Tercero Espinoza L, Marscheider-Weidemann F, Graus W. Can a dysprosium shortage threaten green energy technologies? Energy 2013;49:344–55. doi:10.1016/J.ENERGY.2012.10.043.

[249] Du X, Graedel TE. Global In-Use Stocks of the Rare Earth Elements: A First Estimate. Environ Sci Technol 2011;45:4096–101. doi:10.1021/ES102836S.

[250] Bolinger M, Bolinger G. Land Requirements for Utility-Scale PV: An Empirical Update on Power and Energy Density. IEEE J Photovoltaics 2022;12:589–94. doi:10.1109/JPHOTOV.2021.3136805.

[251] Amatya R, Brushett F, Campanella A, Kavlak G, Macko J, Maurano A, et al. The Future of Solar Energy. 2015.

[252] Kelly TD, Matos GR. Copper statistics - Historical Statistics for Mineral and Material Commodities in the United States. US Geol Surv Data Ser 140 2014;2006:1–5.

[253] Lee G. The aluminum can: America's most successful recycling story that you've never heard-Greenbiz 2019. https://www.greenbiz.com/article/aluminum-can-americas-most-successful-recycling-story-youve-never-heard (accessed December 28, 2021).

[254] Lennon A, Lunardi M, Hallam B, Dias PR. The aluminium demand risk of terawatt photovoltaics for net zero emissions by 2050. Nat Sustain 2022. doi:10.1038/s41893-021-00838-9.

[255] Goonan T. USGS Circular 1196-X: Copper Recycling in the United States in 2004. 2004.

[256] Copper & the Environment: Copper - The World's Most Reusable Resource 2021. https://www.copper.org/environment/lifecycle/g_recycl.html (accessed December 29, 2021).

[257] Ardani K, Denholm P, Mai T, Margolis R, Silverman T, Zuboy J. Solar Futures Study. 2021.

[258] Morgan H. Polysilicon woes will end within 18 months, says Rethink 2022. https://rethinkresearch.biz/articles/polysilicon-woes-will-end-within-18-months-says-rethink/ (accessed September 19, 2022).

[259] Binnemans K, Jones PT, Müller T, Yurramendi L. Rare Earths and the Balance Problem: How to Deal with Changing Markets? J Sustain Metall 2018;4:126–46. doi:10.1007/s40831-018-0162-8.

[260] Department of Environment M, Lakes G. MI Healthy Climate Plan 2022.

[261] Clean Energy Standard (CES) - NYSERDA n.d. https://www.nyserda.ny.gov/All-Programs/clean-energy-standard (accessed June 3, 2022).

[262] Widmer JD, Martin R, Kimiabeigi M. Electric vehicle traction motors without rare earth magnets. Sustain Mater Technol 2015;3:7–13. doi:10.1016/J.SUSMAT.2015.02.001.

[263] Rippel W. Induction Versus DC Brushless Motors | Tesla 2007. https://www.tesla.com/blog/induction-versus-dc-brushless-motors (accessed January 8, 2022).

[264] Dang DH, Thompson KA, Ma L, Nguyen HQ, Luu ST, Duong MTN, et al. Toward the Circular Economy of Rare Earth Elements: A Review of Abundance, Extraction, Applications, and Environmental Impacts. Arch Environ Contam Toxicol 2021;81:521–30. doi:10.1007/S00244-021-00867-7/FIGURES/3.

[265] Olivetti EA, Ceder G, Gaustad GG, Fu X. Lithium-Ion Battery Supply Chain Considerations: Analysis of Potential Bottlenecks in Critical Metals. Joule 2017;1:229–43. doi:10.1016/j.joule.2017.08.019.

[266] E-fuels: a solution for the future of green mobility n.d. https://www.engie.com/en/news/e-fuels-what-are-they (accessed September 13, 2022).

[267] Cuffari B. The Applications of e-Fuels 2018. https://www.azom.com/article.aspx?ArticleID=16740 (accessed September 13, 2022).

[268] Global Lithium-Ion (Li-ion) Batteries Market 2022-2026 - n.d. https://www.globenewswire.com/en/news-release/2022/05/17/2444677/28124/en/Global-Lithium-Ion-Li-ion-Batteries-Market-2022-2026-Robust-Outlook-for-EVs-Opens-New-Avenues-of-Growth-for-Li-ion-Batteries-Market.html (accessed August 6, 2022).

[269] Deizel C. 80% Carpet Rule 2016. https://www.landlordology.com/80-percent-carpet-rule/ (accessed December 6, 2017).

[270] Residential Energy Consumption Survey (RECS) - Data - U.S. Energy Information Administration (EIA) 2015. https://www.eia.gov/consumption/residential/data/2001/index.php?view=consumption (accessed October 17, 2019).

[271] Michigan Residential Code 2009.

[272] ASHRAE. Built Environment Today | ashrae.org n.d. https://www.ashrae.org/File Library/docLib/Technology (accessed December 18, 2017).

[273] Califonia Building Energy Efficiency Standards. 2013.

[274] Energy Cost Calculator for Electric and Gas Water Heaters. 2017.

[275] Bureau of Construction codes. Michigan Residential Code 2003. 2003.

[276] Michigan Energy Code. 2015.

[277] Air Leakage Guide. U.S. Department of Energy; 2012.

[278] Fact Sheet on Air Conditioner, Furnace, and Heat Pump Efficiency Standards Agreement. 2009.

[279] HVAC Design Guidliens n.d.

[280] Pfannenstiel J. Building Energy Efficiency Standards. California Energy Commission; 2005.

[281] Brown EG. Residential Compliance Manual for the 2016 Building Energy Efficiency Standards Title 24, Part 6, and Associated Administrative Regulations in Part 1. 2015.

[282] Weisenmiller R. Residential Compliance Manual. California Energy Commission; 2016.

[283] Parker D. Determining Appropriate Heating and Cooling Thermostat Set points for Building Energy Simulations for Residential Buildings in North America. 2013.

[284] Pataki GE. New York State Energy Conservation Construction Code. Albany,NY: New York State Department of State; 1991.

[285] New York City Energy conservation code. Residential Requirements. New York City Department of Buildings; 2011.

[286] Building HVAC Requirements. New York City Department of Buildings; 2011.

[287] Factsheet from coconino county sustainable building program n.d. http://www.coconino.az.gov/DocumentCenter/View/5475 (accessed December 28, 2017).

[288] International Residential Code for One and Two Family Dwellings. International Code Council; 2006.

[289] IECC compliance guide for homes in Oregon. International Energy Conservation code; 2009.

[290] Energy Trust of Oregon New Homes Air Sealing Pilot II Evaluation Report. 2015.

[291] A Guide to Energy-Efficient Heating and Cooling. United States Environmental Protection Agency; 2009.

[292] Residential pricing options for DTE Energy. 2020.

[293] Residential rates for Los Angeles Department of Water and Power. 2020.

[294] Archived rate plan information of Con Edison of New York. 2020.

[295] Residential Time of Use (Saver Choice) TOU-E rate for Arizona Public Service Electric Company 2020. https://apps.openei.org/USURDB/rate/view/5cacc7715457a393487780e2#1__Basic_Information (accessed August 10, 2022).

[296] Residential Time-Of-Service (Rate 7-TOU) for Portland General Electric Company n.d. https://apps.openei.org/USURDB/rate/view/5cc0d8e05457a35039671080#3__Energy (accessed August 10, 2022).

[297] USEPA. eGRID Summary Tables 2016. n.d.

[298] Jungbluth N, Stucki M, Frischknecht R, Büsser S. Photovoltaics. Authors Updat Autor Überarbeitung Niels Jungbluth, ESU-Services Autorin Überarbeitung Lucia Ciseri Autoren Bearb 2010.

[299] Ahmadi L, Young SB, Fowler M, Fraser RA, Achachlouei MA. A cascaded life cycle: reuse of electric vehicle lithium-ion battery packs in energy storage systems. Int J Life Cycle Assess 2017;22:111–24. doi:10.1007/s11367-015-0959-7.

[300] Commodity Flow Survey United States: Shipment Characteristics by Industry for the United States. 2012.

[301] Schoenwald D, Ellison J. SANDIA REPORT Determination of Duty Cycle for Energy Storage Systems in a Renewables (Solar) Firming Application. n.d.

APPENDIX A: Supplementary Information for Chapter 2

A1. Inputs for the building energy modeling

The building energy modeling was carried out in Building Energy Optimization (BEopt) tool. The inputs for BEopt tool were based on the building and energy codes for the selected cities. To model an average house in each location, the version of building code corresponded to one of the years from the decade in which the highest percentage of houses were constructed in that city. The residential building age data was available at the state level. Therefore, the chosen cities were assumed to have same building age distribution as the corresponding states. The building age distribution for each state is mentioned in Table A1 as shown below.

Table A1. Percentage of houses built in study locations with respect the year in which they were built.

State	Houses built Pre-1950 (%)	Houses built b/w 1950-1969 (%)	Houses built b/w 1970-1989 (%)	Houses built b/w 1990-2009 (%)	Reference
Arizona	3	7	40	50	[70]
California	15	30	35	20	[68]
Michigan	30	28	27	15	[67]
New York	38	32	20	10	[69]
Oregon	15	30	35	20	[66]

Structural and thermal recommendations for components such concrete masonry unit were not mentioned in the earlier versions of the building codes. When that was the case for a city, the earliest code mentioning the concerned material/component was used. The tables below (A2-A7) give the detailed inputs entered in BEopt for all the five study locations.

Table A2. Building components and appliances in residential buildings which are same for all the cities.

Component	Material specification /dimension	Special Remarks	Reference
Carpet area	80 %	N/A	[269]
Ceiling fan	3 fans with standard efficiency	N/A	[270]
Clothes dryer	Electric	Standard usage schedule assumed	
Clothes Washer	Standard	Standard usage schedule assumed	
Cooking Range	Electric	Assumed	
Dishwasher	318 rated kWh, 80 % usage of annual average	Assumed	
Door area	20 sq. ft	Assumed	
Electric baseboard	100 % Efficiency	In some cities the baseboard was not part of the house as per the Building code recommendations	
Exterior finish	Light Vinyl		[271]
Hot water fixtures	2	Assumed	
Humidity Set point	60 %		[272]
Interzonal walls	Light Vinyl	Assumed	
Lighting	20 % CFL Hardwired, 34% CFL plugin	Assumed	
Natural ventilation	Year round, 7 days/week	Assumed	
Overhangs	2ft, on all windows	Assumed	
Plug loads		Includes all loads not explicitly defined in the appliances .Formula for plug loads:Annual electric use [kWh/yr]=1108.1+180.2 * (# of bed rooms) +0.278 *(Finished floor area)	
Refrigerator	Top freezer type,	Assumed 100 % usage	
Roof material	Medium tiles (Mottled Terracotta, buff)	Assumed	
Total Window area	132 sq. ft	Assumed default	
Unfinished Attic	Ceiling R-19, Cellulose, Vented	N/A	[67],[273]
Water heating	Standard electric	N/A	[274]

Table A3. Building component and appliance specification for Detroit, Michigan.

Component	Material Dimension/Specification	Remarks	Reference
Area of House	1954 sq. ft	N/A	[67]
Wooden Wall stud	R-19, Fiberglass Batten, 2 x 4, framing spacing=24 inches	NA	[76]
Concrete Masonry Unit	6 inches hollow, R-12, Closed Cell Spray Foam	NA	[275]
Window type	Double Insulated, Air, H-gain Low-E glass	NA	[276]
Air Leakage	3 ACH50 (Air changes per hour at 50 Pascals)	NA	[277]
Central Air Conditioner	SEER 15	NA	[278]
Ducts	20 % Leakage, R-6	NA	[276]
Cooling set point	76 ^{0}F	NA	[279]
Heating set Point	71 ^{0}F	NA	[279]

Table A4. Building component and appliance specification for Los Angeles, California.

Component	Material Dimension/Specification	Remarks	Reference
Area of House	1583 sq. ft	NA	[68]
Wooden Wall stud	R-13, Fiberglass Batten, 2 x 4, framing spacing=16 inches	NA	[280]
Concrete Masonry Unit	8 inches hollow, R-10 XPS	NA	[280]
Window type	Clear, Double, Air		[281]
Air Leakage	3 ACH50 (Air changes per hour at 50 Pascals)	NA	[277]
Central Air Conditioner	SEER 14	NA	[278]
Ducts	20 % Leakage, R-6	NA	[282]
Cooling set point	76 ^{0}F	NA	[283]
Heating set Point	69 ^{0}F	NA	[283]

Table A5. Building component and appliance specification for New York City, New York.

Component	Material Dimension/Specification	Remarks	Reference
Area of House	1832 sq. ft	NA	[69]
Wooden Wall stud	R-7, Fiberglass Batten, 2 x 4, framing spacing=16 inches	NA	[284]
Concrete Masonry Unit	6 inches hollow, R-12 Polyiso type insulation	NA	[284]
Window type	Double insulated, High-E Low-E glass	NA	[285]
Air Leakage	3 ACH50 (Air changes per hour at 50 Pascals)	NA	[277]
Central Air Conditioner	SEER 15	NA	[278]
Ducts	20 % Leakage, R-8	NA	[285]
Cooling set point	75 ^{0}F	NA	[286]
Heating set Point	70 ^{0}F	NA	[286]

Table A6. Building component and appliance specification for Phoenix, Arizona.

Component	Material Dimension/Specification	Remarks	Reference
Area of House	1798 sq. ft	NA	[70]
Wooden Wall stud	R-7, Fiberglass Batten, 2 x 4, framing spacing=16 inches	NA	[76]
Concrete Masonry Unit	6 inches hollow, R-12 Polyiso type insulation	NA	[287]
Window type	Clear, Double thermal-break, Air	Assumed, no recommendation in building code of Arizona	
Air Leakage	1 ACH50 (Air changes per hour at 50 Pascals)	NA	[288]
Central Air Conditioner	SEER 15	NA	[278]
Ducts	20 % Leakage, R-8	NA	[288]
Cooling set point	78 ^{0}F	NA	[278]
Heating set Point	68 ^{0}F	NA	[278]

Table A7. Building component and appliance specification for Portland, Oregon.

Component	Material Dimension/Specification	Remarks	Reference
Area of House	1906 sq. ft	NA	[66]
Wooden Wall stud	R-13, Fiberglass Batten, 2 x 4, framing spacing=16 inches	NA	[289]
Concrete Masonry Unit	8 inches hollow, R-10, XPS insulation	NA	[289]
Window type	Double insulated, High-E Low-E glass		[289]
Air Leakage	3 ACH50 (Air changes per hour at 50 Pascals)	NA	[290]
Central Air Conditioner	SEER 14	NA	[278]
Ducts	20 % Leakage, R-8	NA	[289]
Cooling set point	78 ^{0}F	NA	[291]
Heating set Point	70 ^{0}F	NA	[291]

A2. Electricity prices in selected locations

The time-of-use pricing structures in the chosen study locations was taken from respective utility websites. Table A8 provides the name of the utilities and the references for the pricing structure for each study location.

Table A8. Utility name and pricing structures for the study locations.

Location	Utility	Reference
Detroit	Detroit Edison	[292]
Los Angeles	Los Angeles Department of Water and Power	[293]
New York City	Consolidated Edison	[294]
Phoenix	Arizona Public Service Electric Company	[295]
Portland	Portland General Electric Company	[296]

A3. Inventory data for the life cycle analysis

Table A9. Data sources for materials and energy used in inventory analysis.

	Details	Reference
Electricity	Greenhouse gas emissions of electricity production according to the North American Electric Reliability Corporation (NERC) in 2016	[297]
Photovoltaic system	Installation of 3kWp slanted-roof installation of multi-Si photovoltaic system without inverter for US	[298]
Second life battery	Data for GWP and CED of the enclosure (30%) and pack manufacturing (100%) of a new LIB from Kim et al. (2016) used to obtain second life battery inventory	[116,299]
New lithium-ion battery	Inventory of first life EV battery based on GWP from Kim et al. (2016)	[116]
Inverter	Production of 500W inverter in the US	[298]
Battery transportation	Average transportation distances for electronics in the US: 1,996 t-km by lorry 16-32 metric ton	[300]

The global warming potential (GWP) and cumulative energy demand (CED) of grid electricity for the five selected locations is calculated using [297] and presented in Figure A1.

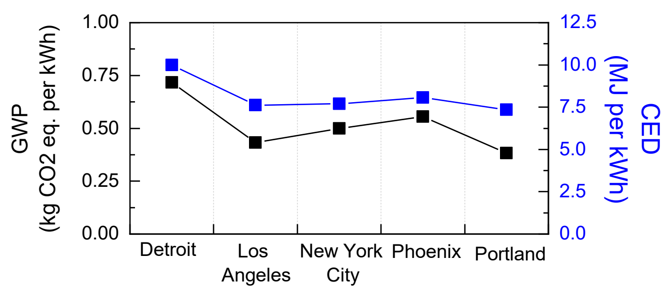

Figure A1. GWP and CED of grid electricity in study locations.

A4. Maximum allowable PV capacities

For 20 house microgrids, the maximum allowable PV capacity is selected as the minimum of the following a) Utility guidelines b) Suitable roof space available for PV installation on rooftop of the 20 houses in the microgrid. The maximum PV capacity used for the optimization exercise in the microgrid study are given in Table A10.

Table A10. Maximum allowable PV capacity used for optimization in 20 house microgrids.

Location	Maximum allowable PV capacity (kW)
Detroit	170 kW
Los Angeles	137 kW
New York City	159 kW
Phoenix	156 kW
Portland	166 kW

The maximum allowable PV capacity for the three selected locations for single house-based home energy storage + EV charging application was similarly derived and is given in Table A11.

Table A11. Maximum allowable PV capacity used for optimization in single house-based home energy storage + EV charging application.

Location	Maximum allowable PV capacity (kW)
Detroit	8.5 kW
New York City	8 kW
Phoenix	7.8 kW

APPENDIX B: Supplementary Information for Chapter 3

B1. Building simulation parameters

The heating and cooling energy demand of the commercial buildings depend on the solar heat gain coefficient (SHGC) calculated based on the window UV-vis spectral characteristics by EnergyPlus 8.9 [1]. The visible transmittance of the windows is also calculated based on the spectral characteristics of the window and shown in Table B1.

Table B1. Solar heat gain coefficient (SHGC) and visible transmittance of the three types of windows considered in this study.

Window type	SHGC	Visible transmittance
Clear glass	0.764	0.812
ClAlPc	0.586	0.643
CyTPFB	0.539	0.686

The heating and cooling energy demand for a commercial building in a given location is determined by heating and cooling energy setpoints. Depending on the building use, some commercial buildings are divided into thermal zones or subsections based on heating and ventilation characteristics from [1]. These setpoints give the suitable range of temperature for each subsection of the building as given in [2–4] .The set point values for the sub-sections of the selected commercial buildings are shown in Table B2.

Table B2. Cooling and heating set-points for the selected commercial buildings and the corresponding subsections to model the heating, ventilation and air conditioning loads.

Building	Subsection	Cooling set point (^{0}C)	Heating set point (^{0}C)
Midrise apartments	Corridor 1	26.6	21.1
	Corridor 2	27.2	15.6
	Corridor 3	27.2	21.1
	Rest of the building	23.9	21.1
Medium office	NA	24.0	21.0
Primary School	NA	24.0	21.0
Large Hotel	NA	24.0	21.0
Hospital	Kitchen	26.0	21.1
	Operating room	18.3	21.1
	Rest of the building	22.2	21.1

For occupancy schedules, each building is divided into zones based on the typical usage on weekdays, weekends and holidays. The occupancy schedule for each commercial building is taken from [5]. The hourly occupancy of different regions of each selected building in the (Table B3-B12).

Midrise apartment

Table B3. Building occupancy (%) for each hour in apartment and office premise of midrise apartment building.

Apartment	Office
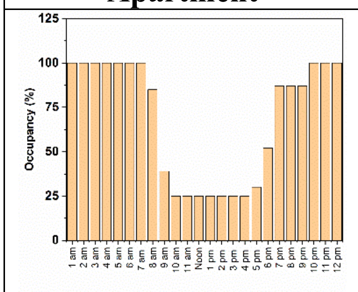	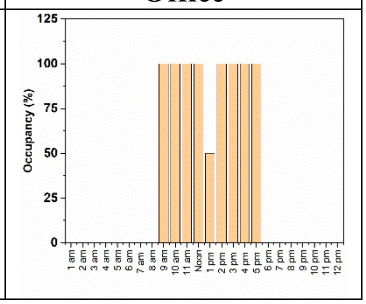

No change in apartment schedule on weekends and 0% occupancy for office on weekends.

Medium office

Table B4. Building occupancy (%) for each hour in medium office on weekdays, Saturday, Sunday, and holidays.

Weekday	Saturday	Sunday and Holiday
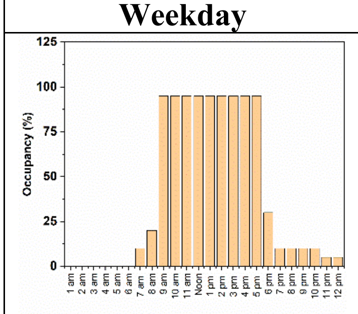	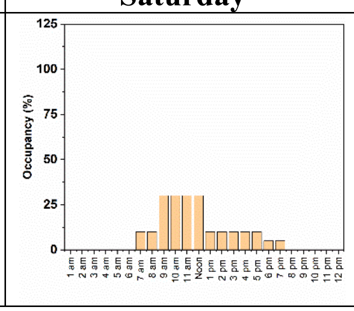	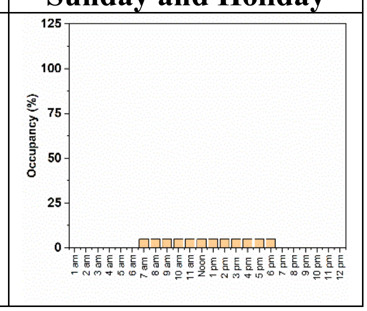

Primary School

Table B5. Building occupancy (%) for each hour in classrooms and study areas of primary schools during study periods and summer.

Study periods	Summer
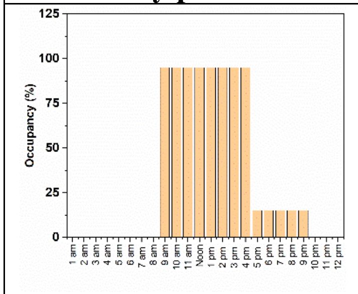	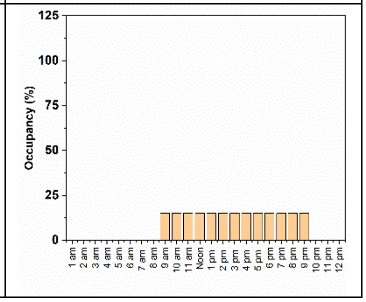

Table B6. Building occupancy (%) for each hour in office areas of primary schools during study periods and summer.

Study periods	Summer
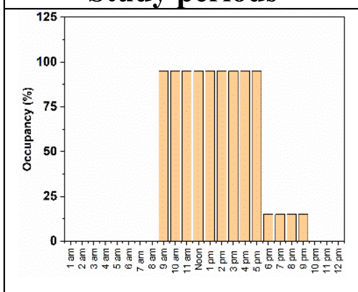	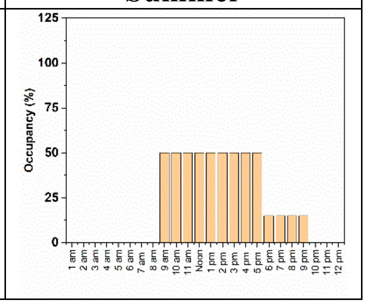

Table B7. Building occupancy (%) for each hour in cafeteria of primary schools during study periods and summer.

Study periods	Summer
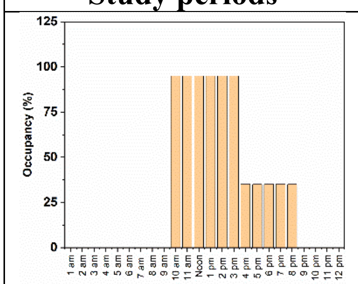	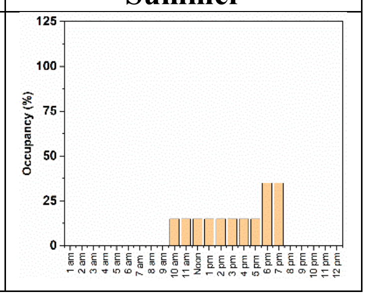

Table B8. Building occupancy (%) for each hour in gym area of primary schools during study periods and summer.

Study periods	Summer
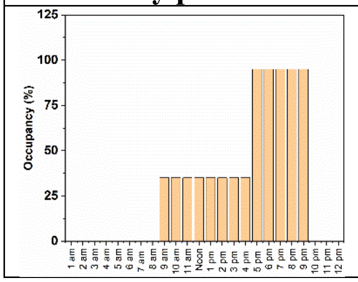	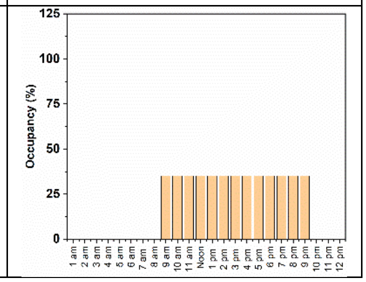

On weekends and holidays the occupancy the primary school is assumed to be 0% throughout the day.

Large hotel

Table B9. Building occupancy (%) for each hour in guest room areas of large hotel building during weekdays, Saturday, Sunday, and holidays.

Weekday	Saturday	Sunday and Holiday
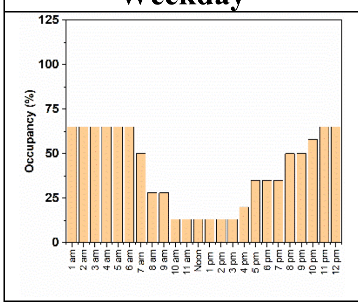	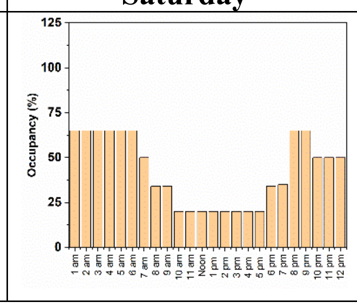	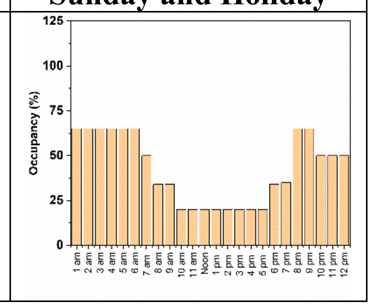

Table B10. Building occupancy (%) for each hour in public spaces of large hotel building during weekdays, Saturday, Sunday, and holidays.

Weekday	Saturday	Sunday and Holiday
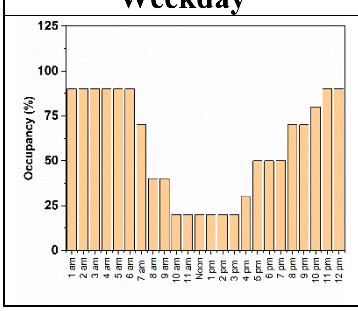	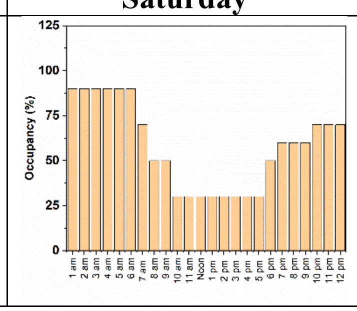	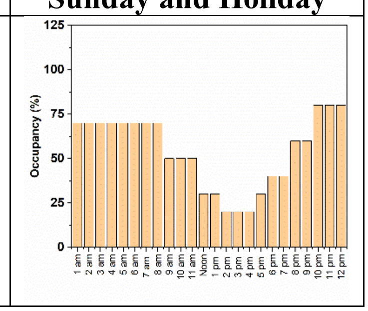

Hospital

Table B11. Building occupancy (%) for each hour in office, lobby, clinic and operation room of hospital building during weekdays, Saturday, Sunday and holidays.

Weekday	Saturday	Sunday and Holiday
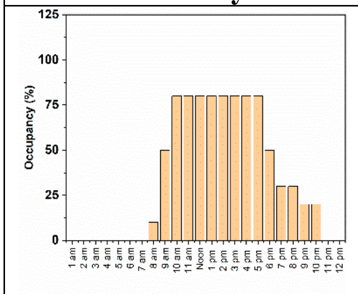	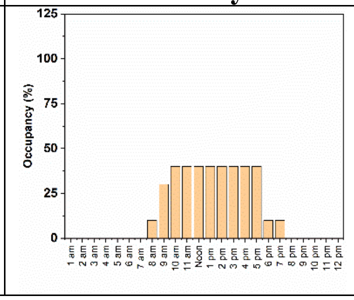	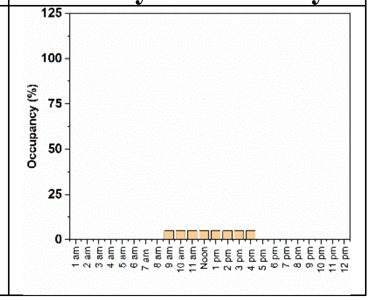

Table B12. Building occupancy (%) for each hour in emergency room, patient room, intensive care unit, nurse station, dining and kitchen of hospital building during weekdays, Saturday, Sunday, and holidays.

Weekday	Saturday	Sunday and Holiday
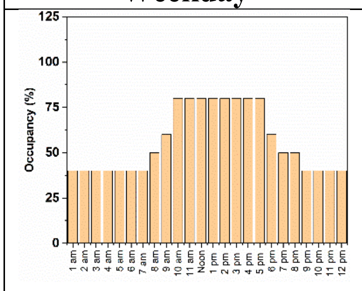	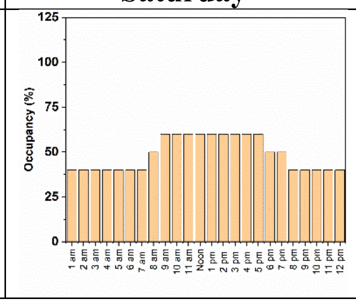	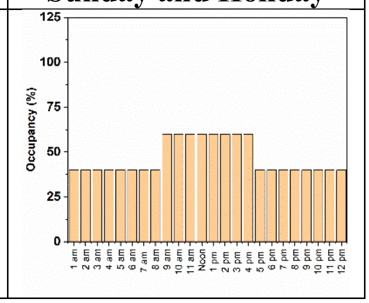

B2. LCA assumptions and processes

Table B13. Data Sources for Materials for LCA.

	Details	**Ref.**
Chloroaluminum phthalocyanine (ClAlPc)	CAS:14154-42-8; synthesis of ClAlPc based on 4:1 ratio of phthalonitrile and aluminum chloride in 1-chlronaphthalene	[6]
Cyanine Heptamethine (ADS815EI)	CAS: not available; identification is available at the reference [7]; synthesis of cy-I based on 2:1 ratio of 1-ethyl-1,2,2-trimethylbenzoindoleninium iodide and 2-chloro-1-formyl-3-(hydroxymethylene)cyclohex-1-ene in acetic anhydride. See Figure B1.	[8]
Potassium tetrakis (pentafluorophenyl)borate (K-TPFB)	CAS:89171-23-3; starting from Bromopentafluorobenzene in diethyl ether and n-Butyllithium added by maintaining temperature at -78°C for 50 min. Then, potassium chloride and D.I. water added into a white suspension in room temperature. See Figure B2.	[9]
Heptamethine-TPFB (Cy-TPFB)	CAS: not available; anion exchange of cyanine heptamethine (Cy-I), from iodide to tetrakis (pentafluorophenyl)borate (TPFB)	[10]
1-ethyl-1,2,2-trimethyl benzoindoleninium iodide	CAS:1640-39-7; 2,3,3-Trimethylbenzoindolenine and iodoethane in toluene heated at 100°C for 20 hours. See Figure B1.	[8]
2,3,3-Trimethylbenzoindolenine	CAS:1640-39-7; reaction of 2-naphthylhydrazine and isopropyl methyl ketone in acetic acid. See Figure B1.	[11]
2-naphthylhydrazine	CAS:2243-57-4; 2-naphthol and hydrazine in autoclave under 60 bar and 85°C for 100 hours. Extracting with dichloromethane and washing with 10% sodium hydroxide. See Figure B1.	[11]
2-naphthol	CAS:135-19-3; heating 2-naphthalenesulfonic acid and sodium hydroxide at 320 °C and precipitating 2-naphthol with concentrated hydrochloric acid. See Figure B1.	[12]
2-naphthalenesulfonic acid	CAS:120-18-3; heating mixture of sulfuric acid and naphthalene at 170 °C for 12 hours and adding CaO. The mixture is filtered, and the calcium salt of the 2-naphthalenesulfonic acid is crystallized. See Figure B1.	[13]
3-Methyl-2-butanone	CAS:598-75-4; stoichiometric calculation of 2-butanone and formaldehyde. See Figure B1.	
Ethyl iodide	CAS:75-03-6; adding iodine into mixture of phosphorus and ethyl alcohol in room temperature for 24 hours and refluxing 2 hours. See Figure B1.	[14]
Potassium acetate	CAS:127-08-2; stoichiometric calculation of acetic acid and potassium hydroxide. See Figure B1.	
Sodium bicarbonate	CAS:144-55-8; Solvay process. See Figure B1.	[15]
2-chloro-1-formyl-3-(hydroxymethylene)cyclohex-1-ene	CAS:61010-04-6; phosphoryl chloride in dichloromethane added in dimethylformamide. Adding cyclohexanone into mixture and refluxing for 2 hours. See Figure B1.	[8]
Butyllithium	CAS:109-72-8; reaction between lithium powder and n-butyl chloride See Figure B2.	[16]
n-butyl chloride	CAS: 109-69-3; reaction between zinc chloride, hydrochloric acid, and butyl alcohol. See Figure B2.	[17]
Zinc chloride	CAS:7646-85-7; stoichiometric calculation of zinc and hydrochloric acid See Figure B2.	
Bromopentafluorobenzene	CAS:344-04-7; bromination of pentafluorobenzene. See Figure B2.	[18]
pentafluorobenzene	CAS:363-72-4; subtraction of fluorine by catalytic reaction. See Figure B2.	[19]
Hexafluorobenzene	CAS:392-56-3; substitution of chlorine to fluorine from hexachlorobenzene. See Figure B2.	[18]
Hexachlorobenzene	CAS:118-74-1; chlorination of benzene. See Figure B2.	[20]
Potassium fluoride	CAS:7789-23-3; stoichiometric calculation of potassium carbonate and hydrogen fluoride. See Figure B2.	

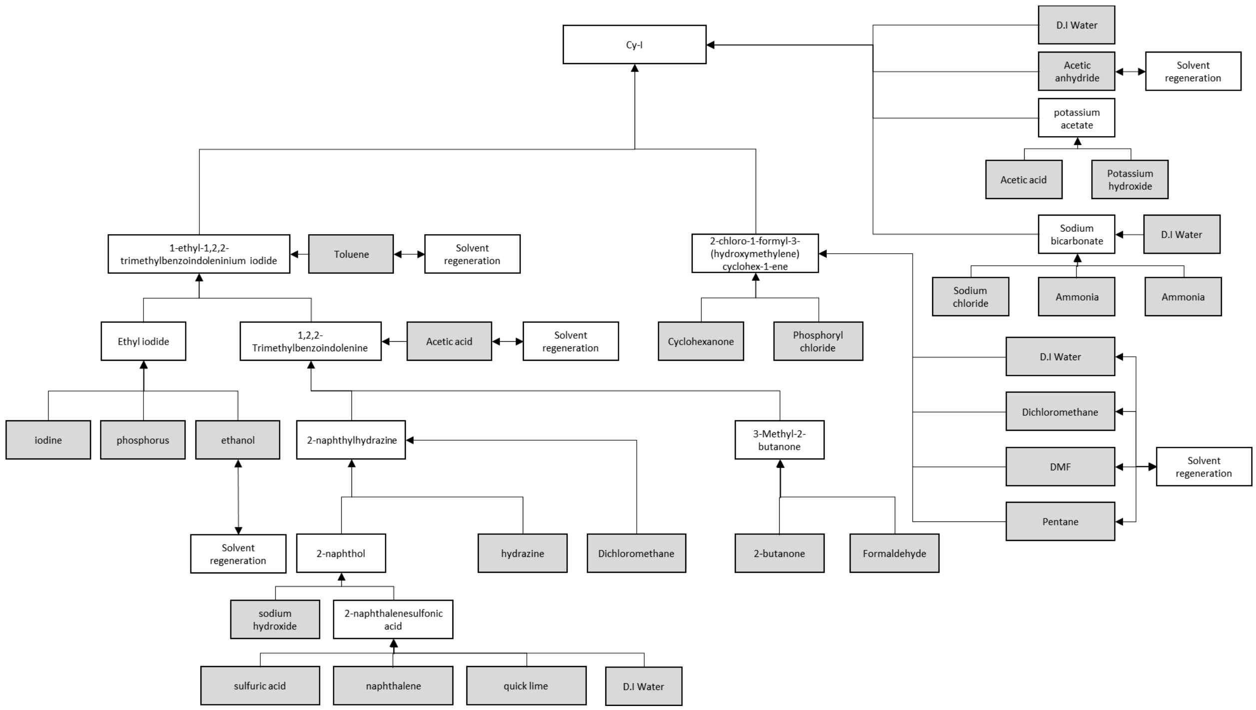

Figure B1. Process flow diagram of cyanine heptamethine.

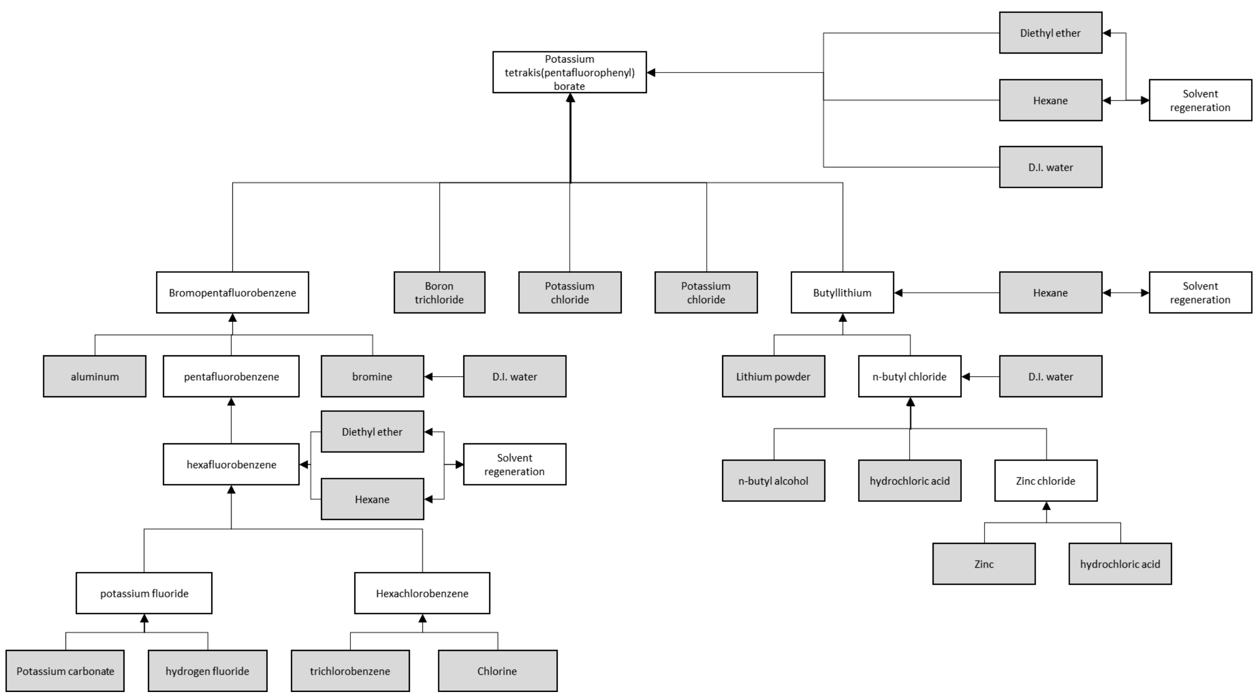

Figure B2. Process flow diagram of Potassium tetrakis (pentafluorophenyl)borate.

B3. Energy conversion efficiency factors from LCA

The supplementary material of [21] summarizes the sources of grid electricity generation in eGRID zones of the selected locations based on [22,23]. The percentage contribution of sources for electricity generation are listed in Table B14.

Table B14. Grid energy source for eGRID zone of each selected location [21].

Unit %	Source	RFCM (Detroit)		CMAX (Los Angeles)		AZNM (Phoenix)		HIOA (Honolulu)	
		2016	**2035**	**2016**	**2035**	**2016**	**2035**	**2016**	**2035**
Fossil	**Coal**	41.5	33.0	4.3	0.0	29.5	22.0	20.7	3.4
	Oil	0.9	0.0	0.1	0.0	0.1	0.0	68.7	11.4
	Gas	31.4	50.0	48.4	22.0	39.8	41.0	0.0	0.0
	Other Fossil	1.9		0.7	0.0	0	0.0	0.9	0.1
	Nuclear	17.5	8.0	9.4	0.0	19.5	17.0	0.0	0.0
Renewable	**Hydro**	0.0	0.3	12.1	17.1	3.5	6.2	0.0	
	Biomass	2.0	0.9	2.9	1.5	0.4	0.2	6.1	5.0
	Wind	4.8	7.6	7	17.8	1.2	2.3	3.2	10.8
	Solar	0.0	0.2	10.6	33.5	2.8	10.2	0.4	69.2
	Geo-thermal	0.0	0.0	4.1	8.0	3.2	1.2	0.0	
	Other	0.0	0.0	0.2	0.0	0	0.0	0.0	

The energy conversion efficiency factors for electricity generation in four locations are taken from [21] based on Table B14. The factors are calculated using LCA for years 2016 and 2035 and values for all other years are calculated using linear interpolation as given in Table B15.

Table B15. Energy conversion efficiency factors for electricity generation in the four selected study locations is shown from 2016-2035.

	Detroit	**Honolulu**	**Los Angeles**	**Phoenix**
2016	0.340	0.277	0.460	0.436
2017	0.339	0.295	0.472	0.438
2018	0.338	0.313	0.484	0.440
2019	0.337	0.331	0.497	0.442
2020	0.337	0.350	0.509	0.444
2021	0.336	0.369	0.521	0.446
2022	0.335	0.387	0.533	0.448
2023	0.334	0.405	0.545	0.450
2024	0.333	0.424	0.558	0.452
2025	0.332	0.442	0.570	0.454
2026	0.332	0.461	0.582	0.456
2027	0.331	0.479	0.594	0.458
2028	0.330	0.498	0.606	0.460
2029	0.329	0.516	0.619	0.462
2030	0.328	0.534	0.631	0.464
2031	0.327	0.553	0.643	0.466
2032	0.326	0.571	0.655	0.468
2033	0.326	0.590	0.668	0.470
2034	0.325	0.608	0.680	0.472
2035	0.324	0.626	0.692	0.474

The energy conversion efficiency factor for natural gas generation in the U.S. (η_{NG}=0.7663) is also taken from [21].

B4. References for the cumulative energy demand vs. efficiency figure

Table B16. References for the cumulative energy demand and power conversion efficiency data for different PV technologies given in the main text.

Type of photovoltaic module	**Source**
TOPV-CyTPFB	This study
TOPV-ClAlPc	[21]
c-Si	[24]
mc-Si	[24]
Organic	[25]
CIGS	[24]
CdTe	[24]

B5. Electricity and natural gas process for the selected locations

Table B17. Electricity and natural gas prices for the selected locations.

Location	Electricity price (¢/kWh)	Natural gas price ($/thousand cubic feet)
Detroit	10.64	6.97
Los Angeles	15.07	8.77
Phoenix	10.41	8.89
Honolulu	24.64	29.62

The inflation was taken as 2%.

B6. Avoided cost and GHGs with ClAlPc TOPVs

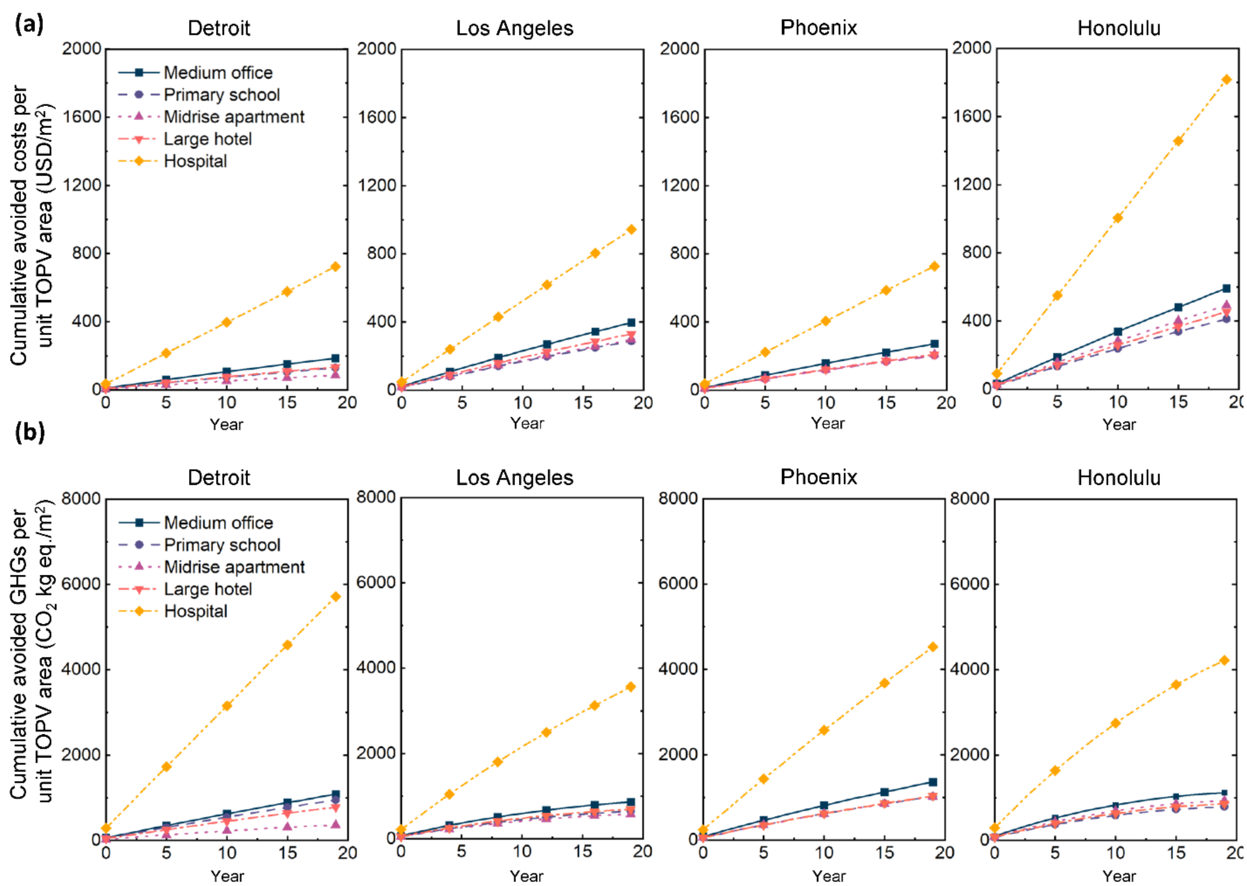

Figure B3. The (a) cumulative avoided cost per unit TOPV area (USD/m^2), and (b) cumulative avoided greenhouse gas (GHG) emissions per unit TOPV area (CO_2 kg eq./m^2) over 20 years in five commercial buildings across the four U.S. locations when the clear glass windows are replaced with ClAlPc TOPV windows.

B7. Duty cycle used for utility-level PV firming applications

The duty cycle for firming applications given by Sandia National Laboratories [301] was used to simulate the minute by minute change in the PV output from utility level plant. The 1-second duty cycle used for this study is shown in Figure B4.

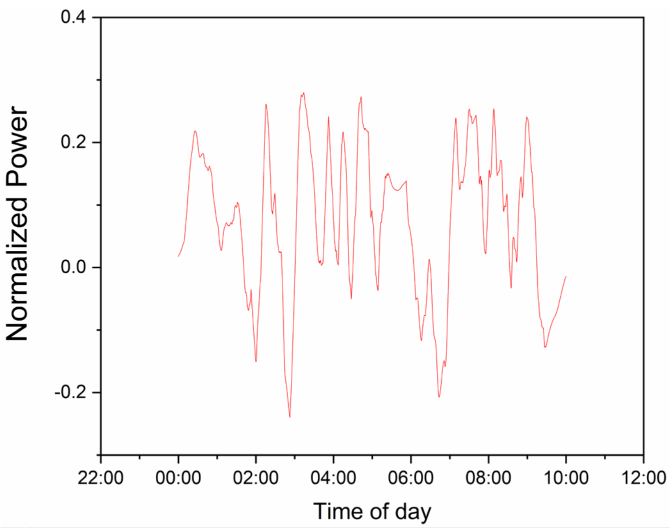

Figure B4: Standard normalized PV power signal over 10 hour time period for testing the PV firming applications.

B8. Detailed results: Component design, economic analysis, and life cycle assessment

Table B18. Results of component design, economic analysis and life cycle assessment for utility-level PV firming application (PVF).

#	Location	Configuration	Component Design					Economic Analysis		Life Cycle Assessment
			PV (MW)	Battery storage (MWh)	Inverter (MW)	Energy Produced (MWh/year)	Grid Purchase (MWh/year)	LCOE (¢/kWh)	Annualized Cost ($/ year)	GWP (kg CO_2 eq. per kWh)
1	DET	PVF0	5	0	3.335	6,780	NA	3.85	261,229	0.052
		PVF1	5	0.269	3.335	7,526	37	3.56	267,516	0.051
		PVF1n	5	0.075	3.335	7,526	37	3.56	268,088	0.051
2	LA	PVF0	5	0	3.335	8,478	NA	3.08	261,281	0.042
		PVF1	5	15.229	3.335	9,146	595	4.79	438,110	0.056
		PVF1n	5	12.995	3.335	9,148	324	7.50	685,869	0.075
3	NYC	PVF0	5	0	3.335	7,095	NA	3.68	261,111	0.050
		PVF1	5	27.289	3.335	8,028	162	6.42	494,416	0.059
		PVF1n	5	22.523	3.335	8,028	165	12.00	929,999	0.095
4	PHX	PVF0	5	0	3.335	9,442	NA	2.77	261,101	0.038
		PVF1	5	26.137	3.335	11,441	169	4.16	475,435	0.042
		PVF1n	5	21.642	3.335	11,441	144	7.76	887,646	0.065
5	PTD	PVF0	5	0	3.335	6,276	NA	4.16	261,101	0.057
		PVF1	5	33.467	3.335	6,899	151	7.02	484,094	0.066
		PVF1n	5	21.889	3.335	6,899	206	13.00	894,995	0.109

APPENDIX C: Supplementary Information for Chapter 4

C1. Material requirement for solar PV plants and wind turbines by 2050

The proportion of mono-crystalline silicon modules in 2050 was assumed as 66% and, while 34% of modules were assumed to be multi-crystalline silicon based on [239]. The per kW silicon, aluminum, and copper required for mono-crystalline silicon is given in Table C1.

Table C1. Material requirement for mono-crystalline silicon modules in 2050.

Material name	Material quantity	Reference
Silicon	2.93 kg	[239]
Aluminum	11.08 kg	
Copper	0.52	

Similarly, the per kW silicon, aluminum, and copper required for multi-crystalline silicon modules in 2050 is given in Table C2.

Table C2. Material requirement for multi-crystalline silicon modules by 2050.

Material name	Material quantity	Reference
Silicon	3.41 kg	[239]
Aluminum	11.97 kg	
Copper	0.57 kg	